Effects of Synthetic Gauge Fields on Quasi-1D Electronic and Spin Systems

Bachana Beradze

A dissertation thesis was submitted to the Faculty of Natural Sciences and Medicine of Ilia State University by the requirements for the degree of Doctor of Philosophy in Physics

Doctoral Program in Physics and Astronomy

supervised by
Prof. Alexander Nersesyan and Prof. George Japaridze

Ilia State University
Tbilisi, 2024

Acknowledgements

I am profoundly grateful to my supervisor, Prof. Alexander Nersesyan, for his invaluable guidance, support, and mentorship throughout my PhD journey, which has shaped my scientific perspective in countless ways. I extend my heartfelt thanks to Prof. George Japaridze for his indispensable support, mentorship, and constructive critique, providing crucial insights throughout this work. I also wish to acknowledge the invaluable support of my colleagues, Mikheil Tsitsishvili, Shota Garuchava, Tatia Sharia, and Erekle Jmukhadze, whose encouragement has been a constant source of motivation. Special thanks go to Marcello Dalmonte, Emanuele Tirrito, Titas Chanda, and Mikheil Tsitsishvili for their collaborative contributions, which significantly enriched and reinforced the findings presented in this thesis. Finally, I would like to express my deepest gratitude to my mother for her unwavering support and encouragement.

My appreciation also goes to the scientific and administrative staff of Ilia State University for providing a supportive environment during my studies. The support from the Shota Rustaveli National Science Foundation of Georgia, SRNSF, Grant No. FR-19-11872, is gratefully acknowledged.

Contents

Acronyms

1D one-dimensional

2D two-dimensional

AT Ashkin-Teller

BCs boundary conditions

BKT Berezinskii-Kosterlitz-Thoules

CDW charge density wave

CFT conformal field theory

DSG double-frequency sine-Gordon

EMT energy-momentum tensor

LL Luttinger liquid

OPE operator product expansion

QAT quantum Ashkin-Teller

RG renormalization group

SG sine-Gordon

TFL triangular flux ladder

TLL Tomonaga-Luttinger liquid

WZNW Wess-Zumino-Novikov-Witten

აბსტრაქტი

ულტრაცივი ფერმი გაზების სისტემები სინთეტური ყალიბური ველების თანაობისას წარმოადგენს შესანიშნავ პლატფორმას, რათა შესწავლილ იქნეს მესრის ფრუსტრაციისა და ეფექტური მაგნიტური ნაკადის ეფექტები, როდესაც ერთ ნაწილაკზე მოსული ნაკადის სიდიდე ახლოსაა ნაკადის ერთი კვანტის მნიშვნელობასთან. მინიმალური თეორიული მოდელი, რომელშიც შესაძლებელია მსგავსი ამოცანის შესწავლა, არის უსპინო ფერმიონების მოდელი ორჯაჭვიანი სამკუთხა კიბის ფორმის მქონე მესერზე პლაკეტის გამჭოლი მაგნიტური ნაკადის თანაობისას. მოცემულ დისერტაციის შესწავლის საგანს წარმოადგენს სწორედ ასეთი მოდელი ნახევრადშევსებული ზონის პირობებში, როდესაც ჯაჭვთა შორის ფერმიონთა გადახტომის ამპლიტუდები ალტერნირებულია ზიგზაგ ბმების გასწვრივ და გაცილებით მცირეა ჯაჭვის გასწვრივ გადახტომის ამპლიტუდასთან შედარებით. ასეთ პირობებში ადგილი აქვს თვისობრივ ცვლილებებს ჯერ კიდევ არაურთიერთქმედი მოდელის ზღვარშიც კი. განსაკუთრებით აღსანიშნავია ტოპოლოგიური ლიფშიცის გადასვლების წანაცვლება ერთ პლაკეტზე მოსული ნაკადის (f) ისეთ მნიშვნელობებზე, რომლებიც ახლოსაა ნაკადის ერთი კვანტის მნიშვნელობასთან ($f \sim 1/2$). სტანდარტულ მართკუთხა კიბეზე არსებული სპექტრის სიმეტრია $k \to \pi - k$ დარღვეულია გეომეტრიული ფრუსტრაცის პირობებში. შედეგად ადგილი აქვს მეტალ-იზოლატორულ გადასვლათა გადაგვარების მოხსნას. ტრანსლაციურად ინვარიანტული სამკუთხა კიბის შემთხვევაში, აღსანიშნავია იზოლირებული დირაკის წერტილის ფორმირება ბრილუენის ზონის საზღვარზე. შედეგად ძირითადი მდგომარეობა $f = 1/2$-სთვის ხდება მეტალური. აღნიშნულ ნაშრომში შესწავლილია ორბიტალური დენების ნაკადზე დამოკიდებულება და დადგენილია ლიფშიცის კრიტიკულ წერტილთა მდებარეობა აღნიშნული დამოკიდებულების განსაკუთრებულ წერტილთა (სინგულარობათა) მდებარეობების შესწავლით როგორც ფიქსირეული ქიმიური პოტენციალის μ, ასევე ფიქსირებული ნაწილაკთა რიცხვის ρ პირობებში. გეომეტრიული ფრუსტრაციით გამოწვეული ნაწილაკ-ხვრელური სიმეტრიის დარღვევას მივყავართ ასიმეტრიამდე ნაწილაკებითა ($\rho > 1$) და ხვრელებით ($\rho < 1$) დოპირების შემთხვევათა შორის, რაც იძლევა თვისობრივად განსხვავებულ შედეგებს ფაზურ დიაგრამაში, ლიფშიცის წერტილების ბუნებისა და ორბიტალური დენების ნაკადზე დამოკიდებულებაში, $\rho = \text{const}$ და $\mu = \text{const}$ შემთხვევებს შორის.

სპექტრში იზოლირებული დირაკის წერტილის არსებობის შედეგად სისტემა ხდება მეტად მგრძნობიარე ნაწილაკთაშორის კორელაციების მიმართ. მიკროსკოპულ დონეზე სისტემას გააჩნია U(1) სიმეტრია, რაც შეესაბამება სრული ფერმიონული მუხტის შენახვას, და დისკრეტული $\mathbb{Z}_2$ სიმეტრია, რაც წარმოადგენს ლუწობისა და ჯაჭვთა გადასმის ოპერაციათა კომბინაციას. ბოზონიზაციის გამონებით ნაჩვენები იქნა, რომ სისტემის ყოფაქცევა და-

ბალ ენერგიებზე აღიწერება ორსიხშიროვანი სინუს-გორდონის (DSG) მოდელით. ამ შესაბამისობაზე დაყრდნობით დადგენულია მეტად მდიდარი ფაზური დიაგრამა. იგი შედგება ტრივიალური და ტოპოლოგიური ზონური იზოლატორის ფაზებისაგან სუსტი ურთიერთქმედების შემთხვევაში, რომლებიც ერთამნეთისგან გამოყოფილია გაუსის ტიპის კრიტიკული მრუდით, ხოლო შედარებით დიდი ურთიერთქმედებისთვის ადგილი აქვს სპონტანურად დარღვეული $\mathbb{Z}_2$ სიმეტრიის მქონე ძლიერ კორელირებულ ფაზას, რომელიც ხასიათდება ჯაჭვთა შორის მუხტის იმბალანსისა და სრული დენის ჩამოყალიბებეით. ამ სამი ფაზის გადაკვეთის წერტილში სისტემაში თავს იჩენს აღმოცენებადი SU(2) სიმეტრია. აღნიშნული არა-აბელური სიემტრია, რომელსაც არ აქვს ადგილი მიკროსკოპულ აღწერაში, დამახისიათებელია მხოლოდ სისტემის დაბალენერგეტიკული ზღვრისთვის როგორც მაგნიტური ნაკადის, ფრუსტრაციისა და მრავალ-ნაწილაკოვანი კორელაციების გაერთიანებული ეფექტი. აღნიშნული კრიტიკული წერტილი ეკუთვნის $SU(2)_1$ ვეს-ზუმინო-ნოვიკოვ-ვიტენის (Wess-Zumino-Novikov-Witten) უნივერსალობის კლასს, რომელიც განიცდის ბიფურკაციას ორი იზინგის ტიპის კრიტკულ მრუდში, რომლებიც ერთმანეთისგან გამოყოფენ ზონური იზოლატორის ფაზებს ძლიერ კორელირებული დარღვეული სიმეტრიის ფაზისაგან.

მოცემულ ნაშრომში დადგენულია დაბალენერგეტიკულ ზღვარში ბიფურკაციის წერტილის მახლობლად მოდელის კავშირი აშკინ-ტელერისა (Ashkin-Teller) და სუსტად დიმერიებულ ნახევარსპინიან ჰეიზენბერგის XXZ მოდელებთან. ჩვენი შედეგები რელევანტურია ისეთი თანამედროვე ექსპერიმენტების კონტექსტში, როგორიცაა ცივი ატომების სისტემები რიდბერგის ტიპის დინამიკით, რომლებშიც უკვე დაიმზირება კორელირებული დინამიკა კიბის ფორმის მქონე სტრუქტურებში.

ნაშრომში წარმოდგენილი რიცხვითი შედეგები (რომლებიც მიღებულ იქნა კოლაბორაციის ფარგლებში) ადასტურებს ჩვენს მიერ მიღებულ თეორილ შედეგებს როგორც ფაზური დიაგრამის ასევე კრიტიკული ყოფაქცევის თვალსაზრისით.

Abstract

Ultracold Fermi gases with synthetic gauge field represent an excellent platform to study the combined effect of lattice frustration and an effective magnetic flux close to one flux quantum per particle. The minimal theoretical model to accomplish this task is a system of spinless fermions on a triangular two-chain flux ladder. In this thesis, we consider this model close to half-filling, with interchain hopping amplitudes alternating along the zigzag bonds of the ladder and being small. In such a setting qualitative changes in the ground state properties of the model in the noninteracting limit, most notably the flux-induced topological Lifshitz transitions are shifted towards the values of the flux per a diatomic plaquette (f) close to the flux quantum ($f \sim 1/2$). Geometrical frustration of the lattice breaks the $k \to \pi - k$ particle-hole spectral symmetry present in non-frustrated ladders. It leads to the splitting of the degeneracies at metal-insulator transitions. A remarkable feature of a translationally invariant triangular ladder is the appearance of an isolated Dirac node at the Brillouin zone boundary, rendering the ground state at $f = 1/2$ semi-metallic. We calculate the flux dependence of the orbital current and identify Lifshitz critical points by the singularities in this dependence at a constant chemical potential μ and constant particle density ρ. The absence of the particle-hole symmetry in the triangular ladder leads to the asymmetry between particle ($\rho > 1$) and hole ($\rho < 1$) doping and to qualitatively different results for the phase diagram, Lifshitz points and the flux dependence of the orbital current in the settings $\rho = \text{const}$ and $\mu = \text{const}$.

The appearance of the isolated Dirac node in the spectrum renders the system very susceptible to interactions. Microscopically, the system exhibits a U(1) symmetry corresponding to the conservation of total fermionic charge, and a discrete $\mathbb{Z}_2$ symmetry – a product of parity transformation and chain permutation. Using bosonization, we show that, in the low-energy limit, the system is described by the quantum double-frequency sine-Gordon (DSG) model. On the basis of this correspondence, a rich phase diagram of the system is obtained. It includes trivial and topological band insulators for weak interactions, separated by a Gaussian critical line, whereas at larger interactions a strongly correlated phase with spontaneously broken $\mathbb{Z}_2$ symmetry sets in, exhibiting a net charge imbalance and non-zero total current. At the intersection of the three phases, the system features a critical point with an emergent SU(2) symmetry. This non-Abelian symmetry, absent in the microscopic description, is realized at low energies as a combined effect of the magnetic flux, frustration, and many-body correlations. The criticality belongs to the $SU(2)_1$ Wess-Zumino-Novikov-Witten universality class. The critical point bifurcates into two Ising critical lines that separate the band insulators from the strong-coupling symmetry broken phase. We establish an analytical connection between the low-energy description of our model around the critical bifurcation point on one hand, and the Ashkin-Teller (AT) model and a weakly dimerized XXZ spin-1/2 chain on the other. Our findings are of interest to up-to-date cold atom experiments utilizing Rydberg dressing, that have

already demonstrated correlated ladder dynamics.

Numerical results (obtained by collaborators) spread throughout the thesis provide additional evidence for the theoretical predictions and help validate the proposed phase diagram and critical behavior of the triangular flux ladder (TFL) model.

The structure of the thesis

The first part, titled "Theoretical and Experimental Background," is structured into four chapters. Chapter 1 begins with an introduction to Abelian bosonization for one-dimensional (1D) spinless fermions, followed by a summary of non-Abelian bosonization of the Heisenberg spin-1/2 chain in Sec. 1.5, offering the necessary theoretical foundation. Chapter 2 discusses the DSG model and its connection with the AT model. Before introducing a model of the TFL (Chapter 4), which is the core subject of the thesis, artificial flux systems are introduced in chapter 3 in the context of cold atoms on optical lattices.

The second part of the thesis is dedicated to an in-depth analysis of the TFL, focusing on configurations where the flux per diatomic plaquette is close to $\varphi_c = \pi$ (in units of the flux quantum), as presented in publications [1] and [2]. Chapter 5 examines the flux-induced topological Lifshitz transitions and diamagnetic currents in the non-interacting TFL. In Sec. 5.5, the topological properties and the corresponding edge states are identified. Inter-particle correlations are explored in Chapter 6 using the bosonization technique.

Part I

Theoretical and experimental background

Chapter 1

Bosonization

1.1 Free fermions in 1D

Free gapless fermions in 1D are equivalent to gapless bosons. Certain interactions between the fermions (forward scattering processes) keep the bosonic Hamiltonian Gaussian and, hence exactly solvable. The solution displays a non-Fermi-liquid behavior of interacting fermions known as the Tomonaga-Luttinger liquid (TLL) characterized by power-law correlations of physical quantities. Those interactions that do not fall into this class (backward spin-flip scattering, Umklapp processes, etc) are expressed in terms of local perturbations which are nonlinear in terms of the bosonic fields (the so-called vertex operators). When these perturbations are relevant in the renormalization group (RG) sense, the problem admits a non-perturbative solution based either on the integrability or scaling arguments. Physically, fundamental fermions acquire a structure of quantum solitons of the corresponding bosonic field theory.

The **U(1) symmetric** model of non-interacting fermions in 1D is given by the Hamiltonian:[1]

$$\mathcal{H}_0 = -t\sum_{j=1}^{N}\left(c_j^\dagger c_{j+1} + c_{j+1}^\dagger c_j\right) - \mu\sum_{j=1}^{N} n_j, \tag{1.1}$$

where $t > 0$ and μ are the hopping amplitude and the chemical potential, respectively. $c_j^\dagger$ and c_j are creation and annihilation operators of spinless fermion at site j satisfying fermion anti-commutation algebra:

$$\{c_i, c_j^\dagger\} = \delta_{ij}, \quad \{c_i^\dagger, c_j^\dagger\} = \{c_i, c_j\} = 0. \tag{1.2}$$

One usually considers a periodic lattice with the first ($j = 1$) and last ($j = N+1$) sites identified with each other and imposing either periodic or antiperiodic boundary conditions

[1]Such a model is not of only pure theoretical interest but arises in a number of physical problems such as the Heisenberg model of 1D quantum antiferromagnet (appendix A) by means of Jordan-Wigner transformation (A.7).

(BCs) on fermion operators. For future convenience, we choose an antiperiodic BCs:

$$c_{j+N} = -c_j. \tag{1.3}$$

The U(1) symmetry acts on the fermion operator as phase transformation:

$$c_j \to e^{-\mathrm{i}\alpha} c_j, \tag{1.4}$$

and leads to the conservation of fermion number:

$$N_e = \sum_{j=1}^{N} n_j, \quad [N_e, \mathscr{H}] = 0. \tag{1.5}$$

In terms of Fourier modes

$$c_j = \frac{1}{\sqrt{N}} \sum_{k\in\mathrm{B.Z.}} e^{\mathrm{i}kja_0} c_k, \tag{1.6}$$

where the summation over momenta k is restricted to the first Brillouin zone (B.Z.) defined by the antiperiodicity:

$$\mathrm{B.Z.} = \left\{ k = \frac{2\pi}{L}\left(n + \frac{1}{2}\right): \quad n = -\frac{N}{2}, -\frac{N}{2}+1, \ldots, -1, 0, 1, \ldots, \frac{N}{2} - 1 \right\}. \tag{1.7}$$

the free part (1.1) is easily diagonalized:

$$\mathscr{H}_0 = \sum_{k\in\mathrm{B.Z.}} \left(\varepsilon_0(k) - \mu\right) c_k^\dagger c_k. \tag{1.8}$$

The one-particle energy spectrum

$$\varepsilon_0(k) = -2t\cos(ka_0), \tag{1.9}$$

is depicted in Fig. 1.1. In the ground state, all one-particle states below the chemical potential are occupied by a single spinless fermion due to Pauli exclusion. Those are states with momentum in the range $|k| < k_\mathrm{F}$ shown with full circles. The empty circles depict empty states. The Fermi momentum is determined from the equation $\varepsilon(k_\mathrm{F}) = \mu$ which gives

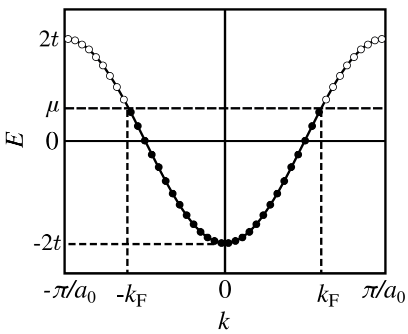

Figure 1.1: One-particle spectrum.

$$k_\mathrm{F} = \frac{1}{a_0} \arccos\left(\frac{\mu}{2t}\right), \tag{1.10}$$

using which one can express the band filling number:

$$\langle n \rangle = \frac{1}{N} \sum_{k\in\mathrm{B.Z.}} \langle c_k^\dagger c_k \rangle \approx \begin{cases} 0, & \mu < -2t, \\ 1 - \frac{1}{\pi}\arccos\left(\frac{\mu}{2t}\right), & |\mu| < 2t, \\ 1, & \mu > 2t. \end{cases} \tag{1.11}$$

Therefore, the chemical potential controls the fermion filling. At $\mu = 0$, the band is half-filled $\langle n \rangle = 1/2$. In what follows, we consider only a half-filled band, hence $\mu = 0$ at all subsequent calculations. In this limit, the model is particle-hole symmetric:

$$c_j \to (-1)^j c_j^\dagger. \tag{1.12}$$

Let us now consider the density-density correlation function

$$\Gamma(i-j) = \left\langle \big(n_i - \langle n \rangle\big)\big(n_j - \langle n \rangle\big) \right\rangle. \tag{1.13}$$

Using Wick's theorem and then passing to the momentum representation, one easily obtains for arbitrary $i \neq j$:

$$\Gamma(i-j) = -\frac{1}{2\pi^2}\frac{1-(-1)^{i-j}}{(i-j)^2}. \tag{1.14}$$

The power-law behavior of correlations highlights the critical nature of the free fermion model (1.1).

It is worth noting that the elementary excitations consist of particle-hole pairs that, once excited, propagate independently as free particles, possessing well-defined quasi-momentum and energy. Each pair is characterized by momentum q and energy

$$\omega(q;k) = \varepsilon_0(k+q) - \varepsilon_0(k), \tag{1.15}$$

forming what is known as the **spinon continuum** as depicted in Fig. 1.2. This graph is of paramount importance to 1D quantum physics. It elucidates that excitations near the origin exhibit a linear dispersion $\omega \approx v|q|$, $|q| \ll k_F$, independent of k, similar to the dispersion relation of long-wavelength sound waves, representing density excitations of a 1D lattice (see Sec. 1.3). In this low energy limit, as it corresponds to long-distance physics and is insensitive to microscopic details of the underlying lattice Hamiltonian, the emergence of universal properties is anticipated.

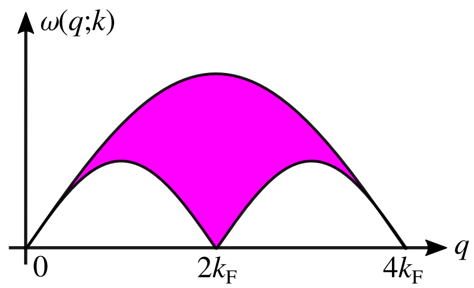

Figure 1.2: Spinon continuum of the half-filled XX model ($h = 0$).

1.2 Continuum description

1.2.1 Low energy Hamiltonian

As mentioned in the previous section, only processes occurring near Fermi points contribute to universal properties. Hence, we linearize the spectrum (1.9) at these points, as illustrated in Fig. 1.3. Expressing $k = \pm k_{\rm F} + p$, where $p \ll k_{\rm F}$ and is quantized as,

$$p_n = \frac{2\pi}{L}\left(n + \frac{1}{2}\right), \tag{1.16}$$

and introducing left (L) and right (R) moving fields as follows:

$$\psi_{\rm L}(p) \equiv c_{k_{\rm F}+p}, \quad \psi_{\rm R}(p) \equiv c_{-k_{\rm F}+p}, \quad |p| \ll \Lambda, \tag{1.17}$$

($\Lambda \sim \frac{1}{a_0}$ is a large momentum cutoff) the Hamiltonian

$$\mathscr{H}_0 = \sum_p vp\Big(:\psi^\dagger_{\rm R}(p)\psi_{\rm R}(p): - :\psi^\dagger_{\rm L}(p)\psi_{\rm L}(p):\Big), \tag{1.18}$$

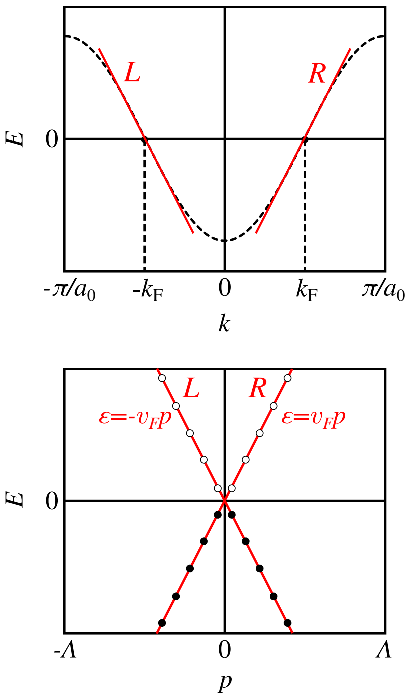

Figure 1.3: Linearized spectrum.

where

$$v \equiv Ja_0, \tag{1.19}$$

is the Fermi velocity at half-filling.

An important observation needs to be made regarding the Hamiltonian (1.18). The vacuum properties of the effective linearized theory differ significantly from those of the original model. All one-particle energy levels below zero are filled in the lowest energy state, while all positive energy levels are empty. Consequently, the ground state, known as the Fermi sea and denoted by $|{\rm F.S.}\rangle$, contains an infinite number of particles, making the ground state energy a divergent quantity.

However, our interest lies in small fluctuations above the ground state, and thus, we can safely set the vacuum energy of the filled Fermi sea to zero: $\langle{\rm F.S.}|\mathscr{H}_0|{\rm F.S.}\rangle = 0$. This is achieved by introducing the following normal ordering operation for right-moving particles:

$$:\psi^\dagger_{\rm R}(p_1)\psi_{\rm R}(p_2): = \begin{cases} \psi^\dagger_{\rm R}(p_1)\psi_{\rm R}(p_2), & p_1 \neq p_2, \\ \psi^\dagger_{\rm R}(p_1)\psi_{\rm R}(p_1), & p_1 = p_2 > 0, \\ -\psi_{\rm R}(p_1)\psi^\dagger_{\rm R}(p_1), & p_1 = p_2 < 0, \end{cases} \tag{1.20}$$

and for left-moving particles:

$$:\psi_{\mathrm{L}}^{\dagger}(p_1)\psi_{\mathrm{L}}(p_2):=\begin{cases}\psi_{\mathrm{L}}^{\dagger}(p_1)\psi_{\mathrm{L}}(p_2), & p_1\neq p_2,\\ \psi_{\mathrm{L}}^{\dagger}(p_1)\psi_{\mathrm{L}}(p_1), & p_1=p_2<0,\\ -\psi_{\mathrm{L}}(p_1)\psi_{\mathrm{L}}^{\dagger}(p_1), & p_1=p_2>0.\end{cases} \tag{1.21}$$

That being said, starting with the Fourier representation (1.6), we approximate the lattice fermion operator at $x\equiv ja_0$ as

$$\begin{aligned} c_j \;\to\; \sqrt{a_0}c(x) &= \sqrt{a_0}\left(e^{\mathrm{i}k_{\mathrm{F}}x}\psi_{\mathrm{R}}(x)+e^{-\mathrm{i}k_{\mathrm{F}}x}\psi_{\mathrm{L}}(x)\right)=\\ &=\sqrt{a_0}\left(\mathrm{i}^j\psi_{\mathrm{R}}(x)+(-\mathrm{i})^j\psi_{\mathrm{L}}(x)\right), \end{aligned} \tag{1.22}$$

expressed in terms of slowly varying fields,

$$\psi_{\mathrm{R}}(x)\equiv\frac{1}{\sqrt{L}}\sum_{|p|\ll\Lambda}e^{\mathrm{i}px}\psi_{\mathrm{R}}(p)\quad\text{and}\quad\psi_{\mathrm{L}}(x)\equiv\frac{1}{\sqrt{L}}\sum_{|p|\ll\Lambda}e^{\mathrm{i}px}\psi_{\mathrm{L}}(p). \tag{1.23}$$

each centered at the corresponding Fermi point (see Fig. 1.3).

Then, the continuum Hamiltonian decouples into two commuting chiral parts:

$$\mathscr{H}_0=\mathscr{H}_0^{(\mathrm{R})}+\mathscr{H}_0^{(\mathrm{L})}=-\mathrm{i}v\int_{-L/2}^{L/2}\mathrm{d}x\left[:\psi_{\mathrm{R}}^{\dagger}(x)\partial_x\psi_{\mathrm{R}}(x):-:\psi_{\mathrm{L}}^{\dagger}(x)\partial_x\psi_{\mathrm{L}}(x):\right]. \tag{1.24}$$

Slowly varying fields still satisfy fermion anticommutation algebra asymptotically in the limit, $|x|\gg\alpha$:

$$\begin{aligned} \left\{\psi_{\mathrm{R}}^{\dagger}(x),\psi_{\mathrm{R}}(y)\right\}&=\left\{\psi_{\mathrm{L}}^{\dagger}(x),\psi_{\mathrm{L}}(y)\right\}=\delta(x-y)\\ \left\{\psi_{\mathrm{R}}^{\dagger}(x),\psi_{\mathrm{L}}^{\dagger}(y)\right\}&=\left\{\psi_{\mathrm{R}}(x),\psi_{\mathrm{L}}(y)\right\}=0. \end{aligned} \tag{1.25}$$

1.2.2 Emergent symmetries

Projecting onto the low-energy sector results in the emergence of a larger symmetry group than that of the original lattice model. The most obvious among these **emergent symmetries** are:

Lorenz invariance

Equation (1.24) represents a second-quantized Hamiltonian of the Dirac equation:

$$\mathrm{i}\frac{\partial}{\partial t}\Psi=\hat{\mathscr{H}}\Psi,\quad \mathscr{H}=-\mathrm{i}v\hat{\sigma}^3\partial_x,\quad \Psi=\begin{pmatrix}\psi_{\mathrm{R}}\\ \psi_{\mathrm{L}}\end{pmatrix} \tag{1.26}$$

where $\hat{\sigma}^3$ is the third Pauli matrix[2] The commonly used formulation of the massless Dirac equation in literature involves multiplying the aforementioned equation by the first Pauli

[2]We choose the representation of Pauli matrices with diagonal $\hat{\sigma}^3$:

$$\hat{\sigma}^1=\begin{pmatrix}0&1\\1&0\end{pmatrix},\quad \hat{\sigma}^2=\begin{pmatrix}0&-\mathrm{i}\\ \mathrm{i}&0\end{pmatrix},\quad \hat{\sigma}^3=\begin{pmatrix}1&0\\0&-1\end{pmatrix}.$$

matrix $\hat{\sigma}^1$ from the left and then dividing by the Fermi velocity. Denoting $x^0 = vt$, $x^1 = x$ and $\partial_\mu = \frac{\partial}{\partial x^\mu}$, the resulting expression is:

$$\mathrm{i}\gamma^\mu \partial_\mu \Psi = 0, \tag{1.27}$$

where

$$\gamma^0 = \hat{\sigma}^1, \quad \gamma^1 = \hat{\sigma}^1 \hat{\sigma}^3 = -\mathrm{i}\hat{\sigma}^2 \tag{1.28}$$

are Dirac γ-matrices satisfying the following Clifford algebra:

$$\{\gamma^\mu, \gamma^\nu\} = 2g^{\mu\nu}, \quad g^{\mu\nu} = \mathrm{diag}(1, -1). \tag{1.29}$$

Then one constructs the manifestly Lorentz invariant Lagrangian

$$\mathscr{L}_\mathrm{M} = \mathrm{i}\Psi^\dagger(\mathbf{x})\gamma^0\gamma^\mu\partial_\mu\Psi(\mathbf{x}), \tag{1.30}$$

and the action functional

$$S_\mathrm{M}[\Psi] = \mathrm{i}\int \mathrm{d}^2\mathbf{x}\, \Psi^\dagger(\mathbf{x})\gamma^0\gamma^\mu\partial_\mu\Psi(\mathbf{x}). \tag{1.31}$$

in Minkowski space-time just by imposing the condition to reproduce (1.27) via the Euler-Lagrange equation. The two components of the Dirac spinor field Ψ satisfy the equal time canonical anticommutation relations:

$$\begin{aligned} &\{\psi_\alpha(t,x), \psi^\dagger_\beta(t,y)\} = \delta_{\alpha\beta}\delta(x-y), \\ &\{\psi_\alpha(t,x), \psi_\beta(t,y)\} = \{\psi^\dagger_\alpha(t,x), \psi^\dagger_\beta(t,y)\} = 0, \quad (\alpha, \beta = \mathrm{R}, \mathrm{L}). \end{aligned} \tag{1.32}$$

Chiral symmetry

Separation of chiral modes in (1.24) renders the model invariant under the wider group $U(1)_\mathrm{R} \times U(1)_\mathrm{L}$ associated with the separate conservation of numbers of right and left movers. This new emergent (chiral) symmetry, under which spinor components transform as

$$\psi_\mathrm{R}(x) \to e^{-\mathrm{i}\alpha}\psi_\mathrm{R}(x), \quad \psi_\mathrm{L}(x) \to e^{-\mathrm{i}\beta}\psi_\mathrm{L}(x), \tag{1.33}$$

is generated by,

$$N_\mathrm{R} = \int \mathrm{d}x\, J_\mathrm{R}(x), \quad N_\mathrm{L} = \int \mathrm{d}x\, J_\mathrm{L}(x), \tag{1.34}$$

respectively, where

$$J_\mathrm{R}(x) \equiv :\psi^\dagger_\mathrm{R}(x)\psi_\mathrm{R}(x): \quad \text{and} \quad J_\mathrm{L}(x) \equiv :\psi^\dagger_\mathrm{L}(x)\psi_\mathrm{L}(x): \tag{1.35}$$

are densities of the right and the left movers, or chiral currents above the filled Fermi sea. Normal ordering guarantees the finite ground state expectation values.

It is instructive to reformulate the chiral symmetry in Lagrangian formalism. We start with the total phase transformation symmetry

$$\Psi \to e^{-\mathrm{i}\alpha}\Psi, \tag{1.36}$$

inherited from the original lattice model. According to Noether's theorem, it results in the total particle number conservation:

$$\partial_\mu J^\mu = 0, \quad J^0 = J_\mathrm{R} + J_\mathrm{L}, \quad J^1 = J_\mathrm{R} - J_\mathrm{L} \quad \Longrightarrow \quad \mathcal{Q} = \int \mathrm{d}x\, J^0 = N_\mathrm{R} + N_\mathrm{L} = \mathrm{const.} \tag{1.37}$$

On the other hand, the additional U(1) symmetry emerges in a continuum limit (which is not present in the original lattice model). First, we construct the matrix

$$\gamma^3 \equiv \gamma^0\gamma^1 = \hat{\sigma}^3,$$

which is diagonal in the given choice of γ-matrices (1.28) and consider the transformation

$$\Psi \to e^{\mathrm{i}\alpha\gamma^3}\Psi. \tag{1.38}$$

It is easy to see, that this is indeed the symmetry transformation of the Lagrangian (1.30), and is called the chiral symmetry. According to Noether's theorem, this implies the conservation of the so-called axial current:

$$\partial_\mu J_3^\mu = 0, \quad J_3^0 = J_\mathrm{R} - J_\mathrm{L}, \quad J_3^1 = J_\mathrm{R} + J_\mathrm{L}. \tag{1.39}$$

The corresponding classically conserved "charge" is the total current:

$$\mathcal{J} = \int \mathrm{d}x\, J_3^0 = N_\mathrm{R} - N_\mathrm{L} = \mathrm{const.}$$

The simultaneous conservation of $\mathcal{Q}$ and $\mathcal{J}$ is equivalent to the separate conservation of N_R and N_L.

On top of this, in large systems $L \to \infty$, the absence of any length scale implies scale invariance, which results in an even larger symmetry group, called the conformal group. A field theory invariant under the conformal group is called a conformal field theory (CFT). Basic facts on CFT are summarized in appendix C.

1.2.3 The concept of Tomonaga-Luttinger liquid

The emergence of new symmetries is not the only peculiarity of the low energy limit. Commutation relations of conserved U(1) currents acquire an anomalous behavior: they are nonzero only for infinite systems and vanish for any finite system. Namely, the following **U(1) Kac-Moody algebra** holds:

$$\langle [J_\mathrm{R}(x_-), J_\mathrm{R}(0)] \rangle = \frac{\mathrm{i}}{2\pi}\partial_-\delta(x_-), \quad \langle [J_\mathrm{L}(x_+), J_\mathrm{L}(0)] \rangle = \frac{i}{2\pi}\partial_+\delta(x_+), \tag{1.40}$$

or at equal times:

$$\langle [J_{\rm R}(x), J_{\rm R}(0)] \rangle = -\langle [J_{\rm L}(x), J_{\rm L}(0)] \rangle = \frac{1}{2\pi i}\partial_x \delta(x). \tag{1.41}$$

It is important to stress that the algebra reflects not the properties of the current operators per se, but the existence of the infinite Dirac sea with all negative energy states filled.

This anomalous algebra leads to the fermion-boson duality enabling us to express the Dirac Hamiltonian (1.24) in the following **Sugawara form**:

$$\mathscr{H}_0 \;=\; -\mathrm{i}v \int \mathrm{d}x \,[:\psi_{\rm R}^\dagger \partial_x \psi_{\rm R}: - :\psi_{\rm L}^\dagger \partial_x \psi_{\rm L}:] \;=\; \pi v \int \mathrm{d}x\,[:J_{\rm R}^2(x): + :J_{\rm L}^2(x):]. \tag{1.42}$$

Indeed, the Sugawara Hamiltonian is the only Hamiltonian that together with (1.41) correctly reproduces the Heisenberg equations of motion for currents:

$$\begin{aligned} \partial_t J_{\rm R}(t,x) &= \mathrm{i}[\mathscr{H}_0, J_{\rm R}] = -v\partial_x J_{\rm R}(t,x), \\ \partial_t J_{\rm L}(t,x) &= \mathrm{i}[\mathscr{H}_0, J_{\rm L}] = v\partial_x J_{\rm L}(t,x). \end{aligned}$$

With the Hamiltonian expressed in terms of fermion density operators, we are one step closer to expressing low-energy excitations as bosonic degrees of freedom with linear dispersion $\omega(q) = v|q|$. To achieve this, let us consider the Fourier mode expansion of U(1) currents:[3]

$$\begin{aligned} J_{\rm R}(x) &= \frac{1}{L}\sum_{q\neq 0} e^{\mathrm{i}qx} J_{\rm R}(q), \quad J_{\rm R}(q) = \sum_p \psi_{\rm R}^\dagger(p)\psi_{\rm R}(p+q), \\ J_{\rm L}(x) &= \frac{1}{L}\sum_{q\neq 0} e^{\mathrm{i}qx} J_{\rm L}(q), \quad J_{\rm L}(q) = \sum_p \psi_{\rm L}^\dagger(p)\psi_{\rm L}(p+q). \end{aligned} \tag{1.43}$$

with momentum q quantized as $q = \frac{2\pi}{L}m$, $m \in \mathbb{Z}$. For inverse transformations, we write:

$$J_{\rm R}(q) = \int \mathrm{d}x\, e^{-\mathrm{i}qx} J_{\rm R}(x), \quad J_{\rm L}(q) = \int \mathrm{d}x\, e^{-\mathrm{i}qx} J_{\rm L}(x). \tag{1.44}$$

Note that not all modes are independent due to the reality condition: $(J_{\rm R}(q))^\dagger = J_{\rm R}(-q)$ and $(J_{\rm L}(q))^\dagger = J_{\rm L}(-q)$.

Then the anomalous algebra (1.41) proves to be nothing but a boson commutation relations:

$$[J_{\rm R}(q), J_{\rm R}(q')] = -[J_{\rm L}(q), J_{\rm L}(q')] = \frac{Lq}{2\pi}\delta_{q+q',0}. \tag{1.45}$$

Indeed, introduction of the following rescaled Bose operators:[4]

$$\beta_q = \mathrm{i}\sqrt{\frac{2\pi}{L|q|}} \begin{cases} J_{\rm R}(q), & q>0, \\ J_{\rm L}(q), & q<0, \end{cases} \qquad \beta_q^\dagger = -\mathrm{i}\sqrt{\frac{2\pi}{L|q|}} \begin{cases} J_{\rm R}(-q), & q>0, \\ J_{\rm L}(-q), & q<0, \end{cases} \tag{1.46}$$

[3]In the present treatment we ignore zero mode contribution to keep the presentation simple.

[4]Extra imaginary factors of i are introduced for future convenience.

(1.45) is rewritten in the more familiar canonical form:

$$[\beta_q, \beta_{q'}^\dagger] = \delta_{qq'}. \tag{1.47}$$

Hence, the following modified expressions for (1.43) mode expansions

$$\begin{aligned} J_{\mathrm{R}}(x) &= \mathrm{i}\sum_{q>0}\sqrt{\frac{q}{2\pi L}}\left(\beta_q e^{\mathrm{i}qx} - \beta_q^\dagger e^{-\mathrm{i}qx}\right), \\ J_{\mathrm{L}}(x) &= -\mathrm{i}\sum_{q>0}\sqrt{\frac{q}{2\pi L}}\left(\beta_{-q} e^{-\mathrm{i}qx} - \beta_{-q}^\dagger e^{\mathrm{i}qx}\right). \end{aligned} \tag{1.48}$$

Substituting in (1.42) leads us to the following **bosonized** form of the Sugawara Hamiltonian:

$$\mathscr{H}_0 = \sum_{q\neq 0} v|q|\left(\beta_q^\dagger \beta_q + \frac{1}{2}\right) + \text{const.} \tag{1.49}$$

The elementary excitations of the model are known as **Tomonaga bosons** and describe particle-hole pairs near the origin of the spinon continuum shown in Fig. 1.2.

1.2.4 Interactions between particles

The most general interactions allowed by the chiral symmetry are given by:

$$\begin{aligned} \mathscr{H}' &= \int \mathrm{d}x\left[g_1\left(J_{\mathrm{R}}^2(x) + J_{\mathrm{L}}^2(x)\right) + g_2 J_{\mathrm{R}}(x) J_{\mathrm{L}}(x)\right] = \\ &= \frac{g_1}{\pi}\sum_{q>0} q\left(\beta_q^\dagger\beta_q + \beta_{-q}\beta_{-q}^\dagger\right) + \frac{g_2}{2\pi}\sum_{q>0} q\left(\beta_q^\dagger\beta_{-q}^\dagger + \beta_{-q}\beta_q\right). \end{aligned} \tag{1.50}$$

In such processes, two particles of the same chirality (g_1) or a pair of opposite chirality particles (g_2) are scattered into an identical pair of particles (forward scattering). Clearly, such interactions leave the bosonic Hamiltonian quadratic and therefore exactly solvable.

Indeed, the total Hamiltonian $\mathscr{H}_{\mathrm{TLL}} = \mathscr{H}_0 + \mathscr{H}'$, known as the **TLL** model, is written as:

$$\mathscr{H}_{\mathrm{TLL}} = \frac{1}{2}\sum_{q>0} q\left[\left(v_{\mathcal{Q}} + v_{\mathcal{J}}\right)\left(\beta_q^\dagger\beta_q + \beta_{-q}\beta_{-q}^\dagger\right) + \left(v_{\mathcal{Q}} - v_{\mathcal{J}}\right)\left(\beta_q^\dagger\beta_{-q}^\dagger + \beta_{-q}\beta_q\right)\right],$$

where

$$v_{\mathcal{Q}} = v + \frac{2g_1 + g_2}{2\pi}, \quad v_{\mathcal{J}} = v + \frac{2g_1 - g_2}{2\pi}.$$

Let us introduce the parametrization $v_{\mathcal{Q}} = \frac{\tilde{v}}{K}$ and $v_{\mathcal{J}} = \tilde{v}K$, where

$$\tilde{v} = \sqrt{v_{\mathcal{Q}} v_{\mathcal{J}}} = v\left(1 + \frac{g_1}{\pi v}\right) + \cdots, \quad K = \sqrt{\frac{v_{\mathcal{Q}}}{v_{\mathcal{J}}}} = 1 - \frac{g_2}{2\pi v} + \cdots, \tag{1.51}$$

are renormalized velocity and so-called **Luttinger liquid (LL) parameter**, respectively, and "$\cdots$" denote higher order corrections. Then using the Bogoliubov transformation:[5]

$$\beta_q = u\tilde{\beta}_q + v\tilde{\beta}^\dagger_{-q}, \quad u = \frac{1}{2}\left(\sqrt{K} + \frac{1}{\sqrt{K}}\right), \quad v = \frac{1}{2}\left(\sqrt{K} - \frac{1}{\sqrt{K}}\right), \tag{1.52}$$

the TLL Hamiltonian can be brought to the following canonical form

$$\mathscr{H}_{\mathrm{TLL}} = \sum_{q\neq 0} \tilde{v}|q|\left(\tilde{\beta}^\dagger_q \tilde{\beta}_q + \frac{1}{2}\right), \tag{1.53}$$

while the rotated currents are simply

$$\begin{aligned} \tilde{J}_{\mathrm{R}}(x) &= \mathrm{i}\sum_{q>0}\sqrt{\frac{q}{2\pi L}}\left(\tilde{\beta}_q e^{\mathrm{i}qx} - \tilde{\beta}^\dagger_q e^{-\mathrm{i}qx}\right), \\ \tilde{J}_{\mathrm{L}}(x) &= -\mathrm{i}\sum_{q>0}\sqrt{\frac{q}{2\pi L}}\left(\tilde{\beta}_{-q} e^{-\mathrm{i}qx} - \tilde{\beta}^\dagger_{-q} e^{\mathrm{i}qx}\right), \end{aligned} \tag{1.54}$$

or including the time dependence

$$\begin{aligned} \tilde{J}_{\mathrm{R}}(x^-) &= \mathrm{i}\sum_{q>0}\sqrt{\frac{q}{2\pi L}}\left(\tilde{\beta}_q e^{-\mathrm{i}qx^-} - \tilde{\beta}^\dagger_q e^{\mathrm{i}qx^-}\right), \\ \tilde{J}_{\mathrm{L}}(x^+) &= -\mathrm{i}\sum_{q>0}\sqrt{\frac{q}{2\pi L}}\left(\tilde{\beta}_{-q} e^{-\mathrm{i}qx^+} - \tilde{\beta}^\dagger_{-q} e^{\mathrm{i}qx^+}\right). \end{aligned} \tag{1.55}$$

[5] Do not confuse the Fermi velocity v with the canonical transformation parameters u, v.

1.3 Massless Gaussian model

In this section, we will reformulate the LL theory as a Gaussian model of the scalar Bose field, which provides a straightforward means of interpreting single fermion operators in terms of bosonic degrees of freedom. Later, this will enable us to address chiral symmetry-breaking terms, such as the Umklapp term, which cannot be solely expressed through chiral currents and do not neatly fit within the traditional LL framework.

The simplest model of the free scalar field $\Phi(x,t)$ in $1+1$ dimensional space-time is known as the massless **Gaussian model** given by the Hamiltonian

$$\mathscr{H} = \frac{v}{2}\int \mathrm{d}x\,\big[v^{-2}(\partial_t\Phi)^2 + (\partial_x\Phi)^2\big] = \frac{v}{2}\int \mathrm{d}x\,\big[\Pi^2 + (\partial_x\Phi)^2\big], \tag{1.56}$$

where v is sound velocity, and

$$\Pi(t,x) = \frac{\delta\mathscr{H}}{\delta(\partial_t\Phi)} = v^{-1}\partial_t\Phi.$$

is the momentum conjugate of Φ. Classically, the field $\Phi(t,x)$ satisfies the wave equation (Euler-Lagrange equation):

$$\partial_\mu\partial^\mu\Phi = \big(\partial_0^2 - \partial_1^2\big)\Phi = 4\partial_+\partial_-\Phi = 0, \tag{1.57}$$

the most general solution of which has the form:

$$\Phi(\mathbf{x}) = \varphi_{\mathrm{R}}(x^-) + \varphi_{\mathrm{L}}(x^+) \tag{1.58}$$

where φ_{R} and φ_{L} are arbitrary functions of light-cone coordinates $x^\pm = vt \pm x = x^0 \pm x^1$. Hence, the field Φ is decomposed into two chiral waves propagating in opposite directions.

From these chiral components, we construct what is known as the dual field:

$$\Theta(\mathbf{x}) = -\varphi_{\mathrm{R}}(x^-) + \varphi_{\mathrm{L}}(x^+), \tag{1.59}$$

following the duality relations:

$$\partial_0\Phi = \partial_1\Theta \quad \text{and} \quad \partial_1\Phi = -\partial_0\Theta. \tag{1.60}$$

In terms of the dual field, canonical momentum

$$\Pi(\mathbf{x}) = \partial_1\Theta(\mathbf{x}), \tag{1.61}$$

hence Eq. (1.56) can be recasted in the following alternate forms

$$\mathscr{H} = \frac{v}{2}\int \mathrm{d}x\,\big[(\partial_1\Theta)^2 + (\partial_1\Phi)^2\big] = v\int \mathrm{d}x\,\big[(\partial_1\varphi_{\mathrm{R}})^2 + (\partial_1\varphi_{\mathrm{L}})^2\big]. \tag{1.62}$$

In passage to quantum theory, classical fields are replaced by corresponding operators. The field operator Φ and its momentum conjugate Π are subject to the following **equal-time** canonical commutation relations

$$\big[\Phi(x^0,x^1), \Pi(x^0,y^1)\big] = \mathrm{i}\delta(x^1 - y^1), \quad (\hbar = 1), \tag{1.63}$$

all other commutators being zero. Alternatively, in terms of the dual field, we write:

$$\begin{aligned}
\left[\Phi(x),\Theta(y)\right] &= \mathrm{i}\theta_{\mathrm{H}}(y-x),\\
\left[\Phi(x),\Phi(y)\right] &= \left[\Theta(x),\Theta(y)\right] = 0.
\end{aligned} \tag{1.64}$$

or, in terms of chiral components, $\varphi_{\mathrm{L}} = \frac{1}{2}(\Phi+\Theta)$ and $\varphi_{\mathrm{R}} = \frac{1}{2}(\Phi-\Theta)$:[6]

$$\begin{aligned}
\left[\varphi_{\mathrm{R}}(x),\varphi_{\mathrm{L}}(y)\right] &= \frac{\mathrm{i}}{4},\\
\left[\varphi_{\mathrm{R}}(x),\varphi_{\mathrm{R}}(y)\right] &= -\left[\varphi_{\mathrm{L}}(x),\varphi_{\mathrm{L}}(y)\right] = \frac{\mathrm{i}}{4}\mathrm{sign} x-y.
\end{aligned} \tag{1.65}$$

1.3.1 Bosonization rules

Imposing periodic boundary conditions $\Phi(x^0,x^1+L) = \Phi(x^0,x^1)$, we expand Φ in Fourier modes:

$$\Phi(\mathbf{x}) = \sum_q e^{\mathrm{i}qx^1}\Phi_q(x^0), \quad q = \frac{2\pi}{L}n, \quad n\in\mathbb{Z}. \tag{1.66}$$

Reality condition implies $\Phi_q^\dagger = \Phi_{-q}$. Hence, the Hamiltonian (1.56) will be

$$\mathscr{H} = \frac{v}{2L}\sum_{q\neq 0}\left[\Pi_q\Pi_{-q} + (qL)^2\Phi_q\Phi_{-q}\right],$$

where

$$\Pi_q(x^0) = \frac{\partial\mathscr{H}}{\partial\left(\partial_0\Phi_q\right)} = L\partial_0\Phi_{-q}.$$

is the momentum conjugate to Φ_q.

The Fourier modes follow the canonical commutation relations:

$$\left[\Phi_q(x^0),\Pi_p(x^0)\right] = \mathrm{i}\delta_{qp}, \tag{1.67}$$

In analogy with the quantum harmonic oscillator, we implement the ladder operators as follows:

$$b_q = \frac{1}{\sqrt{2|q|L}}\left(|q|L\Phi_q + \mathrm{i}\Pi_{-q}\right), \quad q\neq 0,$$

satisfying the standard commutation relations for bosons:

$$\left[b_q,b_p^\dagger\right] = \delta_{qp}.$$

[6]The nonzero commutator between fields of opposite chirality spoils chiral decomposition at the quantum level, which leads to nontrivial properties between the Fourier zero modes of chiral fields. Again, for the simplicity of the presentation, we completely ignore zero modes.

Boson vacuum $|0\rangle$ is annihilated by all destruction operators b_q:

$$b_q\,|0\rangle = 0, \quad \forall q, \tag{1.68}$$

while $b_q^\dagger$ crates, the so-called, **Tomonaga Boson** with momentum q and energy $v|q|$. Then one obtains the following Tomonaga Hamiltonian:

$$\mathscr{H} = \sum_{q\neq 0} v|q|\left(b_q^\dagger b_q + \frac{1}{2}\right). \tag{1.69}$$

Since,

$$\Phi_q = \frac{1}{\sqrt{2|q|L}}\left(b_q + b_{-q}^\dagger\right), \quad q \neq 0,$$

mode expansion (1.66) is written as

$$\Phi(\mathbf{x}) = \sum_{q\neq 0} \frac{1}{\sqrt{2|q|L}}\left[b_q(x^0)e^{\mathrm{i}qx^1} + b_q^\dagger(x^0)e^{-\mathrm{i}qx^1}\right] \tag{1.70}$$

Using the Heisenberg equation of motion for modes gives $b_q(x^0) = e^{-\mathrm{i}|q|x^0}b_q$ and chiral components are expressed explicitly:

$$\begin{aligned}\varphi_{\mathrm{R}}(x^-) &= \sum_{q>0}\frac{1}{\sqrt{2qL}}\left[b_q e^{-\mathrm{i}qx^-} + b_q^\dagger e^{\mathrm{i}qx^-}\right],\\ \varphi_{\mathrm{L}}(x^+) &= \sum_{q>0}\frac{1}{\sqrt{2qL}}\left[b_{-q} e^{-\mathrm{i}qx^+} + b_{-q}^\dagger e^{\mathrm{i}qx^+}\right]\end{aligned} \tag{1.71}$$

Now, comparing (1.69) to (1.49), bosonic and fermionic models are identical to each other provided that $\beta_q \doteq b_q$. With this identification, one may express the U(1) chiral currents in Dirac theory in terms of chiral components of the scalar Bose field, in the bosonized form:[7]

$$J_{\mathrm{R}}(x^-) \doteq -\frac{1}{\sqrt{\pi}}\partial_-\varphi_{\mathrm{R}}(x^-), \quad J_{\mathrm{L}}(x^+) \doteq \frac{1}{\sqrt{\pi}}\partial_+\varphi_{\mathrm{L}}(x^+), \tag{1.72}$$

Substituting these relations in Eq. (1.42) directly provides bosonized Dirac Hamiltonian:

$$-\mathrm{i}v\int \mathrm{d}x\,[:\psi_{\mathrm{R}}^\dagger\partial_x\psi_{\mathrm{R}}: - :\psi_{\mathrm{L}}^\dagger\partial_x\psi_{\mathrm{L}}:] \;\longrightarrow\; \frac{v}{2}\int \mathrm{d}x\,[\Pi^2 + (\partial_x\Phi)^2]. \tag{1.73}$$

As a matter of fact, the conservation of Noether's current and axial current follows from the equation of motion (1.57) of the Bose field and its dual field:

$$\begin{aligned}\partial_\mu J^\mu &= 2\partial_+ J_{\mathrm{R}} + 2\partial_- J_{\mathrm{L}} &&= \frac{1}{\sqrt{\pi}}\partial_+\partial_-\Theta(x^+,x^-) = 0,\\ \partial_\mu J_3^\mu &= 2\partial_+ J_{\mathrm{R}} - 2\partial_- J_{\mathrm{L}} &&= -\frac{1}{\sqrt{\pi}}\partial_+\partial_-\Phi(x^+,x^-) = 0.\end{aligned}$$

[7] The dotted equality signs emphasize that the identification is not operator identity, rather it is identity under correlation functions. In what follows, we use the usual equality sign.

Relations (1.72) accurately map local properties of fermionic and bosonic theories onto each other. However, strictly speaking, the full equivalence between free fermion and free boson theories requires certain constraints on the possible range of values of the Bose field. 1D fermions are $U(1)\otimes U(1)$ (chiral) symmetric, on the other hand, the bosonic theory has $\mathbb{R}\otimes\mathbb{R}$ symmetry (displacements of chiral fields by arbitrary constants leaves the boson Hamiltonian intact). Therefore, to maintain the precise equivalence, one has to consider the so-called compactified boson instead, for which the Bose field has an angular character. Only in such a theory, can the so-called vertex operators be defined and single fermion operators expressed with them. Therefore all sorts of possible interactions (such as Umklapp scattering – see below) can be treated within the bosonization language. Full treatment of compactified boson and its implications are beyond the scope of this short introduction. Instead, we directly jump on to the following definition of the **vertex operators**:

$$e^{\mathrm{i}\beta\varphi_{\mathrm{R}}} \equiv 1+\sum_{n=1}^{\infty}\frac{(\mathrm{i}\beta)^n}{n!}:\varphi_{\mathrm{R}}^n:,\quad e^{\mathrm{i}\bar{\beta}\varphi_{\mathrm{L}}} \equiv 1+\sum_{n=1}^{\infty}\frac{(\mathrm{i}\bar{\beta})^n}{n!}:\varphi_{\mathrm{L}}^n:. \tag{1.74}$$

Normal ordering guarantees finite expectation values. This permits us to introduce the standard boson representation of single fermion operators:

$$\psi_{\mathrm{R}}(x) = \frac{1}{\sqrt{2\pi\alpha}}e^{\mathrm{i}\sqrt{4\pi}\varphi_{\mathrm{R}}(x)},\quad \psi_{\mathrm{L}}(x) = \frac{1}{\sqrt{2\pi\alpha}}e^{-\mathrm{i}\sqrt{4\pi}\varphi_{\mathrm{L}}(x)}. \tag{1.75}$$

It is simple to show that the anticommutation algebra of fermions and the bosonization rules for currents (1.72) as well are correctly reproduced by (1.75), using Backer-Hausdorff formula

$$e^{\hat{A}}e^{\hat{B}} = e^{\hat{A}+\hat{B}}e^{\frac{1}{2}[\hat{A},\hat{B}]}, \tag{1.76}$$

and correlation functions of bosons (see appendix C).

Out of Dirac spinor field $\Psi=(\psi_{\mathrm{R}},\psi_{\mathrm{L}})^{\mathrm{T}}$ one can construct at most four linearly independent fermion bilinears, $\Psi^\dagger(x)\Psi(x)$ and $\Psi^\dagger(x)\hat{\boldsymbol{\sigma}}\Psi(x)$, where $\hat{\boldsymbol{\sigma}}=(\hat{\sigma}^1,\hat{\sigma}^2,\hat{\sigma}^3)$ are Pauli matrices. Diagonal bilinears are the total density and total current in the system, which in bosonization language are,

$$\begin{aligned}\Psi^\dagger(x)\Psi(x) &= J_{\mathrm{R}}(x)+J_{\mathrm{L}}(x) = \frac{1}{\sqrt{\pi}}\partial_x\Phi(x),\\ \Psi^\dagger(x)\hat{\sigma}^3\Psi(x) &= J_{\mathrm{R}}(x)-J_{\mathrm{L}}(x) = -\frac{1}{\sqrt{\pi}}\partial_x\Theta(x).\end{aligned} \tag{1.77}$$

Using Eq. (1.76), the remaining two obtains the form:

$$\begin{aligned}\mathcal{N}_1(x) &\equiv \psi_{\mathrm{R}}^\dagger(x)\psi_{\mathrm{L}}(x)+\mathrm{h.c.} = -\frac{1}{\pi\alpha}\sin\sqrt{4\pi}\Phi(x),\\ \mathcal{N}_2(x) &\equiv -\mathrm{i}\psi_{\mathrm{R}}^\dagger(x)\psi_{\mathrm{L}}(x)+\mathrm{h.c.} = -\frac{1}{\pi\alpha}\cos\sqrt{4\pi}\Phi(x).\end{aligned} \tag{1.78}$$

1.4 Bosonization of interacting fermions

We turn on weak repulsive density-density interaction between the spinless fermions in (1.1):[8]

$$\mathscr{H} = \mathscr{H}_0 + \mathscr{H}_{\text{int}} \tag{1.79}$$

$$\mathscr{H}_{\text{int}} = V \sum_{j=1}^{N} n_j n_{j+1}, \quad V > 0. \tag{1.80}$$

With sufficiently small $V \ll t$, the one-particle energy spectrum is assumed essentially identical to the one obtained for the free model (1.9). Hence the (1.22) is essentially valid and in the continuum limit interaction energy is represented as

$$\mathscr{H}_{\text{int}} \;\to\; g \int \mathrm{d}x : \rho(x)\rho(x+a_0) :, \quad g \equiv V a_0, \tag{1.81}$$

where

$$\rho(x) \;=\; J_{\mathrm{R}}(x) + J_{\mathrm{L}}(x) + (-1)^j \left[: \psi_{\mathrm{R}}^{\dagger}(x)\psi_{\mathrm{L}}(x) : + : \psi_{\mathrm{L}}^{\dagger}(x)\psi_{\mathrm{R}}(x) :\right]. \tag{1.82}$$

is the continuum fermion density. Explicit substitution into (1.81) gives:

$$\mathscr{H}_{\text{int}} \;=\; \int \mathrm{d}x \left[2g\left[: J_{\mathrm{R}}^2(x) : + : J_{\mathrm{L}}^2(x) :\right] + 4g J_{\mathrm{R}}(x) J_{\mathrm{L}}(x)\right] + g \int \mathrm{d}x\, O_{\mathrm{Umk}}(x), \tag{1.83}$$

where

$$O_{\mathrm{Umk}}(x) = - : \left(\psi_{\mathrm{R}}^{\dagger}\psi_{\mathrm{L}}\right)_x \left(\psi_{\mathrm{R}}^{\dagger}\psi_{\mathrm{L}}\right)_{x+a_0} : + \text{h.c.} \tag{1.84}$$

describes the so-called Umklapp processes.

Apart from the Umklapp term, the effective low-energy Hamiltonian of the interacting fermions is given by the following TLL model:

$$\mathscr{H}_{\mathrm{TLL}} \;=\; \frac{\pi\tilde{v}}{2} \int \mathrm{d}x \left[K : (J_{\mathrm{R}} - J_{\mathrm{L}})^2 : + \frac{1}{K} : (J_{\mathrm{R}} + J_{\mathrm{L}})^2 :\right] = \tag{1.85}$$

$$= \frac{\tilde{v}}{2} \int \mathrm{d}x \left[K : (\partial_x \Theta)^2 : + \frac{1}{K} : (\partial_x \Phi)^2 :\right] \tag{1.86}$$

where the renormalized velocity and LL parameter are given by

$$\tilde{v} = v\left(1 + \frac{4g}{\pi v}\right)^{\frac{1}{2}} = v\left(1 + \frac{2g}{\pi v} + O(g^2)\right) \tag{1.87}$$

and

$$K = \left(1 - \frac{4g}{\pi v}\right)^{-\frac{1}{2}} = 1 - \frac{2g}{\pi v} + O(g^2), \tag{1.88}$$

[8]Again, such interactions arise in the Heisenberg model as shown in appendix A.

respectively.

As g increases, the approximate expression for the LL parameter proves inadequate near the phase transition point ($V = 2t$). Fortunately, the 1D fermion model (1.79) is exactly solvable by the Bethe ansatz [3], providing the exact result:

$$K = \frac{\pi}{2\left(\pi - \arccos\frac{V}{2t}\right)}. \tag{1.89}$$

Using the results of the previous section, we obtain

$$O_{\mathrm{Umk}}(x) = \frac{1}{2(\pi\alpha)^2} :\cos\sqrt{16\pi}\Phi(x): + \text{irrelevant terms},$$

hence, up to irrelevant contributions, one obtains:

$$\mathcal{H} = \frac{\tilde{v}}{2}\int \mathrm{d}x \left[K :(\partial_x\Theta)^2: + \frac{1}{K} :(\partial_x\Phi)^2:\right] + \frac{g}{2(\pi\alpha)^2}\int \mathrm{d}x :\cos\sqrt{16\pi}\Phi(x):, \tag{1.90}$$

One usually rescales Bose fields:

$$\Phi \to \sqrt{K}\Phi, \quad \Theta \to \frac{1}{\sqrt{K}}\Theta \tag{1.91}$$

(which clearly preserves Boson commutation relations (1.63)) to bring the Hamiltonian to its canonical sine-Gordon (SG) form

$$\mathcal{H} = \frac{\tilde{v}}{2}\int \mathrm{d}x \left[:(\partial_x\Theta)^2: + :(\partial_x\Phi)^2:\right] + \frac{g}{2(\pi\alpha)^2}\int \mathrm{d}x :\cos\sqrt{16\pi K}\Phi(x):. \tag{1.92}$$

The scaling properties of the SG model are summarised in the appendix D. According to the appendix, the Umklapp term is irrelevant if its scaling dimension $\Delta_{\mathrm{Umk.}} = 4K > 2$ or $K > \frac{1}{2}$. Therefore the effective theory reduces to the free massless Gaussian model or the TLL model,

$$\mathcal{H} = \frac{\tilde{v}}{2}\int \mathrm{d}x \left[:(\partial_x\Theta)^2: + :(\partial_x\Phi)^2:\right], \tag{1.93}$$

From the exact expression of the LL parameter (1.89), this critical region corresponds to $|V| < 2t$ and is characterized by the power-low behavior of correlation functions with K (or g)-dependent critical exponents.

For $V > 2t$, $K < 1/2$, rendering the cosine perturbation relevant and the system flows to a strong coupling regime with a dynamically generated mass gap. The Bose field Φ is locked in one of the following infinitely degenerate classical vacua:

$$\Phi_l = \frac{1}{2}\sqrt{\frac{\pi}{K}}\left(l + \frac{1}{2}\right), \quad l \in \mathbb{Z}. \tag{1.94}$$

To determine the physical properties of the model we need order parameter fields. In the fermion model, the only physical observable is the local fermion density:

$$\begin{aligned}\rho(x) &= J_{\mathrm{R}}(x) + J_{\mathrm{L}}(x) + (-1)^j N^x(x) = \\ &= \sqrt{\frac{K}{\pi}}\partial_x\Phi(x) + \frac{(-1)^j}{\pi\alpha} :\sin\sqrt{4\pi K}\Phi(x):.\end{aligned} \tag{1.95}$$

Its staggered part serves as an order parameter, which vanishes in the critical phase and acquires a nonzero expectation value in the strong coupling regime:

$$(-1)^j n_j \sim \left\langle \sin\sqrt{4\pi K}\Phi \right\rangle = \begin{cases} 0, & V < 2t, \\ C(K)|g|^{\frac{1}{2}\frac{K}{1-2K}}, & V > 2t, \end{cases} \tag{1.96}$$

where $C(K)$ is some known numerical function (see appendix D). It follows that the system develops quasi-long-range charge density wave (CDW) order in the strong coupling regime. CDW spontaneously breaks link parity P_L – reflection with respect to the center of a link of two neighboring sites.

The transition point $K = 1/2$ possesses the hidden microscopic SU(2) symmetry. Namely, the fermion model (1.79) at $V = 2t$ is equivalent to the SU(2) symmetric Heisenberg spin chain:

$$\mathcal{H}_{\text{XXX}} = J\sum_{j=1}^{N} \mathbf{S}_j \cdot \mathbf{S}_{j+1}. \tag{1.97}$$

However, in the Abelian bosonization scheme, the symmetry is lost! This is an obvious result as various spin components in the JW transformation (A.7) are not treated similarly. In the next section, we develop an alternate approach, which explicitly incorporates the underlying symmetry of the model.

1.5 Non-Abelian Bosonization of XXZ chain

Due to obvious reasons, it is preferable to keep the underlying symmetry manifest, which is achieved using non-Abelian bosonization [4, 5]. In this case, one starts with **symmetry-preserving fermionization** (instead of JW transformation) of the spin operators:

$$\mathbf{S}_j \equiv \frac{1}{2} c^{\dagger}_{j,\alpha} \hat{\boldsymbol{\sigma}}_{\alpha\beta} c_{j,\beta}, \tag{1.98}$$

in the SU(2) symmetric Hamiltonian (1.97). Here $c^{\dagger}_{j,\alpha}$ creates electron with spin $\alpha(=\uparrow\downarrow)$ at cite j and $\hat{\boldsymbol{\sigma}} = \left(\hat{\sigma}^1, \hat{\sigma}^2, \hat{\sigma}^3\right)$ is the vector of Pauli matrices. For this representation to work one has to eliminate (excess) states of empty and doubly occupied sites by imposing the condition $\sum\limits_{\sigma=\uparrow,\downarrow} n_{j,\sigma} = 1$ at every lattice site, where $n_{j,\sigma}$ is spin-σ electron density. If this condition is fulfilled, one is left with spin dynamics only. Such a scenario can be realized in a repulsive Hubbard model of 1D electrons (Appendix B). Following this route one proves the low energy limit of the isotropic Heisenberg model to be represented by the critical SU(2)$_1$ Wess-Zumino-Novikov-Witten (WZNW) model with central charge $c = 1$ perturbed by marginally irrelevant current-current perturbation [6]:

$$\mathcal{H}_{\mathrm{XXX}} = \int \mathrm{d}x \left[\frac{2\pi v_s}{3} \left(:\mathbf{J}^2_{\mathrm{R}}: + :\mathbf{J}^2_{\mathrm{L}}: \right) - g_0 \mathbf{J}_{\mathrm{R}} \cdot \mathbf{J}_{\mathrm{L}} \right], \tag{1.99}$$

where $\mathbf{J}_{\mathrm{R,L}}$ are SU(2)$_1$ spin currents satisfying the non-Abelian Kac-Moody algebra:

$$\left[J^a_{\mathrm{R,L}}(x), J^b_{\mathrm{R,L}}(y) \right] = \mathrm{i}\epsilon^{abc} J^c_{\mathrm{R,L}}(x)\delta(x-y) \mp \frac{\mathrm{i}}{4\pi}\delta^{ab}\partial_x \delta(x-y) \tag{1.100}$$

and $v_s \sim g_0 \sim J a_0$.

Using the Abelian bosonization of non-Abelian currents:

$$\begin{aligned} J^{\pm}_{\mathrm{R}} &= \frac{1}{2\pi\alpha} e^{\mp\mathrm{i}\sqrt{2\pi}(\Phi_s - \Theta_s)}, \quad J^{\pm}_{\mathrm{L}} = \frac{1}{2\pi\alpha} e^{\pm\mathrm{i}\sqrt{2\pi}(\Phi_s + \Theta_s)}, \\ J^{z}_{\mathrm{R}} &= \frac{1}{2\sqrt{2\pi}} \partial_x(\Phi_s - \Theta_s), \quad J^{z}_{\mathrm{L}} = \frac{1}{2\sqrt{2\pi}} \partial_x(\Phi_s + \Theta_s), \end{aligned} \tag{1.101}$$

where $J^{\pm}_{\mathrm{R,L}} = J^{x}_{\mathrm{R,L}} \pm \mathrm{i} J^{y}_{\mathrm{R,L}}$, we derive

$$\begin{aligned} \mathcal{H}_{\mathrm{XXX}} \to\ & \frac{v_s}{2} \int \mathrm{d}x \left[(\partial_x \Phi_s)^2 + (\partial_x \Theta_s)^2 \right] - \\ & - \frac{g_0}{8\pi} \int \mathrm{d}x \left[(\partial_x \Phi_s)^2 - (\partial_x \Theta_s)^2 - \frac{2}{\pi\alpha^2} \cos\sqrt{8\pi}\Phi_s \right]. \end{aligned} \tag{1.102}$$

The SU(2) symmetry of the bosonized Hamiltonian is hidden in the robust structure of the perturbation term being determined by the single coupling constant:

$$\mathbf{J}_{\mathrm{R}}(x) \cdot \mathbf{J}_{\mathrm{L}}(x) = \frac{1}{8\pi} \left[(\partial_x \Phi_s)^2 - (\partial_x \Theta_s)^2 - \frac{2}{\pi\alpha^2} \cos\sqrt{8\pi}\Phi_s \right]. \tag{1.103}$$

Then one can use the following continuum form of the spin operator:

$$\begin{aligned} \mathbf{S}_j &\to a_0 \mathbf{S}(x), \\ \mathbf{S}(x) &= \mathbf{J}_{\mathrm{R}}(x) + \mathbf{J}_{\mathrm{L}}(x) + (-1)^j \mathbf{n}(x), \end{aligned} \tag{1.104}$$

where $\mathbf{n}(x)$ is staggered magnetization, to take into account symmetry-breaking perturbations to the XXX model. It must be noted that (1.104) can not be directly substituted into (1.97) to obtain WZNW Hamiltonian, as it produces the wrong sign for the marginal current-current perturbation in Eq. (1.99).

The strongly fluctuating fields of the Heisenberg chain are the dimerization field and the staggered magnetization,

$$(-1)^j \mathbf{S}_j \cdot \mathbf{S}_{j+1} \sim \epsilon(x), \quad (-1)^j \mathbf{S}_j \to \mathbf{n}(x), \tag{1.105}$$

respectively, which constitute the scalar and vector parts of the 2×2 matrix bosonic field, $\hat{g}(x) \sim \epsilon(x) + i\mathbf{n}(x)\cdot\hat{\boldsymbol{\sigma}}$, $\epsilon^2 + \mathbf{n}^2 = \text{const}$, taking values in the SU(2) group and having scaling dimension 1/2. Under Abelian bosonization,

$$\begin{aligned} \epsilon(x) &= \frac{\lambda}{\pi\alpha} \cos\sqrt{2\pi}\Phi_s, \\ \mathbf{n}(x) &= \frac{\lambda}{\pi\alpha}\left(\cos\sqrt{2\pi}\Theta_s, \sin\sqrt{2\pi}\Theta_s, -\sin\sqrt{2\pi}\Phi_s\right) \end{aligned} \tag{1.106}$$

(λ is some nonuniversal numerical constant).

Adding exchange anisotropy $J\rho\sum_j S_j^z S_{j+1}^z$, $\rho = \Delta - 1$, and using 1.104, one obtains:

$$\begin{aligned} \mathcal{H}_{\mathrm{XXZ}} = {} & \frac{\tilde{v}_s}{2}\int \mathrm{d}x \left[(\partial_x\Phi)^2 + (\partial_x\Theta)^2\right] - \\ & - \frac{g_\parallel}{8\pi}\int \mathrm{d}x\left[(\partial_x\Phi)^2 - (\partial_x\Theta)^2\right] + \frac{g_\perp}{(2\pi\alpha)^2}\int \mathrm{d}x \cos\sqrt{8\pi}\Phi, \end{aligned} \tag{1.107}$$

where $\tilde{v}_s \approx v_s(1 + C\alpha\rho)$ is renormalized velocity and

$$g_\parallel = g - C_1\alpha\rho, \quad g_\perp = g + C_2\alpha\rho \tag{1.108}$$

(here $C, C_1, C_2 > 0$ are nonuniversal numerical constants). The criticality near the SU(2) symmetric point fell in the Berezinskii-Kosterlitz-Thoules (BKT) universality class and its scaling properties are summarized by the RG diagram depicted in Fig. 1.4. In the isotropic limit, $\rho \to 0$, only a weak coupling regime is allowed corresponding to the flow along the weak coupling separatrix (black line in the first quadrant). At $\rho > 0$ the initial point of the RG flow is shifted towards a strong coupling line in the crossover sector (upper red line in the Figure) and the system enters a gapped Neel phase with a doubly degenerate ground state [7], while at $\rho < 0$ it shifts towards the weak-coupling anisotropic sector where the model is equivalent to a TLL phase with ρ-dependent critical exponents [8].

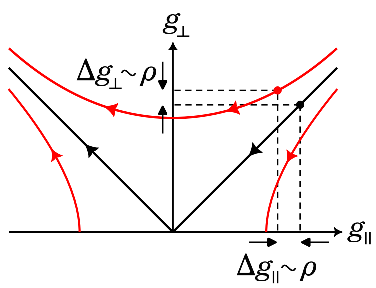

Figure 1.4: (Color online). BKT RG flow for $g_\perp$ and $g_\parallel$ coupling constants.

1.5.1 Dimerized Heisenberg chain

One may consider many different generalizations of (A.1) XXZ model, however, in the present discussion we are most interested in one including dimerization:

$$\mathscr{H}_{\rm Dim} = J\sum_j \left[1+(-1)^j\delta\right]\left[\mathbf{S}_j\cdot\mathbf{S}_{j+1}+\rho S^z_j S^z_{j+1}\right], \quad \rho\equiv\Delta-1. \tag{1.109}$$

In the regime $|\delta|,|\rho| \ll 1$, the model in Eq. (1.109) occurs in the vicinity of the isotropic Heisenberg point, $\delta=\rho=0$, where it is critical with the central charge $c=1$. A finite ρ-term introduces exchange anisotropy. At $\delta=0$ and $\rho>0$ the system is in Neel state, which is site-parity (P_S) symmetric but breaks spontaneously link parity (P_L). At $\rho=0$, $\delta\neq 0$ the chain maintains spin-rotational symmetry but is explicitly dimerized. Its spectrum is massive. The δ-perturbation breaks P_S but preserves P_L (see Fig. 1.5). So, there are two, mutually incompatible by symmetry, "massive" directions at the SU(2) critical point parametrized by the couplings δ and ρ. Their competition leads to splitting the SU(2)$_1$ WZNW criticality into two Ising criticalities as will be shown in the next chapter.

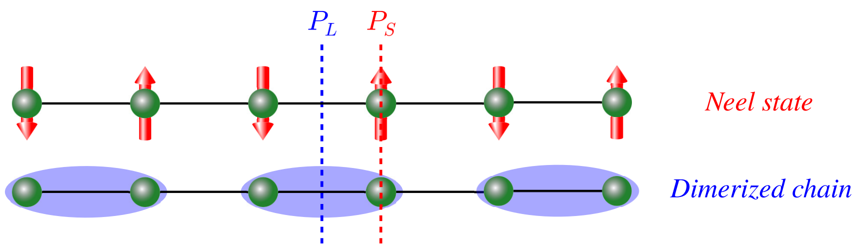

Figure 1.5: Competing orders of staggered XXZ chain.

The scaling limit of the weakly dimerized anisotropic Heisenberg chain is effectively described by the following DSG Hamiltonian:

$$\mathscr{H}_{\rm DSG} = \frac{u_s}{2}\left[(\partial_x\Phi)^2+(\partial_x\Theta)^2\right]+\frac{m}{\pi\alpha}\cos\sqrt{2\pi K_s}\Phi+\frac{g_\perp}{(2\pi\alpha)^2}\cos\sqrt{8\pi K_s}\Phi, \tag{1.110}$$

where $m\sim\delta$, u_s is yet another renormalized velocity and K_s is LL parameter.

Since the model Eq. (1.109) is not integrable, the exact dependence of K_s on the parameters of the model Eq. (1.110) is unknown. However, as a consequence of symmetry, at the SU(2) point $K_s=1$ ($K=1/2$). Moreover, the case $K_s>1$ corresponds to the massless phase of the XXZ chain ($\rho<1$), whereas at $K_s<1$ the Neel phase ($\rho>1$) sets in. Fig. 1.4 depicts the BKT phase diagram of the model in Eq. (1.110) at $m=0$.

Chapter 2

Double-frequency sine-Gordon model

2.1 Quasi-classical analysis

The problem of a CFT perturbed by a single relevant operator is well understood. An example is the SG model, as discussed in Appendix D. In the SG model, a Gaussian CFT with central charge $c = 1$ is perturbed by a single vertex operator.

An interesting scenario arises when the perturbing potential includes two mutually exclusive relevant operators similar to the case of the dimerized Heisenberg model of Sec. 1.5.1. In such cases, the field configurations that minimize one of the operators are incompatible (by symmetry) with those that minimize the other, therefore, the interplay between the two can lead to phase transitions between the two massive quantum field theories by crossing a massless critical point [9, 10].

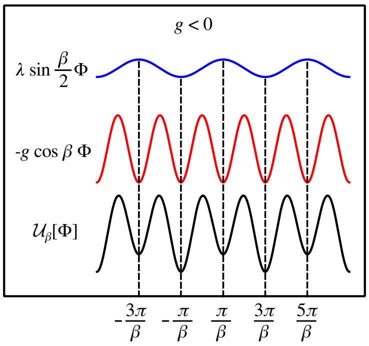

Figure 2.1: Soliton confinement regime.

Below we will consider the DSG model described by the following Hamiltonian density:

$$\begin{aligned}\mathscr{H}_{\mathrm{DSG}}[\Phi] &= \frac{u_s}{2}\left[(\partial_x\Phi)^2 + (\partial_x\Theta)^2\right] + \mathcal{U}_\beta[\Phi],\\ \mathcal{U}_\beta[\Phi] &= \lambda\sin\frac{\beta}{2}\Phi(x) - g\cos\beta\Phi(x),\end{aligned} \tag{2.1}$$

which will play a central role in this thesis. The Hamiltonian (1.110) can be brought to this form by a constant shift in the field $\Phi \to \Phi + \sqrt{\pi/8K_s}$.

We assume $\sqrt{2\pi} \le \beta \le \sqrt{8\pi}$ so that both perturbations are relevant and closed under operator product expansion (OPE). For $g < 0$, arbitrary small λ shifts the degeneracy between neighboring minima of g-term as shown in Fig. 2.1 and leads to soliton confinement [11]. In what follows, we consider $g > 0$, while the sign of λ can be arbitrary due to $\Phi \to -\Phi$ symmetry. In this regime, the existence of the Ising phase transition can be seen by simple quasi-classical analysis of the shape of $U_\beta[\Phi]$ potential. For $0 < g < 0.25\lambda$ each

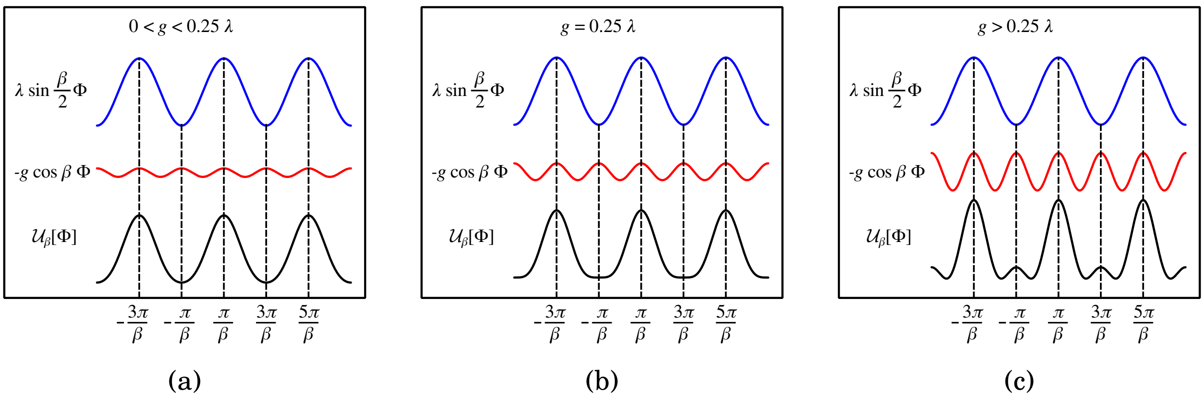

Figure 2.2: (Color online.) Ising transition in the DSG model.

minima of $U_\beta[\Phi]$ is locally equivalent to a quadratic potential well 2.2a, at the (classical) transition point $g = 0.25\lambda$, it deforms into Φ^4 one 2.2b, and for $g > 0.25\lambda$ obtains the structure of double potential well 2.2c. Therefore, in a Ginsburg-Landau sense, the Ising transition occurs with central charge $c = 1/2$ along the (classical) critical line $\lambda_c(g) = 4g$. Taking quantum fluctuations into account leads to power low dependence [9]

$$\lambda_c(g) = g^\nu, \quad \nu = \frac{(32\pi - \beta^2)}{(16\pi - \beta^2}). \tag{2.2}$$

In the following section, we introduce the AT model, a system of particular interest to us. The quantum version of this model – understood in the context of the transfer matrix formalism – known as the quantum Ashkin-Teller (QAT) model, is equivalent to the staggered XXZ model. Consequently, the phase diagram of the QAT model also includes a point with hidden SU(2) symmetry. The behavior of the system in the vicinity of this point is thus described by the DSG Hamiltonian 1.110. The relation between the AT model, considered in the scaling limit, and the DSG model of a scalar field has been anticipated in earlier studies [9, 10, 12, 13, 14].

2.2 Ashkin-Teller model

The classical AT model describes two identical two-dimensional (2D) Ising models coupled by a four-spin interaction. It is defined by the Euclidean action (the energy in units of temperature)

$$S = -\sum_{\langle \mathbf{r},\mathbf{r}'\rangle} \left[K_2\left(\sigma_{1,\mathbf{r}}\sigma_{1,\mathbf{r}'} + \sigma_{2,\mathbf{r}}\sigma_{2,\mathbf{r}'}\right) + K_4 \sigma_{1,\mathbf{r}}\sigma_{1,\mathbf{r}'}\sigma_{2,\mathbf{r}}\sigma_{2,\mathbf{r}'} \right]. \tag{2.3}$$

Here $\sigma_{j,\mathbf{r}} = \pm 1$ are classical Ising spins residing on lattice sites $\mathbf{r}$ of two planes labeled by $j = 1,2$, and K_2, K_4 are positive dimensionless constants. The phase diagram of the AT model (Fig. 2.3) is known to have a self-dual line, $\sinh 2K_2 = e^{-2K_4}$, which is a line of continuously varying critical points [16, 13, 12, 17]. On this line, the AT model is equivalent to the 6-vertex model of 2D statistical physics [18]. At the intersection of the 4-state Potts line $K_2 = K_4$ with the self-dual line the latter bifurcates into two Ising criticalities [13].

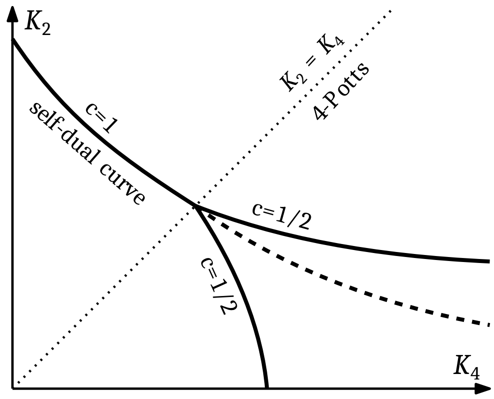

Figure 2.3: The phase diagram of the AT model. Figure extracted from[15].

As is well known [19], by virtue of transfer matrix formalism, 2D classical statistics can be viewed as an imaginary-time (i.e., Euclidean) version of quantum mechanics in 1+1 dimensions. The 1D quantum many-body Hamiltonian corresponding to the 2D AT model was derived in [20]. Passing to a strongly anisotropic 2D lattice with interatomic distances x and τ and four coupling constants, $K_2^{x,\tau}$, $K_4^{x,\tau}$, such that $K_{2,4}^{\tau} \gg K_x^{2,4}$, and then going to the so-called τ-continuum limit [19], one defines the transfer matrix as $T = e^{-\tau H} \approx 1 - \tau H + O(\tau^2)$. With the parametrization

$$4K_2^x = J_+\tau, \quad 4e^{-2K_2^\tau} = J_-\tau, \quad \frac{K_4^x}{K_2^x} = e^{-2(K_2^\tau - K_4^\tau)} = \gamma,$$

the resulting Hamiltonian takes the form of two coupled quantum Ising (QI) chains:

$$\begin{aligned} H = -\frac{1}{4}\sum_{j=1}^{N} \Big[&\left(J_+\hat\sigma^3_{1,j}\hat\sigma^3_{1,j+1} + J_-\hat\sigma^1_{1,j}\right) + \left(J_+\hat\sigma^3_{2,j}\hat\sigma^3_{2,j+1} + J_-\hat\sigma^1_{2,j}\right) + \\ &+ \gamma\left(J_+\hat\sigma^3_{1,j}\hat\sigma^3_{1,j+1}\hat\sigma^3_{2,j}\hat\sigma^3_{2,j+1} + J_-\hat\sigma^1_{1,j}\hat\sigma^1_{2,j}\right)\Big]. \end{aligned} \tag{2.4}$$

The Hamiltonian Eq. (2.4) represents a quantum lattice version of the AT model [20]. At $\gamma = 1$ it possesses a hidden SU(2) symmetry. Indeed, using the nonlocal unitary transformation designed in [20], one shows that (see e.g. Ref. [21], for details)

$$-4\mathbf{S}_{2j}\cdot\mathbf{S}_{2j+1} = \hat\sigma^3_{1,j}\hat\sigma^3_{1,j+1} + \hat\sigma^3_{2,j}\hat\sigma^3_{2,j+1} + \hat\sigma^3_{1,j}\hat\sigma^3_{1,j+1}\hat\sigma^3_{2,j}\hat\sigma^3_{2,j+1}, \tag{2.5}$$

$$-4\mathbf{S}_{2j-1}\cdot\mathbf{S}_{2j} = \hat\sigma^1_{1,j} + \hat\sigma^1_{2,j} + \hat\sigma^1_{1,j}\hat\sigma^1_{2j}, \tag{2.6}$$

where $\mathbf{S}_{2j}$ and $\mathbf{S}_{2j+1}$ are spin-1/2 operators defined on even and odd sublattices of a new lattice with $2N$ sites. Introducing the notations $J_{\pm} = J(1 \pm \delta)$, $\gamma = 1 + \rho$ one maps the model Eq. (2.4) onto a staggered XXZ spin-1/2 chain [20] of Eq. (1.109).

Let us stress again that the relationship between the Ising operators of the QAT model in Eq. (2.4) and the spin operators of the XXZ chain in Eq. (1.109) is highly nonlocal and nonlinear.

Although the model Eq. (1.110) was derived in the vicinity of the XXX point, it maintains its applicability to a broader region of the parameter space where $K_s < 1$. In particular, there exists a 'decoupling' point $K_s = 1/2$ where the DSG model can be mapped onto two non-critical (disordered) Ising models coupled by an interaction $\sim \sigma_1\sigma_2$ [9, 10]. However, in that region, the two mutually dual Ising critical lines are well separated and their merging point is not accessible. On the contrary, the present discussion, relying on the equivalence with the staggered XXZ spin chain, treats the DSG model as a weakly perturbed $\mathrm{SU}(2)_1$ WZNW model at exactly the bifurcation point; Fig 4.2. Therefore, the appearance of the SU(2) symmetric point is no surprise.

Before ending the section, we would like to add a further comment on the nature of the bifurcation point. In literature, the bifurcation point in the classical 2D AT model is identified as the termination point of the self-dual Gaussian line – a point where it intersects with a 4-state Potts line; Fig. 2.3. Conventionally, the AT model is formulated in terms of Ising variables. As we have discussed, a representation of the 1D QAT model exists in terms of a staggered XXZ spin chain, which is highly nonlocal with respect to the original Ising-spin representation. It is this new spin-chain representation that reveals the hidden SU(2)-symmetry of the bifurcation point. Consider, for example, two identical decoupled quantum Ising models close to the critical point, with an apparent discrete $\mathbb{Z}_2 \otimes \mathbb{Z}_2$ symmetry. Each chain is equivalent to a theory of massive Majorana fermion. But, for two identical Ising models, the emerging Majorana model has a continuous O(2)-symmetry, generated by planar rotations of the Majorana vector $\xi = (\xi_1, \xi_2)$. To reconcile the two pictures, one refers to the fact that the three equivalent representations of the quantum Ising model, two in terms of Ising order and disorder operators and one more in terms of a Majorana fermion, are all mutually nonlocal. This is why the symmetries found in different representations need not coincide.

Chapter 3

Experimental background

3.1 Overview

The effects caused by an external magnetic field that quantizes the spectrum of charged carriers in crystalline lattices has long been one of the fundamental problems in condensed matter physics [22, 23, 24, 25, 26, 27, 28, 29]. The interplay of the applied magnetic field, dynamical correlations between the particles, and superimposed geometrical lattice frustration has become the subject of intense research in recent years. The main objects of these studies are Fermi and Bose gases on ladders, which are minimal quasi-1D structures that can accommodate finite magnetic fluxes through elementary plaquettes. The kinetic frustration caused by the magnetic field, as well as the geometrical frustration present in structures like triangular and Creutz ladders, dramatically change the properties of a system when the flux per particle is close to one (more generally, rational fraction of) flux quantum [30, 31]. In naturally existing quasi-1D electron systems fields so strong could hardly be achieved. Moreover, in such objects, the possibility of focusing on purely orbital effects of the magnetic flux would be obscured by the Zeeman splitting of the electron spin states. Fortunately, ultracold atoms represent an excellent opportunity to circumvent these limitations. It has been demonstrated [32] that, in systems of neutral atoms on optical lattices, Raman-assisted tunneling in 2D optical lattices generates synthetic gauge fields and thus makes large effective fluxes feasible. Moreover, lattice connectivity in optical multi-leg flux ladders can be ensured by extra synthetic dimensions which can be engineered taking advantage of the internal atomic degrees of freedom [33, 34].

The properties of bosonic and fermionic flux ladders have been the subject of many theoretical and experimental studies [35, 36, 37, 38, 39, 40, 41, 42, 43, 44, 45, 46, 47, 48, 49, 50]. Ground state phases and their topological properties, chiral boundary currents, and topological Lifshitz transitions taking place in ladders on varying flux have been investigated. Lifshitz transitions connect phases with different numbers of Fermi points in the band spectrum and reveal themselves through the singularities in the flux dependence of the persistent orbital current and its derivative – the charge stiffness. The existence of cusps in this dependence for a half-filled standard (square) ladder was indicated in Refs. [39, 40] and more recently in Refs. [41, 45]. Away from half-filling, the behavior of the orbital current as a function of the flux essentially depends on which quantity, the particle density $\rho = N_f/N$ (canonical ensemble) or the chemical potential μ (grand canonical ensemble), is chosen to be a fixed parameter [45]. In standard experiments with ultracold atoms, the density is fixed. However, interesting proposals to control the chemical potential in such systems have recently been reported. These include the splitting of 2D ultracold atom systems into a physical sample of a homogeneous density and a dilute reservoir using advances in quantum gas microscopy [51], realization of two-terminal configurations based on holographic techniques for the study of Landauer transport [52], and the effective control of chemical potentials using Rabi coupling between different hyperfine levels of the atomic species [53].

Experimental setups involving ultra-cold atoms, trapped in optical tweezer arrays and laser-coupled to highly excited Rydberg states, have demonstrated, in recent years, the remarkable potential for simulating strongly-correlated quantum phases of many-body systems under controllable experimental conditions [54, 55, 56, 57, 58, 59, 60]. Rydberg atom platforms, where large and long-lived van der Waals type interactions between Rydberg states can extend over relatively long distances (tunable even up to a few microns), provide unique opportunities to probe the many-body system at single-site levels with high experimental precision and control [61] – a feat that is unattainable in conventional cold atoms in optical lattices governed by Hubbard-like physics (see e.g., [62]).

In a typical experimental scenario of optical tweezer arrays, Rydberg states are populated with the dynamics between the Rydberg states being much faster compared to the respective atomic motion. Such a setup of Rydberg arrays is often described by interacting spin-1/2 models [63, 64] paving the way to study frustrated magnetism in a controllable laboratory setting [65, 66, 67, 68], and offers various fascinating phenomena both in 1D and 2D settings (see e.g., [54, 69, 60, 70, 67, 66, 71, 68, 72, 73]).

In an alternative experimental scenario, the ground states of trapped ultra-cold atoms in optical lattices are weakly coupled to virtually populated Rydberg states – the so-called 'Rydberg dressing' – resulting in generalized Hubbard-like systems with tunable long-range interactions [74, 75, 76, 77]. The dynamics of such Rydberg-dressed systems lie in the intermediate regime between the conventional Hubbard models describing ultra-cold atoms on optical lattices and the frozen Rydberg gases trapped in optical tweezers. In 1D with a single bosonic field, Rydberg dressed systems show exotic critical behavior like cluster Luttinger liquids [78] and emergent supersymmetric critical transition [79]. In 2D settings, these systems are associated with anomalous dynamics and glassy behavior [80, 81]. Along with these theoretical endeavors, the many-body dynamics of Hubbard models with long-range Rydberg-dressed interactions in 2D have been realized in a recent experiment [82].

While the aforementioned cases are mostly focused on either 1D or 2D geometries, in this thesis, we consider the intermediate regime between these two – a ladder geometry that can accommodate interactions and magnetic terms possible in 2D geometries, while simultaneously being tractable by analytical and numerical methods that are suitable for 1D systems. In recent years, ladder systems with Rydberg dynamics have been subjected to various theoretical works, that include coupled cluster Luttinger liquids and coupled supersymmetric critical transitions [83, 84, 85], Ising criticality by order-by-disorder mechanism [86], chiral 3-state Potts criticality [87] – among many others.

Here we consider the scenario of an optical lattice system on a two-leg triangular ladder geometry where ultra-cold spinless fermions are trapped and subjected to a synthetic magnetic flux by means of Raman-assisted tunneling [32, 33, 34, 88]. Moreover, the fermions can be coupled to Rydberg states (i.e., the Rydberg dressing) by off-resonant laser driving that can trigger controllable interactions between the fermions. The system exhibits a U(1) symmetry corresponding to the conservation of total fermion number, and a discrete $\mathbb{Z}_2$ symmetry coming from the joint operation of parity transformation and chain inversion. This minimal setting beyond 1D allows for the exploration of the interplay between the magnetic flux, interactions, and the geometrical frustrations, and the associated emerging phenomena, that can be investigated using well-established analytical and numerical techniques.

3.2 Synthetic magnetic flux in optical lattices

In a typical experimental scenario of a system of neutral atoms on optical lattices, nonzero uniform magnetic flux can be realized via Raman-assisted tunneling of the atoms. Initially, one prepares a 2D optical lattice by standing wave laser fields. It is assumed that the lattice traps atoms with only two internal hyperfine states $|g\rangle$ and $|e\rangle$ such that adjusting the polarization of the lasers which confine the particles in the x-direction makes it possible to place the potential wells trapping atoms in the different internal states in an alternate order in x-direction as in Fig. 3.1a.

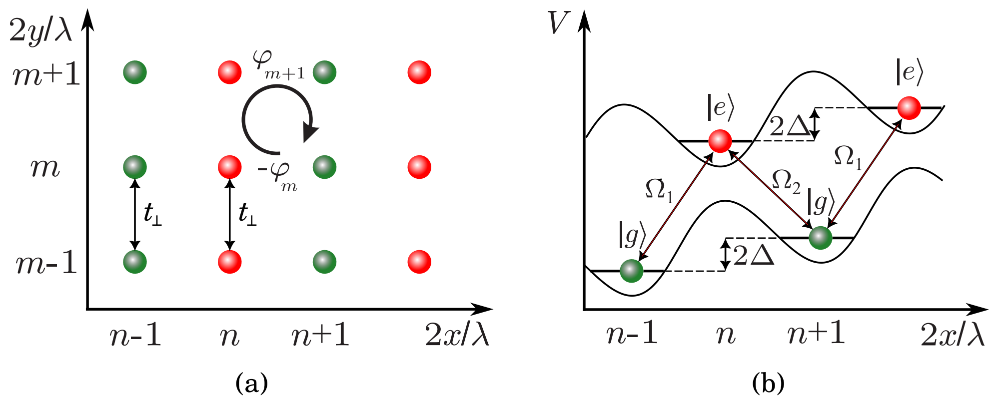

Figure 3.1: (Color online.) The experimental setup consists of atoms trapped in an optical lattice, as illustrated in the figure. In this system, green spheres represent atoms in the ground state $|g\rangle$, while red spheres denote atoms in the excited state $|e\rangle$. (a) Optical Lattice: Atoms are arranged in a 2D optical lattice. Hopping along the y-direction is purely due to kinetic energy and is unaffected by the applied lasers. This process is described by the hopping matrix element $t_\perp$, which remains identical for atoms in both the $|e\rangle$ and $|g\rangle$ states. In contrast, hopping along the x-direction is influenced by additional lasers, creating a distinct hopping pattern. (b) Trapping Potential in the x-Direction: In the x-direction, adjacent lattice sites are offset by an energy Δ due to a static inhomogeneous electric field. This creates an energy imbalance between neighboring sites. Two lasers, Ω_1 and Ω_2, are used to induce transitions between the atomic states. Laser Ω_1 is resonant for transitions between $|g\rangle \leftrightarrow |e\rangle$, while Ω_2 drives transitions between $|e\rangle \leftrightarrow |g\rangle$, due to the offset between lattice sites. Because the spatial phase of the lasers Ω_1 and Ω_2 varies, atoms hopping around one plaquette accumulate phase shifts of $2\pi\alpha = -\phi_m + 0 + \phi_{m+1} + 0$, where the phase is given by $\phi_m = \frac{q\lambda}{4\pi}m$. Figure extracted from [88]

Also, it is assumed that the tunneling (due to kinetic energy) in x-direction is suppressed by energy offset Δ as shown in Fig. 3.1b. One way to accomplish this is by introducing a static electric field $E(x) = \delta E x$ in the x-direction. If both internal states $|g\rangle$ and $|e\rangle$ have the same static polarizability μ, this yields $\Delta \sim \mu\delta E\lambda$. At the same time, the tunneling amplitude $t_\perp$ due to kinetic energy in y-direction being the same for particles in both states, is unaffected.

Then the additional two lasers are superimposed to induce Raman transitions between $|g\rangle$ and $|e\rangle$ states, and therefore mimic tunneling in x-direction. Each of the lasers is a running plane wave chosen to give rise to space-dependent Rabi frequencies of the form

$$\Omega_{1,2} = \Omega e^{\pm \mathrm{i} q y}, \tag{3.1}$$

where $\Omega > 0$ is the magnitude of the Rabi frequencies with $\pm\Delta$ detunings, respectively (see Fig. 3.1b). Then it can be shown that under specific conditions (see [88] for details) the system can be described by the following second quantized Hamiltonian:

$$\mathscr{H} = -t_{\parallel} \sum_{n,m} e^{\mathrm{i}2\pi\alpha m} a^{\dagger}_{n,m} a_{n+1,m} - t_{\perp} \sum_{n,m} a^{\dagger}_{n,m} a_{n,m+1}, \tag{3.2}$$

where $\alpha = \frac{q\lambda}{4\pi}$. This is equivalent to a Hamiltonian for electrons with charge e moving on a lattice in an external magnetic field $B = \frac{2\pi\alpha}{Ae}$.

Chapter 4

The System

4.1 The TFL in the context of optical lattices

We consider a paradigmatic spinless fermionic system on a two-leg triangular ladder in the presence of external magnetic flux as shown in Fig. 4.1. Its Hamiltonian is given by

$$H = H_0 + H_{\text{int}}, \tag{4.1}$$

$$H_0 = -t_0 \sum_{j,\sigma=\pm} \Big(e^{-i\pi\sigma f} c^\dagger_{j,\sigma} c_{j+1,\sigma} + \text{h.c.} \Big) - \sum_j \Big(t_1 c^\dagger_{j,+} c_{j,-} + t_2 c^\dagger_{j,+} c_{j-1,-} + \text{h.c.} \Big), \tag{4.2}$$

$$H_{\text{int}} = V \sum_j \hat{n}_{j,+} \big(\hat{n}_{j,-} + \hat{n}_{j-1,-} \big). \tag{4.3}$$

Here $c_{j,\sigma}$ and $c^\dagger_{j,\sigma}$ are annihilation and creation operators for a spinless fermion on the chain $\sigma = \pm$ with j labeling diatomic unit cells, $\hat{n}_{j,\sigma} = c^\dagger_{j,\sigma} c_{j,\sigma}$ are occupation number operators, t_0 and $t_{1,2}$ are the intra- and interchain tunneling amplitudes, and $f = \Phi_\square/\phi_0$ is the magnetic flux per rectangular plaquette measured in units of the flux quantum $\phi_0 = \frac{hc}{e}$. H_{int} stands for the nearest-neighbor density-density interaction of amplitude V between fermions residing on top and bottom chains. We work at the regime of half-filling.

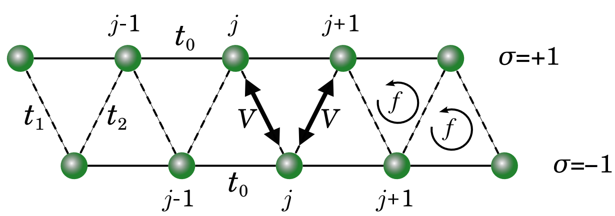

Figure 4.1: (Color online.) Spinless fermions on a two-leg triangular ladder. The integer j labels the diatomic unit cells. t_0, t_1, and t_2 stand for the amplitudes of single-particle nearest-neighbor hopping along the chains and between them. We consider $f = 1/2$ flux per triangular plaquettes (in units of π) and interchain nearest-neighbor interaction of strength V.

The dynamics we are interested in is relevant to cold atom gases in optical lattices, in the presence of off-resonant laser drive to Rydberg states (the Rydberg dressing) [74, 75, 76, 77]. In particular, laser-dressing to p-states generated a strong anisotropic interaction: the latter can be made very strong vertically, and very weak horizontally, realizing the interaction pattern described by H_{int} [65, 79]. Such couplings have been recently realized experimentally in Ref. [82], while distance selection (which could also be utilized for our case here) has also been demonstrated in Ref. [89]. The tunneling dynamics can instead be engineered utilizing laser-assisted tunneling [88] as described in the previous section. We note that the system is also relevant for experiments with trapped ions [90].

4.2 Overview of the phase diagram

Yet the non-interacting Hamiltonian H_0 shows surprisingly rich physics. It has been shown, that in the regime of weak interchain hopping, $0 < t_{1,2} \ll t_0$, the effect of the geometric frustration is most pronounced in the limit $|t_1 - t_2| \ll t_1 + t_2$ and $f \to 1/2$. In this regime, the flux renormalizes the chemical potential leading to a whole cascade of flux-induced Lifshitz transitions between the phases with 4, 2, 1, and 0 numbers of Fermi points.

At $f = 1/2$ the low-energy excitations, as described by the dispersion relations

$$\omega(k)_\pm = \pm\sqrt{4t_0^2 \sin^2 k + t_1^2 + t_2^2 + 2t_1 t_2 \cos k}\ , \tag{4.4}$$

are represented by two branches of massive Dirac fermions, with momenta close to $k = 0$ and $k = \pi$ in the Brillouin zone, and with masses $M = t_1 + t_2$ and $m = t_1 - t_2$, respectively. We will be referring to them as *heavy* (M) and *light* (m) fermionic sectors. The degree of frustration in the non-interacting case can be quantified by the ratio $\delta = \frac{t_2}{t_1} = \frac{M-m}{M+m}$. The model is maximally frustrated in the $m \to 0$ limit. At $f = 1/2$ the ground state of a half-filled ladder with $m \neq 0$ is insulating. Under the same conditions with $m = 0$, the presence of a Dirac node at $k = \pi$ renders the spectrum of the ladder gapless. Such a system is very susceptible to correlations between the particles.

The Hamiltonian (4.1) possesses a $\mathbb{Z}_2$-symmetry which we label by $\mathscr{P}$: it is a product of parity transformation ($j \to -j$) and permutation of the chains ($\sigma \to -\sigma$). Obviously, H has a global U(1) symmetry related to the conservation of the total particle number. However, except for the limit of two decoupled chains ($t_1 = t_2 = 0,\ f = 0$), the total fermionic Hamiltonian H does not display an apparent SU(2) symmetry for any values of the parameters of the model. One of the main results of this thesis is the demonstration that, in fact, in the massless case ($m = t_1 - t_2 = 0$) at a certain value of the coupling constant V the system occurs in a critical state with central charge $c = 1$, where it is characterized by the emergent non-Abelian SU(2) symmetry.

In a symmetric flux ladder ($m = 0$) at $f = 1/2$, at some critical value V_c of the interaction constant, the system undergoes a transition from a TLL phase ($V < V_c$) to a long-range ordered phase ($V > V_c$) with a spontaneously broken discrete $\mathscr{P}$-symmetry. The ordered phase is characterized by a finite interchain charge transfer and a nonzero spontaneous current along the ladder. Starting from the broken-symmetry phase and increasing the zigzag asymmetry m or decreasing V, one observes two Ising critical lines (with central charge $c = 1/2$), signifying transitions to two band insulator phases, one of them being topological ($m < 0$) while the other non-topological ($m > 0$). We show that the two Ising critical lines merge at an AT bifurcation point $V = V_c$, $m = 0$, as shown in Fig. 4.2. We show, both analytically and numerically, that at this point the symmetry of the underlying criticality is promoted to SU(2)$_1$ WZNW universality class. The emergence of this SU(2) criticality is a remarkable property of the originally Abelian model of spinless fermions on a triangular ladder, emerging at low energies as a combined effect of frustration, flux, and correlations.

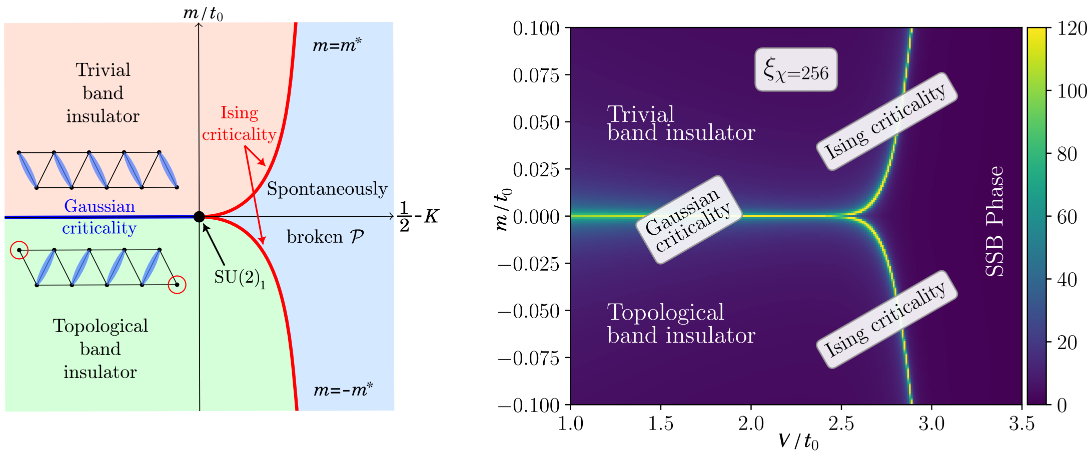

(a) (b)

Figure 4.2: (Color online.) (a) The phase diagram of the DSG model (Eq. (6.31)) that dictates the low-energy description of the lattice Hamiltonian (4.1). The blue line corresponds to U(1) Gaussian criticality, with $c = 1$. The black dot at the origin is the SU(2)$_1$ critical point, with $c = 1$. Two red lines are the Ising criticalities, with $m = \pm m^*$ critical lines and $c = 1/2$. In the band insulator phases, shaded in orange and green, the dimerization is non-zero along t_1 and t_2 links. The orange and green regions correspond to trivial and topological (see Appendix 5.5) band insulator phases, respectively. The region shaded in blue corresponds to the phase with spontaneously broken $\mathscr{P}$ symmetry-a combination of parity and chain interchange operations. This phase is characterized by the non-zero total current along the chains, which is proportional to the charge imbalance between the chains. (b) The phase diagram of the lattice Hamiltonian (4.1) obtained by iDMRG simulations. We plot the correlation length ξ_χ for the iMPS bond dimension $\chi = 256$ in the $(m, V/t_0)$-plane. Diverging values of the correlation length clearly indicate that the critical line at $m = 0$ bifurcates into two critical lines at around $V/t_0 \simeq 2.45$ akin to the DSG model. Apart from these critical lines, all the phases are gapped, and these phases are trivial and topological band insulators and two-fold degenerate spontaneous symmetry-broken (SSB) phase.

Part II

The triangular flux ladder

Chapter 5

Free fermion TFL

5.1 Spectrum and symmetry analysis

In momentum representation

$$H_0 = \sum_k \psi_k^\dagger \hat{\mathscr{H}}_k \psi_k, \quad \psi_k = \begin{pmatrix} c_{k+} \\ c_{k-} \end{pmatrix} \tag{5.1}$$

Here

$$\hat{\mathscr{H}}_k = \epsilon(k) - \mathbf{h}(k) \cdot \hat{\boldsymbol{\sigma}} \tag{5.2}$$

is a 2×2 matrix form of the first quantized Hamiltonian whose scalar and vector parts are given by

$$\begin{aligned} \epsilon(k) &= -2t_0 \cos(\pi f) \cos k, \\ \mathbf{h}(k) &= (t_1 + t_2 \cos k, t_2 \sin k, 2t_0 \sin(\pi f) \sin k). \end{aligned} \tag{5.3}$$

The quasi-momentum k, measured in units of inverse lattice spacing $\frac{1}{a_0}$, varies within the Brillouin zone, $|k| < \pi$, and the Pauli matrices $\hat{\boldsymbol{\sigma}} = (\hat{\sigma}^1, \hat{\sigma}^2, \hat{\sigma}^3)$ act in the 2D space of the Nambu spinor ψ_k. The spectrum of H_0 consists of two bands labeled by the index $s = \pm$:

$$E_s(k) = -2t_0 \cos(\pi f) \cos k + sE_k, \quad E_k = |\mathbf{h}(k)| \tag{5.4}$$

Throughout this thesis, we assume that the interchain tunneling amplitudes are positive and small, $0 < t_{1,2} \ll t_0$. Moreover, we restrict consideration to the case when the particle density $\rho = N^{-1} \sum_{j\sigma} \langle c_{j\sigma}^\dagger c_{j\sigma} \rangle$ is equal or close to 1. Accordingly, the chemical potential is small, $|\mu| \ll 2t_0$.

In the standard ladder (either $t_1 = 0$ or $t_2 = 0$), for any f the band spectrum (5.4) has the property [39, 40]:

$$E_s(k + \pi) = -E_{-s}(k) \tag{5.5}$$

This symmetry is generated by a staggered particle-hole (ph) transformation of the fermionic operators, $c_{k\sigma} \to c^{\dagger}_{k+\pi,-\sigma}$. As a result, if the particle density is fixed at $\rho = 1$, Eq. (5.5) necessarily leads to a half-filled band spectrum and vanishing chemical potential, and vice versa. The spectral properties of the standard ladder at $\rho < 1$ and $\rho > 1$ (equivalently, for the values of the chemical potential $\pm\mu$) are equivalent. In the metallic phase of a half-filled ladder, the Fermi momenta at any f form pairs $\pm(k_{\mathrm{F}}, \pi - k_{\mathrm{F}})$.

As follows from (5.4), this is not the case for a TFL ($t_1 t_2 \neq 0$), where geometrical lattice frustration makes the band splitting momentum-dependent. In Eq. (5.2) the "magnetic field" $|\mathbf{h}(k)|$ is not invariant under the transformation $k \to \pi \pm k$, and the perfect nesting property (5.5) is absent. As a consequence, for a general set of the parameters of the TFL, if the particle density is fixed at $\rho = 1$, the corresponding value of the chemical potential $\mu \neq 0$; inversely, if $\mu = 0$, then $\rho \neq 1$. The properties of the TFL at $\rho < 1$ and $\rho > 1$ are different. For a special value of the flux, $f = 1/2$, the Hamiltonian takes the Bloch form $\hat{\mathscr{H}}_k = -\mathbf{h}(k) \cdot \boldsymbol{\sigma}$ which implies the $(E, -E)$ symmetry of the band spectrum. Nevertheless, the $k \to \pi - k$ symmetry is absent at $f = 1/2$ as well.

At weak interchain tunneling the loss of the ph-symmetry and all qualitative changes in the structure of the spectrum are most pronounced in the limit $|t_1 - t_2| \ll t_1 + t_2$ and for the values of the flux f close to $1/2$. Using the parametrization

$$f = \frac{1}{2} - \frac{\kappa}{2\pi t_0}, \quad |\kappa| \ll 2t_0 \tag{5.6}$$

and replacing (5.4) by the approximate expression

$$E_{\pm}(k) \simeq -\kappa \cos k \pm \sqrt{4t_0^2 \sin^2 k + t_1^2 + t_2^2 + 2t_1 t_2 \cos k} + O(\kappa^2) \tag{5.7}$$

we find that the low-energy states of the spectrum, $|E_{\pm}(k)| \ll 2t_0$, are located close to the points $k = 0$ and $k = \pi$, where excitations are described in terms of two groups of "massive Dirac fermions":

$$|k| \ll 1: \quad E_{\pm}(k) \simeq -\kappa \pm \sqrt{k^2 v_{\mathrm{F}}^2 + M^2} \tag{5.8}$$

$$|k - \pi| \ll 1: \quad E_{\pm}(k) \simeq \kappa \pm \sqrt{(k-\pi)^2 v_{\mathrm{F}}^2 + m^2} \tag{5.9}$$

Here $M = t_1 + t_2$, $m = t_1 - t_2$ and $v_{\mathrm{F}} = 2t_0 a_0$ is the Fermi velocity (here we drop small corrections to v_{F} of the order $O(t_{1,2}^2)$). Both masses are small compared to $2t_0$.

In fact, the same type of spectrum characterizes a family of frustrated two-leg ladders encapsulated in the asymmetric Creutz model, shown in Fig. 5.1. Apart from the standard on-rung interchain tunneling ($t_{\perp}$), this model includes hopping across the diagonals of elementary plaquettes, parametrized by two independent amplitudes $\tilde{t}_1$ and $\tilde{t}_2$. The case $\tilde{t}_1 = \tilde{t}_2 = 0$, $t_{\perp} \neq 0$ corresponds to a standard (non-frustrated) ladder. At $\tilde{t}_1 = \tilde{t}_2 \neq 0$ Fig. 5.1 represents a symmetric Creutz ladder [46]. At $\tilde{t}_2 = 0$ one of the diagonals of the

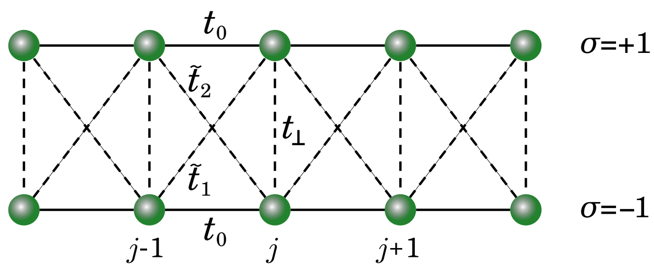

Figure 5.1: Asymmetric Creutz ladder.

plaquette is disabled and the lattice becomes topologically equivalent to a triangular ladder with alternating interchain tunneling amplitudes $t_\perp$ and $\tilde{t}_1$; in the notations of the model (4.2) the latter coincide with t_1 and t_2, respectively.

In the presence of the flux f the Hamiltonian $\hat{\mathscr{H}}_k$ of the asymmetric Creutz ladder has the form (5.2) with

$$\mathbf{h}(k) = \{t_\perp + (\tilde{t}_1 + \tilde{t}_2)\cos k, (\tilde{t}_1 - \tilde{t}_2)\sin k, 2t_0 \sin(\pi f)\sin k\}$$

The low-energy part of its spectrum is given by formulas (5.8), (5.9) with the Dirac masses $M = t_\perp + \tilde{t}_1 + \tilde{t}_2$ and $m = t_\perp - \tilde{t}_1 - \tilde{t}_2$. The asymmetry parameter $\tilde{t}_1 - \tilde{t}_2$ is the measure of geometrical frustration of the model of Fig. 5.1. The TFL is the maximally frustrated member of this family. In the rest of this thesis, we will only deal with the TFL.

Turning back to the model (5.2)–(5.3), we choose for certainty $t_1 \geq t_2 \geq 0$ and introduce a frustration parameter

$$\delta = \frac{t_2}{t_1} = \frac{M-m}{M+m}, \qquad 0 \leq \delta \leq 1 \tag{5.10}$$

In the standard ladder ($\delta = 0$), the $k \to k+\pi$ symmetry keeps the masses equal; Fig. 5.2a. Geometrical frustration ($\delta \neq 0$) makes the Dirac masses different: see Fig. 5.2b. The difference is most striking in the translationally invariant case ($m \to 0$) when the degree of frustration reaches its maximum, $\delta \to 1$; Fig. 5.2c. While at $f = 1/2$ ($\kappa = 0$), the ground state of a half-filled standard ladder is insulating, under the same conditions the presence of a Dirac node at $k = \pi$ renders the spectrum of the symmetric TFL gapless [1] (Fig. 5.2c).

The appearance of the parameter κ in the expressions (5.8), (5.9) makes the spectrum deformable: when κ is varied, the parts of the dispersion curves at $k \sim 0$ and $k \sim \pi$ "move" along the energy axis in opposite directions. This fact explains the existence of flux-induced topological Lifshitz transitions [91] between ground state phases with different numbers of Fermi points. Moreover, it also indicates that, as long as $|\mu|, M, |m| \ll 2t_0$, all these transitions take place in the vicinity of the point $f = 1/2$, i.e. at small κ. The

[1] In fact, the location of the lowest-energy states close to the zone boundary $k = \pi$ is a robust property of the model valid as long as $|t_1 - t_2| \ll |t_1 + t_2|$ irrespective of the magnitude of the ratios $t_{1,2}/t_0$. On the other hand, a local minimum of E_k at $k = 0$ only exists under the condition $t_1 t_2 < 4t_0^2$; otherwise E_k has a local maximum at $k = 0$.

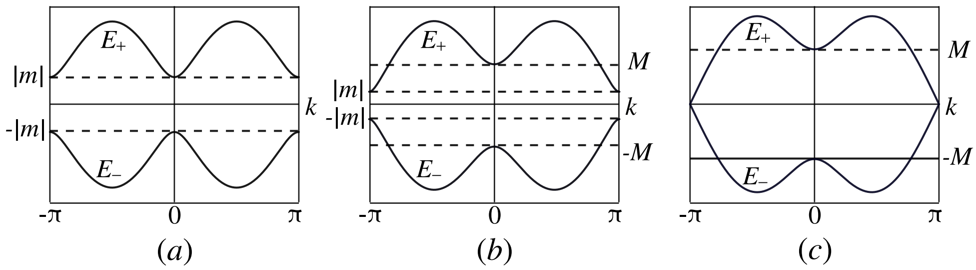

Figure 5.2: Band spectrum at $f = 1/2$ (a) in the standard ladder, (b) in the triangular ladder at $m \neq 0$, (c) in the triangular ladder at $m = 0$.

difference between the mass gaps M and $|m|$ affects the ground state phase diagram and the sequence of Lifshitz transitions in a TFL even at $\mu = 0$. The transitions show up in the experimentally observable singularities in the flux dependence of the orbital current and the anomalies of the charge stiffness of the system. A discussion on this issue in the context of square flux ladders, together with relevant references to ongoing experimental work can be found in the recent publication [45].

To complete this section, let us briefly comment on the topological properties of the insulating phases of the noninteracting TFL. For instance, at $f = 1/2$ such phases are realized at $m \neq 0$ under the condition that $-|m| < \mu < |m|$. With $M > 0$, there are two insulating phases corresponding to opposite signs of the mass m (of course, the thermodynamical properties depend only on $|m|$). The topological properties of a gapped ground state can be inferred from the 2×2 matrix structure of the Bloch Hamiltonian $\hat{\mathscr{H}}_k = -\mathbf{h}(k)\cdot\hat{\boldsymbol{\sigma}}$ in Eq. (5.2). Despite the different structure of the Nambu spinors, the first quantized Hamiltonian $\hat{\mathscr{H}}_k$ of the TFL and that of the 1D spinless p-wave superconductor (Kitaev's model) [92, 93] have the same matrix form and same symmetry properties of the "magnetic" field $\mathbf{h}(k)$ under transformation $k \to -k$. According to conventional definitions (see e.g. Ref. [94]), a matrix Hamiltonian $\hat{\mathscr{H}}_k$ possesses time reversal ($\mathcal{T}$), charge-conjugation ($\mathcal{C}$) and chiral ($\mathcal{S}$) symmetry if the following conditions

$$
\begin{aligned}
U_{\mathcal{T}} \hat{\mathscr{H}}_k^* U_{\mathcal{T}}^{-1} &= \hat{\mathscr{H}}_{-k} \\
U_{\mathcal{C}} \hat{\mathscr{H}}_k^* U_{\mathcal{C}}^{-1} &= -\hat{\mathscr{H}}_{-k} \\
U_{\mathcal{S}} \hat{\mathscr{H}}_k U_{\mathcal{S}}^{-1} &= -\hat{\mathscr{H}}_k
\end{aligned}
$$

are satisfied (here the Us are unitary matrices). Apparently, charge conjugation symmetry is present (with $U_{\mathcal{C}} = \sigma_3$), whereas time reversal and chiral symmetries are explicitly broken. These facts place the TFL into the symmetry class D [94]. In this class, maps of the Brillouin zone to the sphere traversed by a unit vector $\mathbf{h}(k)/|\mathbf{h}(k)|$ form a $\mathbb{Z}_2$ group. Following the same arguments as those in [93], one finds out that homotopically nontrivial maps take place at $m < 0$ (more generally at $Mm < 0$). Thus the insulating ground state of the TFL at $m < 0$ is topologically nontrivial, characterized by a nonzero Zak phase $\phi_{\text{Zak}} = \pi$, whereas the phase at $m > 0$ is non-topological ($\phi_{\text{Zak}} = 0$). It is clear that the insulating phase of a standard ladder with $M = m$ is topologically trivial. We will return to this subject in Sec. 5.5 where topological zero modes are identified and once again in Sec. 6.2.2 where parity and string order parameters are obtained in a weak coupling regime.

5.2 Orbital current

The gauge invariant current through a directed link $\langle n, n+1\rangle$ of the chain σ is defined as

$$J^{\sigma}_{j,j+1} = -\mathrm{i}t_0 c^{\dagger}_{j\sigma} c_{j+1,\sigma} e^{-\mathrm{i}\pi\sigma f} + \text{h.c.}, \quad (\sigma = \pm)$$

The second quantized total and relative current operators are given by

$$J_{\text{tot}} = N^{-1}\sum_{n\sigma} J^{\sigma}_{n,n+1} = N^{-1}\sum_{k}\psi^{\dagger}_{k}\hat{J}_{\text{tot}}(k)\psi_{k} \tag{5.11}$$

$$J_{\text{rel}} = N^{-1}\sum_{n\sigma}\sigma J^{\sigma}_{n,n+1} = N^{-1}\sum_{k}\psi^{\dagger}_{k}\hat{J}_{\text{rel}}(k)\psi_{k}, \tag{5.12}$$

where

$$\hat{J}_{\text{tot}}(k) = 2t_0\left[\cos(\pi f)\sin k - \hat{\sigma}^3\sin(\pi f)\cos k\right] \tag{5.13}$$

$$\hat{J}_{\text{rel}}(k) = 2t_0\left[\hat{\sigma}^3\cos(\pi f)\sin k - \sin(\pi f)\cos k\right] \tag{5.14}$$

are first quantized 2×2 matrix versions of the currents in the chain basis. The Hamiltonian (5.2) is invariant under parity transformation P ($k \to -k$) combined with the interchange of the two chains of the ladder P_{12} ($\sigma \to -\sigma$):

$$\mathscr{P} = PP_{12}, \quad \mathscr{P}\hat{\mathscr{H}}_k\mathscr{P}^{-1} = \hat{\sigma}^1\hat{\mathscr{H}}_{-k}\hat{\sigma}^1 = \hat{\mathscr{H}}_k \tag{5.15}$$

Under $\mathscr{P}$ the total current $\hat{J}_{\text{tot}}(k)$ changes its sign. Therefore, as long as this symmetry remains unbroken, which is an obvious case for the noninteracting model, the expectation value of the total current vanishes. This conclusion changes in strongly correlated phases of interacting fermions in which $\mathscr{P}$-symmetry is spontaneously broken; Sec. 6.2. On the other hand, the operator $\hat{J}_{\text{rel}}(k)$ remains invariant under $\mathscr{P}$ and, hence, except for special values of f, its expectation value is nonzero. Thus, at $f \neq 0$, the ground state of the TFL is characterized by a nonzero orbital current $\langle\hat{J}_{\text{rel}}\rangle$ flowing in opposite directions on the upper and lower chains (Fig. 5.3).

The ground state expectation value of the orbital current is given by

$$\mathcal{J}(f) \equiv \langle J_{\text{rel}}\rangle = \frac{2t_0}{N}\sum_{k\sigma}\langle c^{\dagger}_{k\sigma}c_{k\sigma}\rangle\left[\sigma\sin k\cos(\pi f) - \cos k\sin(\pi f)\right] \tag{5.16}$$

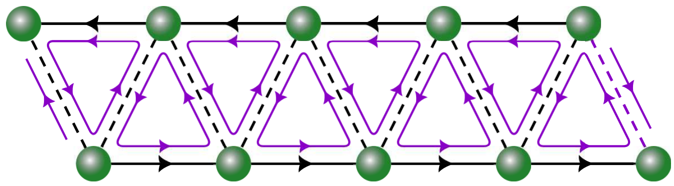

Figure 5.3: Right and left fermions propagate along the upper ($\sigma = +$) and lower ($\sigma = -$) chains, respectively. Net local currents along the zigzag links vanish.

The occupation numbers $\langle c^{\dagger}_{k\sigma} c_{k\sigma}\rangle$ can be easily computed using Matsubara Green's function in the 2×2 matrix representation, $\hat{G}(k,\varepsilon) = \left(\mathrm{i}\varepsilon + \mu - \hat{\mathcal{H}}_k\right)^{-1}$, with $\hat{\mathcal{H}}_k$ given by (5.2). Using the Fourier representation in imaginary time formalism,

$$\hat{G}(k,\tau) = \int \frac{\mathrm{d}\varepsilon}{2\pi} e^{-\mathrm{i}\varepsilon\tau} \hat{G}(k,\varepsilon),$$

occupation numbers will have the form:

$$\langle c^{\dagger}_{k\sigma} c_{k\sigma}\rangle = \lim_{\tau\to 0-} \hat{G}_{\sigma,\sigma}(k,\tau).$$

Now, representing the Matsubara Greens function as:

$$\hat{G}(k,\varepsilon) \;=\; \left[\left(\mathrm{i}\varepsilon + \mu - \xi(k)\right)\mathbb{1} + \mathbf{h}(k)\cdot\hat{\boldsymbol{\sigma}}\right]^{-1} \;=\; \frac{\left(\mathrm{i}\varepsilon + \mu - \xi(k)\right) - \mathbf{h}(k)\cdot\hat{\boldsymbol{\sigma}}}{\left(\mathrm{i}\varepsilon + \mu - \xi(k)\right)^2 - |\mathbf{h}(k)|^2},$$

and replacing momentum summation in (5.16) by integration, one obtains the following expression for the relative current:

$$\begin{aligned}
\mathcal{J}(f) &= -\frac{2t_0}{\pi}\int_0^{\pi} \mathrm{d}k\, \mathcal{F}(k;f),\\
\mathcal{F}(k;f) &= \frac{t_0 \sin(2\pi f)\sin^2 k}{E_k}[n_+(k) - n_-(k)] + \cos k \sin(\pi f)[n_+(k) + n_-(k)],
\end{aligned} \tag{5.17}$$

where E_k is given by (5.4) and $n_{\pm}(k) = \theta\left[\mu - E_{\pm}(k)\right]$ are the ground state Fermi distribution functions for the upper and lower bands, $\theta(x)$ being the Heaviside step function. As follows from (5.17), the orbital current is contributed by *all* occupied states of the two-band spectrum and, as has been mentioned earlier [39, 40], does not represent an infrared phenomenon.

For arbitrary values of the chemical potential μ the current vanishes at integer values of the flux, $f = 0, \pm 1, \pm 2, \ldots$, and has the periodicity property $\mathcal{J}(f+2) = \mathcal{J}(f)$. At the special value $f = 1/2$:

$$\mathcal{J}(1/2) = -\frac{2t_0}{\pi}\int_0^{\pi} \mathrm{d}k \cos k [n_+(k) + n_-(k)] \tag{5.18}$$

When $m \neq 0$ and μ lies within the spectral gap (see Fig. 5.2b), $-|m| \leq \mu \leq |m|$, the ground state is insulating with an empty upper band $E_+(k)$ and fully filled lower band $E_-(k)$. In this case for all k $n_+(k) = 0$, $n_-(k) = 1$, and the integral in (5.18) vanishes: $\mathcal{J}(1/2)|_{\rm insul} = 0$. This result is valid for all $f = l + 1/2$ as long as the ground state is insulating. If $\mu > |m|$ or $\mu < -|m|$, a "Fermi surface" appears and the ground state becomes metallic with a finite $k_{\rm F}$, in which case $\mathcal{J}(1/2) \sim \sin k_{\rm F} \neq 0$.

Shifting the flux by one flux quantum, $f \to f+1$, or inverting it with respect to the point 1/2, $f \to 1-f$, generates a non-staggered ph-transformation of the band spectrum, $E_s(k, 1\pm f) = -E_{-s}(k, f)$. Accordingly $n_\pm(k; 1-f, \mu) = 1 - n_\mp(k; f, -\mu)$. Then from the definition (5.17) it follows that

$$\mathcal{J}(f+1;\mu) = \mathcal{J}(f;-\mu), \tag{5.19}$$

$$\mathcal{J}(1-f;\mu) = -\mathcal{J}(f;-\mu). \tag{5.20}$$

When the current is defined at a fixed density ρ, the above transformation should be replaced by

$$\mathcal{J}(f+1;\rho) = \mathcal{J}(f;2-\rho), \tag{5.21}$$

$$\mathcal{J}(1-f;\rho) = -\mathcal{J}(f;2-\rho). \tag{5.22}$$

Thus, in the TFL, the orbital current is symmetric (antisymmetric) under transformations $f \to f+1$ ($f \to 1-f$) combined with particle-hole transformations $\mu \to -\mu$ or $\rho \to 2-\rho$. For comparison, for a standard ladder, the spectral property (5.5) makes the current symmetric under the change $\mu \to -\mu$, and $\mathcal{J}(f)$ is a periodic function of the flux with the period $\Delta f = 1$.

5.3 C-IC transitions at $\mu = $ const

At $f \ll 1$ the current is proportional to the flux and the difference between the standard and triangular ladders is not significant. Below we concentrate on the region $|f - 1/2| \ll 1$. Here we will assume that the TFL is in contact with a reservoir that supports a fixed value of the chemical potential $\mu = 0$. This value of μ is chosen only for the sake of simplicity of the discussion. We will show that the geometrical frustration of the TFL splits the Lifshitz (metal-insulator) transition of the square ladder into two consecutive transitions taking place at $\kappa = |m|$ and $\kappa = M$. In the vicinity of these transitions, the current is a nonanalytic function of the flux.

Using (5.6) and the expression (5.7) valid at small κ, we represent the current as

$$\mathcal{J}(\kappa) = -\frac{1}{\pi}\sum_{s=\pm}\int_0^\pi {\rm d}k\, \Phi_s(k) n_s(k), \tag{5.23}$$

$$\Phi_s(k) = W\cos k + s\frac{\kappa \sin^2 k}{\mathscr{E}_k},$$

$$\mathscr{E}(k) = \sqrt{\sin^2 k + \tau_1^2 + \tau_2^2 + 2\tau_1\tau_2 \cos k}$$

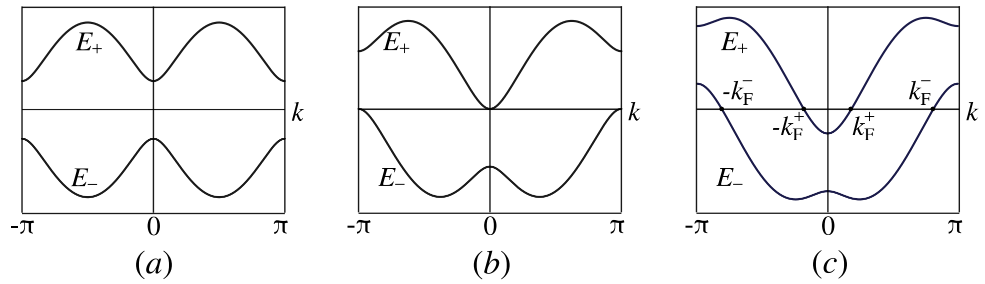

Figure 5.4: Commensurate-incommensurate transition in a standard ladder. a) Insulating phase at $\kappa < |m|$; b) critical point $\kappa = |m|$; c) metallic phase at $\kappa > |m|$.

where $W = 2t_0$ and $\tau_{1,2} = t_{1,2}/W \ll 1$. We start with the insulating phase at $m \neq 0$, Fig. 5.2b, realized at $\kappa < |m|$. For this phase $n_+(k) = 0$, $n_-(k) = 1$ for all k, and the orbital current is a linear function of κ. With the logarithmic accuracy

$$\mathcal{J}_0(\kappa) = \frac{C_0}{\pi}\kappa,$$
$$C_0 = \int_0^\pi \mathrm{d}k \, \frac{\sin^2 k}{\mathcal{E}_k} = 2 - \frac{1}{2W^2}\left(M^2 \ln\frac{W}{M} + m^2 \ln\frac{W}{|m|}\right) \tag{5.24}$$

For the insulating phase of the standard ladder, the result is not much different: one only has to set in (5.24) $M = m$. The difference emerges when the transitions to metallic phases are compared. For a half-filled standard ladder, the ph-symmetry (5.5) implies that if for some κ, $E_+(0) = 0$, then necessarily $E_-(\pi) = 0$. Fig. 5.4b shows the spectrum at the doubly degenerate critical point $\kappa = m = t_1$. As follows from Fig. 5.4c, at $\kappa > m$ the ground state becomes metallic with *four* Fermi points, $\pm k_0$, and $\pm(\pi - k_0)$. In this phase, close to the critical point $k_0 = \sqrt{\kappa^2 - m^2}/v_F$. One then finds that

$$\mathcal{J}(\kappa) = \mathcal{J}_0(\kappa) + \mathcal{J}_{\mathrm{sing}}(\kappa) \tag{5.25}$$

where the singular part of the current displays a square-root dependence on κ, typical for a quantum commensurate-incommensurate (C-IC) transition [95, 96]:

$$\mathcal{J}_{\mathrm{sing}}(\kappa) = -\frac{W}{\pi}\left(\int_0^{k_0} + \int_0^{\pi - k_0}\right) \mathrm{d}k \cos k = -\frac{2}{\pi}\sqrt{\kappa^2 - m^2} + O[(\kappa^2 - m^2)^{3/2}]. \tag{5.26}$$

As already mentioned, in the TFL, an arbitrarily weak frustration ($\delta \ll 1$) removes the degeneracy of the two mass gaps, which leads to two Lifshitz transitions. Increasing κ in the insulating phase, Fig. 5.2b, one first observes a transition at $\kappa = |m|$, where $E_-(\pi; |m|) = 0$ with $E_+(0; |m|) > 0$. This is a transition to a metallic phase with *two* Fermi points, shown in Fig.5.5a. This phase is realized in the region $|m| < \kappa < M$. Close to the critical point $0 < \kappa - |m| \ll |m|$ one obtains $\mathcal{J}_{\mathrm{sing}}(\kappa) \simeq \pi^{-1}\sqrt{\kappa^2 - m^2}$. Further increasing κ leads to the second Lifshitz transition to a metallic phase with *four* Fermi points, Fig. 5.5b. This transition occurs at $\kappa = M$ where $E_+(0; M) = 0$. One then finds that $\mathcal{J}_{\mathrm{sing}}(\kappa) \simeq -\pi^{-1}\sqrt{\kappa^2 - M^2}$ at $0 < \kappa - M \ll M$. At larger values of κ, namely at

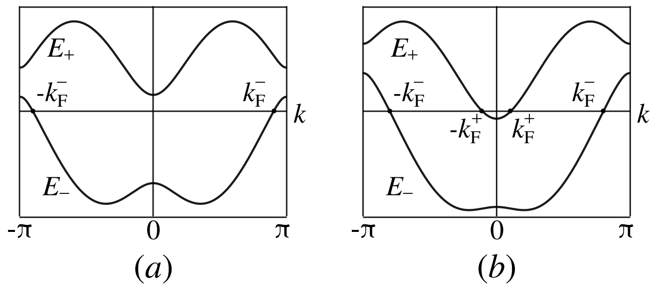

Figure 5.5: Commensurate-incommensurate transition in a TFL. a) 2FP metallic phase at $|m| < \kappa < M$; b) 4FP metallic phase at $\kappa > M$.

$M \ll \kappa \ll W \ln^{-1/2}(W/M)$, the current is easily shown to be inversely proportional to κ: $\mathcal{J}(\kappa) \simeq (M^2 + m^2)/2\pi\kappa$.

At $m \to 0$, the insulating phase of the TFL disappears, implying that the transition at $\kappa = |m|$ disappears as well. The phase at $0 < \kappa < M$ is metallic with *two* Fermi points. The current in this region is a linear function of κ but with a different slope as compared to Eq. (5.24):

$$\mathcal{J}(\kappa) = \frac{\kappa}{\pi}\left(1 - \frac{M^2}{2W^2}\ln\frac{W}{M}\right) \tag{5.27}$$

At $\kappa = M$ the ladder crosses over to the metallic state with four Fermi points. The flux dependence of the orbital current at $m \neq 0$ and small κ is shown in Figs.5.6. The quantity diverging at the C-IC transitions is the relative charge stiffness defined as a response function [97, 98]

$$D = \frac{1}{2\phi_0}\frac{\partial \mathcal{J}}{\partial f} = -\frac{\pi t_0}{\phi_0}\frac{\partial \mathcal{J}}{\partial \kappa}. \tag{5.28}$$

In the context of usual C-IC transitions taking place in the charge or spin excitations of various 1D Fermi systems [99], the quantity D is similar to the compressibility or spin susceptibility. We see that when the frustration ratio δ, Eq. (5.10), is nonzero, the single peak of D at the metal-insulator transition of the standard ladder splits into two peaks that move apart as δ is increased (Figs.5.6). In the vicinity of these transitions $D(\kappa)$ displays universal square-root singularities [95, 96]:

$$D(\kappa) \simeq \frac{t_0}{\phi_0}\frac{\kappa_c}{\sqrt{\kappa^2 - \kappa_c^2}}\theta(\kappa^2 - \kappa_c^2) \tag{5.29}$$

with $\kappa_c = |m|$ or M.

Ground state phases and the transitions between them at a small nonzero μ can be categorized along the same lines. At a constant $\mu \neq 0$ all Lifshitz transitions accessed by varying the flux belong to the C-IC universality class, with a typical behavior of the charge stiffness given by (5.29). The reason for that is simple. A generic C-IC transition is a transition from an insulator with a parabolic two-band spectrum to a metal, taking

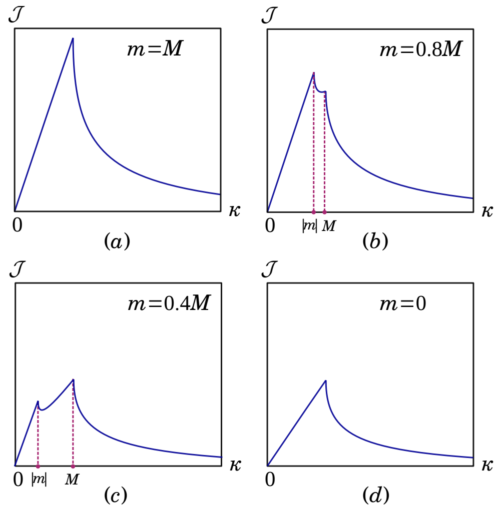

Figure 5.6: Orbital current at a fixed chemical potential $\mu = 0$ and small κ for different values of $|m|$, with $M = 0.4t_0$. (a) A single Lifshitz transition in a standard ladder, $|m| = M$; (b) and (c) – a sequence of two transitions at $|m| < M$; (d) a single transition at $\kappa = M$ when $m \to 0$.

place when varying chemical potential leads to the appearance of extra particles(holes) in the conduction (valence) band. In the TFL with a constant μ the deformation of the two-band spectrum caused by a small κ can be recast as the appearance of variable effective chemical potentials in the Dirac-like parts of the spectrum in the regions $k \sim 0$ and π. Repopulation of these low-energy states in each of these regions occurs independently and at different values of κ. Therefore, each of these transitions is of the C-IC type.

5.4 Phase diagram and orbital current at $\rho = \text{const}$

In this section, we discuss the effect of the flux on the spectrum, orbital current, and phase diagram of the noninteracting TFL at a constant density, fixed at a value: $\rho = 1 + n$, $|n| \ll 1$. Such a setup is typical for ultracold atoms on optical lattices. As before, we assume that $|f - 1/2| \ll 1$. Except for the special case $\rho = 1$, Lifshitz transitions at $\rho = \text{const}$ are different from those that occur at $\mu = \text{const}$. Moreover, as we show below, contrary to the standard ladder, in the TFL the absence of *ph*-symmetry makes the pictures at hole doping ($n < 0$) and particle doping ($n > 0$) qualitatively different.

At $\kappa > (M + |m|)/2$ the two bands of the spectrum overlap. If the chemical potential is located between the energies $E_+(0)$ and $E_-(\pi)$, i.e. $M - \kappa < \mu < \kappa - |m|$, the ground state is metallic with four Fermi points $\pm k_F^+$, $\pm k_F^-$ in the spectrum. We will call this state the 4FP-phase. Imposing an additional restriction upon the density,

$$\pi|n| < \frac{\sqrt{M^2 - m^2}}{W} \tag{5.30}$$

we disregard the situation when $\mu < E_-(0)$ and all four Fermi points belong to the $E_-(k)$ band. Starting from the 4FP phase we will then trace its evolution as κ is decreased. At a constant density $\rho \neq 1$ the Fermi momenta $k_F^{\pm}$ are subject to the constraint $k_{\rm F}^+ + k_{\rm F}^- = \pi(1+n)$. Since $|\kappa| \ll W$ and $|n| \ll 1$, $k_{\rm F}^+$ and $k_{\rm F}^-$ are close to the points $k = 0$ and π, respectively, where the spectrum has the Dirac form (5.8) and (5.9). Therefore we can set $k_{\rm F}^+ = p_+$, $k_{\rm F}^- = \pi - p_-$, where the momenta $p_\pm$ are small, positive and satisfy

$$p_+ - p_- = \pi n \tag{5.31}$$

At given values of the Dirac masses the dependence of $p_\pm$ and μ on the flux is described by the equations

$$\sqrt{p_+^2 v_{\rm F}^2 + M^2} = \kappa + \mu, \quad \sqrt{p_-^2 v_{\rm F}^2 + m^2} = \kappa - \mu \tag{5.32}$$

valid in the 4FP phase for any sign of n.

5.4.1 $\rho < 1$ ($n < 0$)

According to (5.31) at $n < 0$ one has $p_+ < p_-$. The momentum p_+ decreases with κ and vanishes at some critical value $\kappa = \kappa_c$ where the band $E_+(k)$ gets empty. This is a Lifshitz transition at which the number of Fermi points changes from four to two (Fig. 5.7b); we label the new state as the 2FP phase. The critical values of κ and μ are given by $\kappa_c = (M + Q_m)/2$, $\mu_c = (M - Q_m)/2$, where $Q_m = \sqrt{(\pi n)^2 v_{\rm F}^2 + m^2}$. As shown below, the dependence $p_+ = p_+(\kappa)$ at small $\kappa - \kappa_c$ determines the singularities in the flux dependence of the orbital current near the transition.

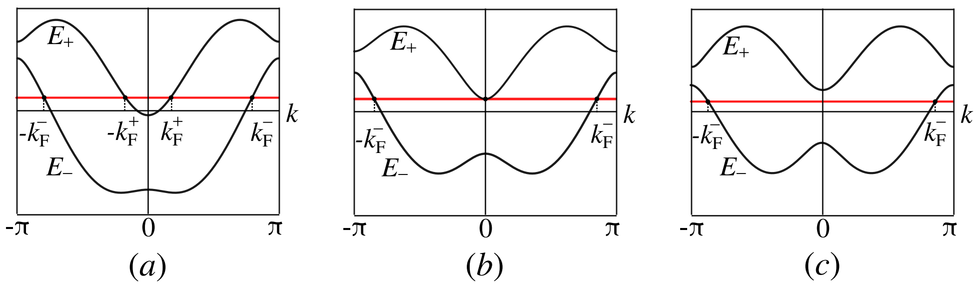

Figure 5.7: Case $\rho < 1$. (a) 4FP metallic phase at $\kappa > \kappa_c$; (b) Lifshitz critical point at $\kappa = \kappa_c$; (c) 2FP metallic phase at $\kappa < \kappa_c$.

From (5.31 and (5.32) one derives the quadratic equation for p_+ valid in the 4FP-phase

$$Ap_+^2 + Bp_+ - C = 0, \quad \kappa > \kappa_c \tag{5.33}$$

where

$$A = 1 - \left(\frac{\pi|n|}{2\kappa}\right)^2, \quad B = \pi|n|\left(1 + \frac{\kappa_c\mu_c}{\kappa^2}\right), \quad C = \left(1 - \frac{\mu_c^2}{\kappa^2}\right)(\kappa^2 - \kappa_c^2) \tag{5.34}$$

Obviously $B > 0$. Since $\kappa > \kappa_c > \mu_c$, the coefficient C is positive as well. One also finds that

$$\frac{\pi|n|}{2\kappa} \leq \frac{\pi|n|}{M + \sqrt{(\pi n)^2 + m^2}} < 1$$

implying that $A > 0$. Focusing on the vicinity of the Lifshitz point we introduce the small parameter $\zeta = (\kappa - \kappa_c)/\kappa_c$, $0 < \zeta \ll 1$. The solution of Eq. (5.33) satisfying the boundary condition $p_+(0) = 0$ reads

$$p_+(\zeta) = \frac{M\pi|n|}{A(M+Q_m)}\left[\sqrt{1+(\zeta/\zeta_0)} - 1\right], \quad \zeta_0 = \frac{1}{2A}\frac{M(\pi n W)^2}{Q_m(M+Q_m)^2} \tag{5.35}$$

Eq. (5.35) is applicable at any $|n| \ll 1$. Assuming that $A \lesssim 1$ and $M \gg |m|$ one easily checks that for any $|n| \ll 1$ the parameter $\zeta_0 \ll 1$. Therefore there are two regions of small ζ. In the immediate vicinity of the transition point, $0 < \zeta \ll \zeta_0$, the dependence $p_+(\zeta)$ is linear

$$p_+ = \frac{1}{v_{\mathrm{F}}}\frac{Q_m(M+Q_m)}{W^2(\pi|n|)}\zeta \tag{5.36}$$

At larger deviations from the criticality, $\zeta_0 \ll \zeta \ll 1$, this dependence crosses over to the square-root asymptotics

$$p_+ = \frac{1}{W}\sqrt{\frac{2MQ_m\zeta}{A}} \tag{5.37}$$

typical for a C-IC transition. In the limit $n \to 0$ ($\rho \to 1^-$) $\zeta_0 \to 0$ and the square-root dependence becomes exact: $p_+ = \sqrt{2M|m|\zeta}$.

At $\kappa < \kappa_c$ the spectrum describes the metallic 2FP phase, Fig. 5.7c, in which k_{F}^- stays fixed at the value $\pi(1-|n|)$ and does not depend on κ. As long as $\rho < 1$, the lower band $E_-(k)$ remains partially filled, so the 2FP phase is stable down to the point $\kappa = 0$ ($f = 1/2$). Thus, on hole doping the ground state of the TFL with $m \neq 0$ always remains metallic. On decreasing κ one finds a single Lifshitz transition separating the 4FP and 2FP phases.

In the 2FP phase, the chemical potential is given by $\mu(\kappa) = \kappa - \sqrt{(\pi n)^2 W^2 + m^2}0$. When $\rho \to 1^-$ ($n \to 0^-$), μ reaches the top of the band $E_-(k)$ (see Fig. 5.8a)

$$\lim_{n\to 0} \mu(\kappa) = \kappa - |m| \tag{5.38}$$

and the latter becomes fully filled. At $m \neq 0$ the upper and lower bands are separated by a finite gap $2|m|$. However, at $m = 0$ a Dirac node appears in the spectrum of the π-fermions at the energy $E_-(\pi) = \kappa$, and the chemical potential is located just at this energy: $\mu = \kappa$. This is a semi-metallic phase with a single Dirac point and a fully filled "Dirac sea"; see Fig. 5.8b.

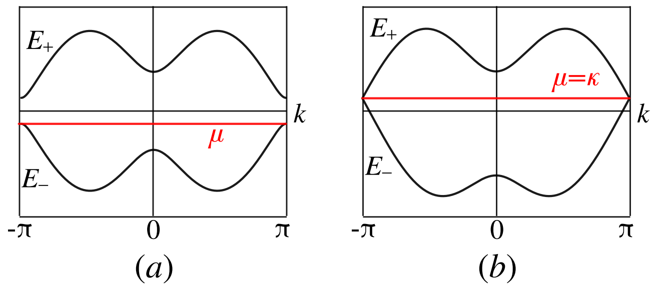

Figure 5.8: $\rho = 1^-$. (a) $m \neq 0$; (b) $m = 0$.

Let us now estimate the orbital current at $\rho <$. According to the definition (5.23), in the 4FP phase, the current is a sum of the contributions of the partially filled upper and lower bands:

$$\mathcal{J}_{4\mathrm{FP}}(\kappa) = \mathcal{J}_+(\kappa) + \mathcal{J}_-(\kappa) = -\frac{1}{\pi}\sum_{s=\pm}\int_0^{k_F^s} \mathrm{d}k\,\Phi_s(k) \tag{5.39}$$

where $k_\mathrm{F}^- = \pi - p_+$ and $k_\mathrm{F}^+ = p_+$ is given by (5.35). Since $k_\mathrm{F}^+ \ll 1$, in the leading order

$$\mathcal{J}_+ = -\frac{W}{\pi}p_+ + O(p_+^3). \tag{5.40}$$

For $\mathcal{J}_-$ we have

$$\mathcal{J}_- = -\frac{1}{\pi}\left(\int_0^\pi - \int_{\pi-p_-}^\pi\right)\mathrm{d}k\left(2t_0\cos k - \frac{\kappa\sin^2 k}{\mathcal{E}_k}\right) \equiv \mathcal{J}_0 + \mathcal{J}_1. \tag{5.41}$$

Here $\mathcal{J}_0 = C_0\kappa/\pi$ given by (5.24) is the current in the band insulator phase, contributed by the fully filled band $E_-(k)$. For the integral $\mathcal{J}_1$ we obtain

$$\mathcal{J}_1 = -\frac{W}{\pi}\sin\tilde{p}_+ - \frac{C_1\kappa}{\pi}, \quad C_1 = \frac{m^2}{4W^2}(\sinh 2\alpha_0 - 2\alpha_0) \tag{5.42}$$

where $\tilde{p}_+ = p_+ + \pi|n|$, $\sinh\alpha_0 = \tilde{p}_+/|m|$. So, in the lowest order in the small parameters k_F^+ and $|n|$ the current in the 4FP phase can be written as

$$\mathcal{J}_{4\mathrm{FP}}(\kappa) = -W|n| - \frac{2W}{\pi}k_\mathrm{F}^+ + \frac{C_0 - C_1}{\pi}\kappa, \quad \kappa > \kappa_c \tag{5.43}$$

In the 2FP phase the upper band does not contribute to the current, so the latter is obtained from (5.43) by setting $p_+ = 0$. At $\kappa < \kappa_c$ the parameter C_1 depends only on the density $|n|$ and for any ratio $\pi|n|W/|m|$ is small compared to C_0. Neglecting small corrections of the order of $M^2\ln M$, we can write

$$\mathcal{J}_{2\mathrm{FP}}(\kappa) = \frac{2}{\pi}(\kappa - \kappa_0), \quad \kappa_0 = t_0\pi|n| \quad (\kappa < \kappa_c). \tag{5.44}$$

We see that, in the 2FP phase, the vacuum current is a linear function of κ. The point where it changes the sign is determined by the hole density $|n|$. The fact that $\mathcal{J}_{2\mathrm{FP}}(0) \neq 0$

is not unexpected. It reflects the lack of the ph-symmetry of the model and the absence of the $\rho \to 2-\rho$ invariance of the thermodynamic quantities (see the discussion in Sec. 5.2).

Comparing (5.43) and (5.44) and taking into account (5.36) we observe that the current is continuous across the 2FP-to-4FP Lifshitz transition but exhibits a cusp at $\kappa = \kappa_c$. As a result, at the critical point the relative charge stiffness $D(\kappa)$, Eq. (5.28), which is proportional to the derivative $\partial\mathcal{J}/\partial\kappa$, undergoes a jump:

$$\left.\frac{\partial \mathcal{J}_{2\mathrm{FP}}}{\partial \kappa}\right|_{\kappa_c} \equiv \lim_{\kappa\to\kappa_c-0} \frac{\partial \mathcal{J}(\kappa)}{\partial\kappa} = \frac{2}{\pi}, \tag{5.45}$$

$$\left.\frac{\partial \mathcal{J}_{4\mathrm{FP}}}{\partial \kappa}\right|_{\kappa_c} \equiv \lim_{\kappa\to\kappa_c+0} \frac{\partial \mathcal{J}(\kappa)}{\partial\kappa} = \frac{2}{\pi}\left[1-\sqrt{1+\left(\frac{m}{\pi n W}\right)^2}\right],\ n\neq 0 \tag{5.46}$$

(In deriving formula (5.46) we neglected a small relative correction proportional to $\partial C_1/\partial p_+$). Thus, at a constant density but away from half-filling the square-root dependence of the current on the flux at the Lifshitz transition ($\kappa \to \kappa_c$), pertinent to C-IC transition in a grand-canonical ensemble, is replaced by a linear one. A similar situation has been described earlier [100] in the study of the magnetization process of isolated 1D Fermi systems at a fixed particle number, and, more recently, in the context of standard ladders away from 1/2-filling [45].

5.4.2 $\rho > 1$ ($n > 0$)

Here again, we start from the four-Fermi-point metallic state which we now label as the 4FP-1 phase. At $n > 0$ we have $p_+ > p_-$. On decreasing κ the first Lifshitz point $\kappa = \kappa_{c1}$ is reached, Fig. 5.9a, at which $p_- = 0$ and the band $E_-(k)$ gets completely filled. The partial filling of the upper band $E_+(k)$ within the interval $|k| < k_F^+$ reflects the existence of a finite particle doping ($n = \rho - 1 > 0$). At the transition, the number of Fermi points changes from four to two. We will label this phase as 2FP-1. We note that under the substitutions $p_+ \leftrightarrow p_-$, $M \leftrightarrow |m|$, $n \leftrightarrow -n$, $\mu \leftrightarrow -\mu$ the already discussed 4FP-2FP Lifshitz transition at $\rho < 1$ exactly maps to the 4FP1-2FP1 transition at $\rho > 1$. Therefore the critical values of κ and μ are given by $\kappa_{c1} = (Q_M + |m|)/2$, $\mu_{c1} = (Q_M - |m|)/2$, with $Q_M = \sqrt{(\pi n)^2 W^2 + M^2}$, and, in the vicinity of the Lifshitz point, the flux dependence of the momentum $p_-(\kappa)$ is given by

$$p_- = \frac{|m|\pi n}{A(|m|+Q_M)}\left[\sqrt{1+\frac{\zeta}{\zeta_1}}-1\right], \quad \zeta_1 = \frac{1}{2A}\frac{|m|(\pi n W)^2}{Q_M(|m|+Q_M)^2} \ll 1 \tag{5.47}$$

where $\zeta_1 = (\kappa - \kappa_{c1})/\kappa_{c1}$ $(0 < \zeta \ll 1)$. As in the $\rho < 1$ case, in (5.47) there are no restrictions on n except for $n \ll 1$. The smallness of ζ_1 implies the existence of the linear ($p_- \sim \zeta$) and square-root ($p_- \sim \sqrt{\zeta}$) asymptotics in the regions $\zeta \ll \zeta_1$ and $\zeta_1 \ll \zeta \ll 1$, respectively.

With k_F^+ fixed at the value $k_F^+ = \pi n > 0$, on decreasing κ with m kept finite one finds the second Lifshitz point $\kappa = \kappa_{c2} < \kappa_{c1}$ at which the chemical potential reaches the value

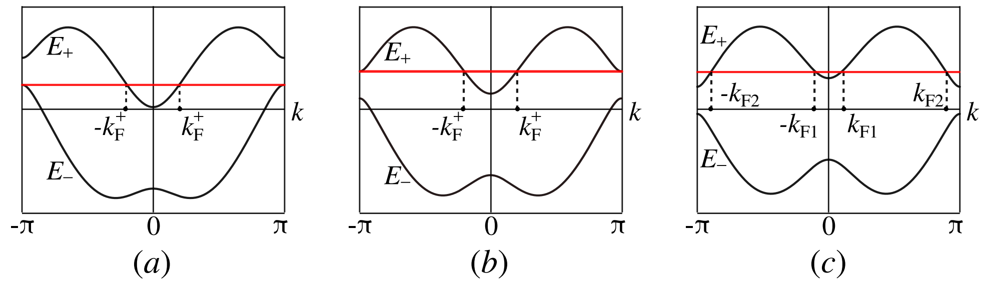

Figure 5.9: Case $\rho > 1$. (a) Lifshitz transition at $\kappa = \kappa_{c1}$ between 4FP-1 to 2FP-1 phases; (b) Lifshitz transition at $\kappa = \kappa_{c2}$ between 2FP-1 to 4FP-2 phases; (c) 4FP-2 metallic phase at $\kappa < \kappa_{c2}$.

$\mu = E_+(\pi)$ (see Fig. 5.9b). The spectrum displays a re-entrant transition to another 4FP metallic phase which we denote by 4FP-2 (Fig. 5.9c). One finds that $\kappa_{c2} = (Q_M - |m|)/2$, $\mu_{c2} = (Q_M + |m|)/2$. This critical point belongs to the region $(M + |m|)/2 < \kappa \ll W$ if the density of doped particles $n > n^*$, where $n^* = \frac{2}{\pi W}\sqrt{|m|(M + |m|)}$. At a lower density, $n < n^*$, the point κ_{c2} is located at smaller values of κ: $(M - |m|)/2 < \kappa < (M + |m|)/2$, with $p_2 \to 0$ as $\kappa \to \kappa_{c2} - 0$.

As shown in Fig. 5.9c, in the 4FP-2 phase the four Fermi points $\pm k_{F1}$ and $\pm k_{F2}$ are all located in the upper band $E_+(k)$ and are subject to the condition $k^+_{F1} + (\pi - k^+_{F2}) = \pi n$. They can be parametrized as $k_{F1} = \pi n - p_2$, $k_{F2} = \pi - p_2$ $(0 < p_2 \ll 1)$. At the transition $(\kappa = \kappa_{c2})$ $p_2 = 0$. Following the same procedure as before we obtain

$$p_2 = \frac{(\pi n)|m|}{A(Q_M - |m|)}\left[\sqrt{1 + \frac{\zeta}{\zeta_2}} - 1\right], \quad \zeta_2 = \frac{|m|(\pi n W)^2}{2AQ_M(Q_M - |m|)^2}, \tag{5.48}$$

where $\zeta_2 = (\kappa_{c2} - \kappa)/\kappa_{c2} > 0$ $(\zeta_2 \ll 1)$.

Further decreasing κ in the 4FP-2 phase one passes to the region $\kappa < (M - |m|)/2$. The spectrum is shown in Fig. 5.10a. The Fermi momenta k_{F1} and k_{F2} are parametrized as $k_{F1} = p_1$, $\pi - k_{F2} = \pi n - p_1$. p_1 and μ are determined by the equations

$$\sqrt{p_1^2 v_F^2 + M^2} = \mu + \kappa, \quad \sqrt{(\pi n - p_1)^2 v_F^2 + m^2} = \mu - \kappa. \tag{5.49}$$

There exists the third Lifshitz transition at $\kappa = \kappa_{c3}$ at which $\mu = E_+(0)$, $p_1 = 0$; see Fig. 5.10b. We find that $\kappa_{c3} = (M - Q_m)/2$, $\mu_{c3} = (M + Q_m)/2$. The requirement $\kappa_{c3} > 0$ is ensured by the condition (5.30) which sets the upper limit for n. From Eqs. (5.49) one obtains the quadratic equation valid at $\kappa > \kappa_{c3}$:

$$\left[1 - \frac{(\pi n)^2 W^2}{4\kappa^2}\right](p_1 v_F)^2 - (\pi n W)\left(1 + \frac{\mu_{c3}\kappa_{c3}}{\kappa^2}\right)(p_1 v_F) + \left(\frac{\mu_{c3}^2}{\kappa^2} - 1\right)\left(\kappa^2 - \kappa_{c3}^2\right) = 0 \tag{5.50}$$

Contrary to all previous cases, a physically acceptable solution of Eq. (5.50) only exists if $\pi n W > 2\kappa$. This brings the allowed doped particle density n to the interval

$$\frac{M^2 - m^2}{2MW} < \pi n < \frac{\sqrt{M^2 - m^2}}{W}. \tag{5.51}$$

Taking the limit $M \gg |m|$, one then concludes that the transition at $\kappa = \kappa_{c3}$ and the onset of the 2FP-2 phase is only possible at $n \sim M/W$. Choosing $|1-(\pi n W)^2/\kappa_{c3}^2| \sim 1$, $Q_m \gtrsim M$, $\pi n W \sim M$ we find that

$$p_1(\zeta_3) \sim \sqrt{\zeta_0+\zeta_3} - \sqrt{\zeta_0}, \quad \zeta_0 \sim \frac{(\pi n)^2 W^2 M}{(M-Q_m)^2 Q_m}, \tag{5.52}$$

where $\zeta_3 = (\kappa - \kappa_{c3})/\kappa_{c3}$. Since $\zeta_0 \sim 1$, only the linear dependence of the momentum p_1 on ζ_3 at $\zeta_3 \ll 1$ is realized. There is no crossover to a square-root asymptotics in this case.

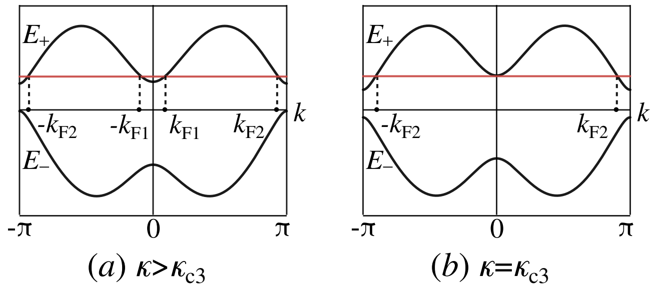

Figure 5.10: Lifshitz transition from 4FP-2 to 2FP-2 at $\rho > 1$.

Thus, contrary to the case $\rho < 1$ in which only one Lifshitz transition takes place, at $\rho > 1$ and $m \neq 0$, on increasing the flux towards the value 1/2 (decreasing κ towards zero) the spectrum of the system undergoes three consecutive Lifshitz transitions

$$\begin{aligned}
\kappa = \kappa_{c1}: &\quad \text{4FP-1 metal} \to \text{2FP-1 metal} \\
\kappa = \kappa_{c2}: &\quad \text{2FP-1 metal} \to \text{4FP-2 metal} \\
\kappa = \kappa_{c3}: &\quad \text{4FP-2 metal} \to \text{2FP-2 metal}
\end{aligned}$$

where $\kappa_{c1} > \kappa_{c2} > \kappa_{c3}$. In the vicinity of each transition, the behavior of the orbital current at $\rho > 1$ is similar to the already considered case $\rho < 1$. Fig. 5.11 shows the flux dependence of the orbital current of a particle-doped ladder ($\rho > 1$) for both signs of $\kappa = 2\pi t_0(1/2 - f)$. Note that due to the symmetry property (5.22), in Fig. 5.11 the region $\kappa < 0$ with $\rho = 1.1$ can be mapped to the region $\kappa > 0$ with $\rho = 0.9$. Therefore Fig. 5.11 actually demonstrates the clear asymmetry in the flux dependence of the current for particle and hole-doped samples (three Lifshitz transitions versus one).

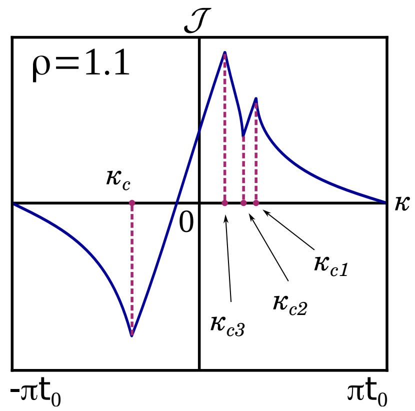

Figure 5.11: Cusps in the flux dependence of the orbital current at $\rho > 1$.

In the 2FP-2 metallic phase the Fermi momentum k_{F2}^+ is fixed by the condition $k_{F2}^+ = \pi(1-n)$. The chemical potential is given by $\mu = \kappa + \sqrt{(\pi n)^2 + m^2}$. At $n \to 0^+$, $\rho \to 1^+$, the band $E_+(k)$ becomes empty with the chemical potential attached to its bottom:

$$\lim_{n\to 0} \mu(\kappa) = \kappa + |m| \tag{5.53}$$

Comparing Figs.5.8a and 5.12, and formulas (5.38) and (5.53), respectively, we observe that at $\rho \to 1$ the chemical potential displays a discontinuity:

$$\mu_\pm(\kappa) \equiv \lim_{\rho \to 1^\pm} \mu(\kappa) = \kappa \pm |m| \tag{5.54}$$

Since the classic paper by Lieb and Wu [101] this fact is regarded as a direct manifestation of the insulating nature of the ground state of a system. In fact, for a system with a given particle number n with the ground state energy $E_0(N)$, the chemical potentials $\mu_\pm$ are defined as $\mu_+ = E_0(N+1) - E_0(N)$ and $\mu_- = E_0(N) - E_0(N-1)$. The finite difference $\mu_+ - \mu_- = 2|m| > 0$ then defines the spectral gap of the insulating state.

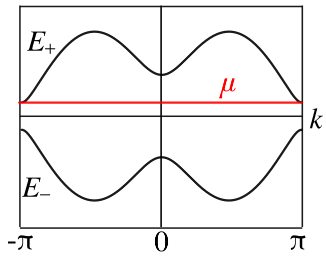

Figure 5.12: $\rho \to 1+$, $m \neq 0$

We complete the discussion by noting that the limit $\rho \to 1$ is unambiguous when the $k \sim \pi$ fermions are massless: $m = 0$. In this case, the ground state of the system is always metallic, characterized by a single Dirac point in the spectrum.

5.5 Boundary modes in the topological phase

Consider a semi-infinite sample, in which the diatomic unit cells are labeled as $n = 1,2,\ldots,\infty$. Let us adopt the continuum limit of this model by taking into account both Dirac-like low-energy modes with masses $M = t_1 + t_2$ and $m = t_1 - t_2$, $|M|,|m| \ll t_0$. Then we can write

$$c_{j,\sigma} \to \sqrt{a_0}\Big[(-1)^j \psi_\sigma(x) + \bar{\psi}_{-\sigma}(x)\Big], \quad (\sigma = \pm), \tag{5.55}$$

where $\psi_\sigma(x)$ and $\bar{\psi}_\sigma(x)$ are fermionic fields describing single-particle excitations with momenta close to π and 0, respectively. Adding an additional rung $n = 0$ to the open end of the ladder we impose boundary conditions

$$c_{0,\sigma} = 0 \;\to\; \psi_\sigma(0) + \bar{\psi}_{-\sigma}(0) = 0, \quad (\sigma = \pm). \tag{5.56}$$

Denoting by $\{u(x), v(x)\}$ and $\{\tilde{u}(x), \tilde{v}(x)\}$ the components of the 2-spinor wave functions $w(x)$ and $\tilde{w}(x)$ associated with the field operators $\psi(x)$ and $\bar{\psi}(x)$, from (5.56) we obtain

$$u(0) + \tilde{v}(0) = 0, \quad v(0) + \tilde{u}(0) = 0.$$

This leads to the following constraint imposed on the boundary spinors:

$$w(0) = \begin{pmatrix} u(0) \\ v(0) \end{pmatrix}, \quad \tilde{w}(0) = \begin{pmatrix} \tilde{u}(0) \\ \tilde{v}(0) \end{pmatrix} = -\hat{\sigma}^1 w(0). \tag{5.57}$$

The boundary zero modes corresponding to these functions satisfy the equations

$$\big[-\mathrm{i}v_{\mathrm{F}}(\sigma_3 + \tau\sigma_2) - m\sigma_1\big] w(x) = 0, \tag{5.58}$$

$$\big[-\mathrm{i}v_{\mathrm{F}}(\sigma_3 + \tau\sigma_2) - M\sigma_1\big] \tilde{w}(x) = 0, \quad x \ge 0. \tag{5.59}$$

The kinetic energy in Eqs. (5.58) and (5.59) is diagonalized by an SU(2) toration of the spinors around the $\hat{\sigma}^1$-axis:

$$\psi = U\zeta, \quad \bar{\psi} = U\tilde{\zeta}, \tag{5.60}$$

where

$$\zeta = \begin{pmatrix} z_1 \\ z_2 \end{pmatrix}, \quad \tilde{\zeta} = \begin{pmatrix} \tilde{z}_1 \\ \tilde{z}_2 \end{pmatrix}, \tag{5.61}$$

and the unitary matrix U is given by

$$\begin{aligned} U &= u + \mathrm{i}v\hat{\sigma}^1, & u^2 + v^2 &= 1, \\ u^2 - v^2 &\equiv \cos\gamma = \frac{1}{\sqrt{1+\tau^2}}, & 2uv &\equiv \sin\gamma = \frac{\tau}{\sqrt{1+\tau^2}}. \end{aligned} \tag{5.62}$$

The spinors ζ and $\tilde{\zeta}$ satisfy canonical Dirac equations for zero modes:

$$(-\mathrm{i}\tilde{v}\sigma_3\partial_x - m\sigma_1)\zeta(x) = 0,$$
$$(-\mathrm{i}\tilde{v}\sigma_3\partial_x - M\sigma_1)\tilde{\zeta}(x) = 0.$$

On the semi-axis $x \geq 0$ their solution reads

$$\zeta(x) = \zeta_0 \begin{pmatrix} 1 \\ \mathrm{i}s_m \end{pmatrix} e^{-|m|x/\tilde{v}},$$
$$\tilde{\zeta}(x) = \tilde{\zeta}_0 \begin{pmatrix} 1 \\ \mathrm{i}s_M \end{pmatrix} e^{-|M|x/\tilde{v}}, \tag{5.63}$$

where ζ_0 and $\tilde{\zeta}_0$ are normalization coefficients and $s_m = \operatorname{sgn} m$, $s_M = \operatorname{sgn} M$.

Using the transformations (5.60) we obtain

$$w(x) = \chi_0 \begin{pmatrix} u - vs_m \\ \mathrm{i}(v + us_m) \end{pmatrix} e^{-|m|x/\tilde{v}}, \tag{5.64}$$

$$\tilde{w}(x) = \tilde{\chi}_0 \begin{pmatrix} u - vs_M \\ \mathrm{i}(v + us_M) \end{pmatrix} e^{-|M|x/\tilde{v}}. \tag{5.65}$$

On the other hand, according to the boundary condition (5.57):

$$\tilde{w}(x) = -\chi_0 \begin{pmatrix} \mathrm{i}(v + us_m) \\ u - vs_m \end{pmatrix} e^{-|M|x/\tilde{v}}. \tag{5.66}$$

Then we obtain

$$\tilde{\zeta}_0(u - vs_M) = -\mathrm{i}\zeta_0(v + us_m),$$
$$\mathrm{i}\tilde{\zeta}_0(v + us_M) = -\zeta_0(u - vs_m),$$

implying that

$$\frac{\tilde{\zeta}_0}{\zeta_0} = \frac{-\mathrm{i}(v + us_m)}{u - vs_M} = \frac{\mathrm{i}(u - vs_m)}{v + us_M}. \tag{5.67}$$

From the last equation, it follows that

$$(u - vs_m)(u - vs_M) + (v + us_m)(v + us_M) = 1 + s_m s_M = 0, \tag{5.68}$$

which leads to the conclusion that a normalizable boundary zero mode only exists – and hence, according to the bulk-boundary theorem, the ground state is topologically nontrivial – if the masses m and M have different signs:

$$s_m s_M = -1 \quad \to \quad Mm < 0. \tag{5.69}$$

With the convention $M > 0$ adopted here, the ground state represents a topological insulator if $m < 0$ and is topologically trivial at $m > 0$.

The total wave function for the boundary zero mode has the structure

$$\Upsilon(x) = (-1)^{x/a_0} w(x) + \tilde{w}(x), \quad x \geq 0, \tag{5.70}$$

where $w(x)$ and $\tilde{w}(x)$ are given by expressions (5.64) and (5.65), respectively, in which the condition (5.69) has to be taken into account. If $|M| \gg |m|$, then $\tilde{w}(x)$ exponentially decays at short distances, $x \sim \tilde{v}/|M|$. At longer distances, $x \gtrsim \tilde{v}/|m|$, there exists an exponential tail of the boundary wave function contributed by the light fermions.

In Sec. 6.2.2 it is shown that under the conditions $K > 1/2$ and $m \neq 0$, for both signs of the "light" mass m the ladder displays a band insulator phase with massive Dirac fermions being elementary low-energy excitations. Since (apart from a possible formation of excitonic states) at $K > 1/2$ interaction effects basically reduce to renormalization of the single-particle mass gap, Eq. (6.44), the results obtained here can be extended to the interacting cases provided that the interaction remains irrelevant in the RG sense.

Chapter 6

Inter-particle correlation in TFL

6.1 Weakly coupled TFL: Effective bosonized model

Treating the interacting model, we concentrate on the limit of weak repulsive interaction, $V \ll W$. In the low-energy range, i.e., $E \sim |m| \ll M \ll W$, the most important states reside in the light sector. Interaction H_{int} induces scattering processes within and between the light and heavy sectors. In the low-energy range under consideration, the interaction in the heavy sector is of minor importance, because the finite mass M cuts off infrared divergences of the scattering amplitudes. Integrating out the heavy modes reduces to renormalization of the parameters of the effective Hamiltonian of the light sector. Assuming that all these renormalizations are taken into account, in what follows we will concentrate on the fermionic modes with momenta $k \sim \pi$ and small mass gap m and define the continuum limit for the lattice fermionic operators by using the correspondence

$$c_{j\sigma} \to \sqrt{a_0}(-1)^j \psi_\sigma(x), \quad (\sigma = \pm) \tag{6.1}$$

where $\psi_\sigma(x)$ are slowly varying fermionic fields describing single-particle excitations with momenta close to the zone boundary $k = \pi$, and a_0 is the lattice constant along the chain which we set to 1. Accordingly, in the light sector, the unperturbed Hamiltonian density of the light fermionic modes takes the following continuum form

$$\mathscr{H}_0(x) = \Psi^\dagger(x)\left[-\mathrm{i}v_{\mathrm{F}}\left(\hat\sigma^3 + \tau\hat\sigma^2\right) + m\hat\sigma^1\right]\Psi(x), \quad \text{with} \quad \Psi = \begin{pmatrix}\psi_+\\ \psi_-\end{pmatrix}, \tag{6.2}$$

The kinetic energy in Eq. (6.2) is brought to a canonical Dirac form by an SU(2) rotation of the spinor Ψ

$$\Psi(x) = U\chi(x), \quad \chi = \begin{pmatrix}R\\ L\end{pmatrix}, \tag{6.3}$$

where the unitary matrix U is given in Eq. 6.3. As a consequence, in the rotated (band) basis the Hamiltonian density $\mathscr{H}_0$ becomes

$$\mathscr{H}_0(x) = \chi^\dagger(x)\big(-\mathrm{i}\tilde{v}\hat{\sigma}^3\partial_x - m\hat{\sigma}^1\big)\chi(x), \tag{6.4}$$

where $\tilde{v} = v_\mathrm{F}\sqrt{1+\tau^2}$ is the renormalized velocity. It is important to realize that the role of the frustration parameter τ is not exhausted by the above velocity renormalization of the single-particle excitations. As we show below, in the continuum limit, frustration in the $\tau^2 V$-order generates pair-hopping scattering processes which, in the rotated basis, are responsible for the onset of a strong-coupling phase with broken $\mathscr{P}$ symmetry.

6.1.1 Physical observables

Unitary rotation (6.3) affects the definition of usual local physical observables. It must be specified in which bases (chain or band) they are defined.

In the continuum limit, after projecting onto the low-energy sector, the fluctuation parts of local physical fields, defined in the chain representation, take the following form:

- Local densities on each chain:

$$\begin{aligned} :\hat{n}_{j\sigma}: \equiv : c^\dagger_{j,\sigma}c_{j,\sigma}: \;&\rightarrow\; a_0\rho_\sigma(x), \\ \rho_\sigma(x) =: \psi^\dagger_\sigma(x)\psi_\sigma(x) :&= \frac{1}{2}\Psi^\dagger(\mathbb{1}+\sigma\hat{\sigma}^3)\Psi. \end{aligned} \tag{6.5}$$

- Longitudinal currents on each chain at $f = 1/2$:

$$\begin{aligned} :J^\sigma_{j,j+1} :&= -\mathrm{i}t_0\left(: c^\dagger_{j,\sigma}c_{j+1,\sigma} : e^{-i\pi\sigma f} - \text{h.c.}\right)\Big|_{f=1/2} \\ &= -t_0\sigma\left(: c^\dagger_{j,\sigma}c_{j+1,\sigma} : + \text{h.c.}\right) \\ &\rightarrow \sigma v_\mathrm{F} : \psi^\dagger_\sigma(x)\psi_\sigma(x) : + \,O(v_\mathrm{F}a_0) \;\equiv\; j^0_\sigma(x), \end{aligned}$$

  implying that, due to their chiral nature, in the leading order at $a_0 \to 0$, local densities and longitudinal currents coincide up to a prefactor v_F:

$$j^0_\sigma(x) = \sigma v_\mathrm{F}\rho_\sigma(x). \tag{6.6}$$

- Interchain currents on t_1 and t_2 zigzag links:

$$\begin{aligned} :J^{+-}_{j,j} :&\equiv -\mathrm{i}t_1 : \left(c^\dagger_{j,+}c_{j,-} - \text{h.c.}\right) : \;\rightarrow\; t_1 a_0 \Psi^\dagger(x)\hat{\sigma}^2\Psi(x), \\ :J^{-+}_{j,j+1} :&\equiv -\mathrm{i}t_2 : \left(c^\dagger_{j,-}c_{j+1,+} - \text{h.c.}\right) : \rightarrow\; t_2 a_0 \Psi^\dagger(x)\hat{\sigma}^2\Psi(x). \end{aligned}$$

  At $t_1 = t_2$ ($m = 0$) and $a_0 \to 0$ with $v_\mathrm{F} = 2t_0a_0 = \text{const}$, the currents along the oriented t_1 and t_2 links coincide:

$$\begin{aligned} :J^{+-}_{j,j} :\rightarrow j_z(x), \quad :J^{-+}_{j,j+1} :\rightarrow j_z(x), \\ j_z(x) = v_\mathrm{F}\tau : \Psi^\dagger(x)\hat{\sigma}^2\Psi(x) : . \end{aligned} \tag{6.7}$$

- Bond-density fields:

$$\begin{aligned} B_{n,n} &=: c^{\dagger}_{n,+} c_{n,-} : + \text{h.c.} \to a_0 B(x), \\ B_{n,n+1} &=: c^{\dagger}_{n,+} c_{n-1,-} : + \text{h.c.} \to -a_0 B(x), \\ B(x) &=: \Psi^{\dagger}(x) \hat{\sigma}^1 \Psi(x) : . \end{aligned} \tag{6.8}$$

In formulas (6.5-6.8), normal ordering prescription is defined as $:\hat{A} := \hat{A} - \langle \hat{A} \rangle_0$, where averaging is done over the vacuum of the noninteracting model at $f = 1/2$ and $m = 0$. From formulas (6.5) and (6.6) it follows that the total current $j_0 = \sum_\sigma j_0^\sigma$ of the zigzag ladder at $f = 1/2$ is proportional to the relative particle density

$$j_0(x) = v_{\mathrm{F}} \rho_{\mathrm{rel}}(x). \tag{6.9}$$

Under transformations (6.3) fermion bilinears transform as:

$$\begin{aligned} \Psi^{\dagger}(x)\Psi(x) &\to \chi^{\dagger}(x)\chi(x), \\ \Psi^{\dagger}(x)\hat{\sigma}^1\Psi(x) &\to \chi^{\dagger}(x)\hat{\sigma}^1\chi(x), \\ \Psi^{\dagger}(x)\hat{\sigma}^2\Psi(x) &\to \cos\gamma\ \chi^{\dagger}(x)\hat{\sigma}^2\chi(x) + \sin\gamma\ \chi^{\dagger}(x)\hat{\sigma}^3\chi(x), \\ \Psi^{\dagger}(x)\hat{\sigma}^3\Psi(x) &\to -\sin\gamma\ \chi^{\dagger}(x)\hat{\sigma}^2\chi(x) + \cos\gamma\ \chi^{\dagger}(x)\hat{\sigma}^3\chi(x), \end{aligned}$$

therefore, all the above operators obtain the following expressions in the band representation:

$$\rho_+(x) = \frac{1}{v_{\mathrm{F}}} j_0^+(x) = u^2 J_{\mathrm{R}}(x) + v^2 J_{\mathrm{L}}(x) - uv\mathcal{N}_2(x), \tag{6.10}$$

$$\rho_-(x) = -\frac{1}{v_{\mathrm{F}}} j_0^-(x) = v^2 J_{\mathrm{R}}(x) + u^2 J_{\mathrm{L}}(x) + uv\mathcal{N}_2(x), \tag{6.11}$$

$$j_z(x) = v_{\mathrm{F}}\tau\left[2uv(J_{\mathrm{R}}(x) - J_{\mathrm{L}}(x)) + (u^2 - v^2)\mathcal{N}_2(x)\right], \tag{6.12}$$

$$B(x) = \mathcal{N}_1(x). \tag{6.13}$$

Here $J_{\mathrm{R}}(x) =: R^{\dagger}(x)R(x):$ and $J_{\mathrm{L}}(x) =: L^{\dagger}(x)L(x):$ are U(1) chiral fermionic currents defined in the band basis (see e.g., Ref. [99]), and $\mathcal{N}_{1,2}$ are Dirac mass bilinears:

$$\mathcal{N}_1(x) = \chi^{\dagger}(x)\hat{\sigma}^1\chi(x) =: R^{\dagger}(x)L(x): + : L^{\dagger}(x)R(x):, \tag{6.14}$$

$$\mathcal{N}_2(x) = \chi^{\dagger}(x)\hat{\sigma}^2\chi(x) = -\mathrm{i}\Big[: R^{\dagger}(x)L(x): - : L^{\dagger}(x)R(x):\Big]. \tag{6.15}$$

The expressions (6.12), (6.13) are the leading terms of the expansion in small a_0. Under the $\mathcal{P}$-transformation

$$\begin{aligned} R(x) &\to L(-x), & L(x) &\to R(-x), \\ J_{\mathrm{R}}(x) &\to J_{\mathrm{L}}(-x), & J_{\mathrm{L}}(x) &\to J_P(-x), \\ \mathcal{N}_1(x) &\to \mathcal{N}_1(-x), & \mathcal{N}_2(x) &\to -\mathcal{N}_2(-x). \end{aligned} \tag{6.16}$$

Here a comment is in order. In models of 1D lattice fermions with a half-filled band, operators with the structure (6.14), (6.15) are associated with spatially modulated (staggered) order parameter fields. In those cases, the fermionic bilinears $R^\dagger L$, $L^\dagger R$ emerge due to hybridization of single-particle states near two opposite Fermi points, with the momentum transfer close to $2k_\mathrm{F} = \pi$. In the present model, there is only one Dirac point in the low-energy spectrum, and the particle-hole fields with momentum transfer π are all short-ranged. In fact, the appearance of the fermionic bilinear $\mathcal{N}_2$ in the asymptotic expressions (6.10)–(6.12) is entirely due to the τ-deformation of the kinetic energy (6.2), that is geometrical frustration of the zigzag ladder.

Using the results of the Sec. 1.3.1 we derive the bosonized expressions of the local physical operators:

$$\rho_\mathrm{tot}(x) = \sum_\sigma \rho_\sigma(x) = \sqrt{\frac{K}{\pi}}\partial_x\Phi(x), \tag{6.17}$$

$$\rho_\mathrm{rel}(x) = \sum_\sigma \sigma\rho_\sigma(x) = \frac{1}{v_\mathrm{F}}j_0(x) = -\frac{1}{\sqrt{1+\tau^2}}\Big[\frac{1}{\sqrt{\pi K}}\partial_x\Theta(x) - \Big(\frac{\tau}{\pi\alpha}\Big) : \cos\sqrt{4\pi K}\Phi(x) : \Big], \tag{6.18}$$

$$j_z(x) = -\frac{v_\mathrm{F}}{\sqrt{1+\tau^2}}\Big[\frac{\tau^2}{\sqrt{\pi K}}\partial_x\Theta(x) + \Big(\frac{\tau}{\pi\alpha}\Big) : \cos\sqrt{4\pi K}\Phi(x) : \Big], \tag{6.19}$$

$$B(x) = -\frac{1}{\pi\alpha} : \sin\sqrt{4\pi K}\Phi(x) : . \tag{6.20}$$

6.1.2 Bosonization of interactions

In the continuum limit, neglecting higher order corrections in a_0, the interaction term (4.3) in chain basis is given by

$$H_\mathrm{int} \to 2g\int \mathrm{d}x\,\rho_+(x)\rho_-(x) = \frac{g}{2}\int \mathrm{d}x\,\big[\big(:\Psi^\dagger\Psi:\big)^2 - \big(:\Psi^\dagger\hat\sigma^3\Psi:\big)^2\big], \quad g = Va_0, \tag{6.21}$$

Therefore the total Hamiltonian before the rotation becomes:

$$H[\Psi] = \int \mathrm{d}x\,\Big\{\Psi^\dagger(x)[-\mathrm{i}v_\mathrm{F}(\hat\sigma^3 + \tau\hat\sigma^2)\partial_x - m\hat\sigma^1]\Psi(x) + \frac{g}{2}\big(:\Psi^\dagger\Psi:\big)^2 - \frac{g}{2}\big(:\Psi^\dagger\hat\sigma^3\Psi:\big)^2\Big\}.$$

After the rotation with arbitrary angle γ, apart from usual interactions (forward- and back-scattering terms), one obtains terms proportional to

$$:\chi^\dagger\hat\sigma^3\chi::\chi^\dagger\hat\sigma^2\chi: = \big(J_\mathrm{R}(x) - J_\mathrm{R}(x)\big)\cdot\mathcal{N}_2(x). \tag{6.22}$$

In a usual scenario, such anomalous terms come with rapidly oscillating prefactor $(-1)^{x/a_0}$ and vanish on integration. However, in the present case, densities do not include rapidly oscillating staggered parts and (6.22) necessarily contribute to the Hamiltonian.

On the other hand, using Wick's theorem we derive the following OPE:[1]

$$:\chi^\dagger\hat\sigma^3\chi::\chi^\dagger\hat\sigma^2\chi: = \lim_{y\to x}\big(J_\mathrm{R}(x) - J_\mathrm{L}(x)\big)\cdot\mathcal{N}_2(y) = -\frac{\mathrm{i}}{\pi}\chi^\dagger\hat\sigma^2\partial_x\chi, \tag{6.23}$$

[1]Here we have used the following correlation functions of chiral fields:

$$\langle \mathrm{R}^\dagger(x)\mathrm{R}(y)\rangle = \langle \mathrm{R}(x)\mathrm{R}^\dagger(y)\rangle = \frac{\mathrm{i}}{2\pi}\frac{1}{x-y+\mathrm{i}\delta}; \quad \langle \mathrm{L}^\dagger(x)\mathrm{L}(y)\rangle = \langle \mathrm{L}(x)\mathrm{L}^\dagger(y)\rangle = -\frac{\mathrm{i}}{2\pi}\frac{1}{x-y-\mathrm{i}\delta}.$$

which exactly coincides with the frustration term in the kinetic energy. Therefore, the total Hamiltonian at an arbitrary angle of rotation admits the form:

$$\begin{aligned} H[\chi] = \int \mathrm{d}x \Big\{ \chi^\dagger(x)\Big[-\mathrm{i}v_\mathrm{F}\Big[\big(\cos\gamma + \tau\sin\gamma\big)\hat{\sigma}^3 + \\ + \Big(-\sin\gamma + \tau\cos\gamma + \frac{g}{\pi v_\mathrm{F}}\cos\gamma\sin\gamma\Big)\hat{\sigma}^2\Big]\partial_x - m\tau^x\Big]\chi(x) + \\ + \frac{g}{2}(:\chi^\dagger\chi:)^2 - \frac{g}{2}\cos^2\gamma(:\chi^\dagger\hat{\sigma}^3\chi:)^2 - \frac{g}{2}\sin^2\gamma(:\chi^\dagger\hat{\sigma}^2\chi:)^2 \Big\}. \end{aligned}$$

In order to eliminate $\hat{\sigma}^2$ term from the kinetic energy, we impose the condition

$$-\sin\gamma + \tau\cos\gamma + \frac{g}{\pi v_\mathrm{F}}\cos\gamma\sin\gamma = 0. \tag{6.24}$$

For small τ and weak interaction, $\sin\gamma \approx \gamma$, $\cos\gamma \approx 1$, and

$$\gamma \approx \tau\Big(1 + \frac{g}{\pi v_\mathrm{F}}\Big). \tag{6.25}$$

Therefore, in this order of accuracy, the appearance of an anomalous term in the interaction is equivalent to the following renormalization of the frustration parameter:

$$\tau \;\to\; \tau' = \tau + \frac{g\tau}{\pi v_\mathrm{F}}. \tag{6.26}$$

Assuming the suitable renormalizations being taken into account, we omit primes in what follows and write:

$$\begin{aligned} H[\Psi] = \int \mathrm{d}x \Big\{ \chi^\dagger(x)\big(-\mathrm{i}\bar{v}\hat{\sigma}^3\partial_x - m\tau^x\big)\chi(x) + \\ + \frac{g}{2}(\chi^\dagger\chi)^2 - \frac{g\cos^2\gamma}{2}(:\chi^\dagger\hat{\sigma}^3\chi:)^2 - \frac{g\sin^2\gamma}{2}(:\chi^\dagger\hat{\sigma}^2\chi:)^2 \Big\}, \end{aligned} \tag{6.27}$$

where $\bar{v} = v_\mathrm{F}\sqrt{1+\tau^2}$.

Now, by the Sugawara construction (1.42) the Hamiltonian admits the representation:

$$\begin{aligned} \mathscr{H}(x) &= \mathscr{H}_0(x) + \mathscr{H}_\mathrm{int}(x) \\ &= \pi v^* \left[:J_\mathrm{R}^2(x): + :J_\mathrm{L}^2(x):\right] - mB(x) + 2gJ_\mathrm{R}(x)J_\mathrm{L}(x) + \lambda\mathscr{O}_\mathrm{ph}(x), \end{aligned} \tag{6.28}$$

where the Dirac-mass operator $B(x)$ is defined in Eq. (6.8) and Eq. (6.13), $v^* = \bar{v} + \lambda/\pi$ is the Fermi velocity with an extra renormalization caused by interactions,

$$\lambda = \frac{\tau^2 g}{2(1+\tau^2)}, \tag{6.29}$$

and

$$\mathscr{O}_\mathrm{ph}(x) =: \Big(R^\dagger L\Big)_x \Big(R^\dagger L\Big)_{x+a} : + \mathrm{h.c.} \tag{6.30}$$

is the interband pair-hopping operator.

Using the transformation properties of the fermionic fields, chiral currents, and mass bilinears under $\mathscr{P}$ (see Eqs. (6.16)), we find that $[\mathscr{H}, \mathscr{P}] = 0$.

Following the standard bosonization rules summarized in Sec. 1.3.1, one readily finds that the fully bosonized effective Hamiltonian (6.28) has the structure of the DSG model [9, 10]:

$$\begin{aligned}\mathscr{H}(x) =& \frac{v_c}{2}\left[:\Pi^2(x): + :(\partial_x \Phi(x))^2:\right] \\ &+ \frac{m}{\pi\alpha} :\sin\sqrt{4\pi K}\Phi(x): - \frac{\lambda}{2(\pi\alpha)^2} :\cos\sqrt{16\pi K}\Phi(x):,\end{aligned} \tag{6.31}$$

where $v_c = v^*\left[1 + O(g^2)\right]$, and

$$K = 1 - \frac{g}{2\pi v^*} + O(g^2) \tag{6.32}$$

is the Luttinger-liquid parameter. It decreases upon increasing the interchain repulsion g; however, its parametrization Eq. (6.32) is only universal at small values of g. Since the model at hand is not integrable, the exact analytical expression of $K = K(g)$ beyond the weak coupling limit is not known. We need to rely on numerical tools to get the dependence of K at large values of g (see Fig. 6.1). Nevertheless, below we treat K as an independent phenomenological parameter of the model.

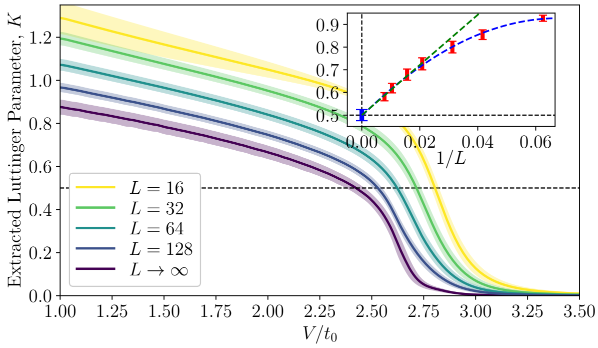

Figure 6.1: (Color online.) The extracted values of the Luttinger parameter K for different system sizes using the scaling form of the bipartite fluctuations of local U(1) operator O: $\mathscr{F}_l(O) = \langle(\sum_{n\le l} O_n)^2\rangle - \langle\sum_{n\le l} O_n\rangle^2 \sim \frac{K}{\pi^2}\ln\left[\frac{L}{\pi}\sin(\pi l/L)\right] + \text{const.}$ along the $m = 0$ line. The shaded regions denote the error bars. The estimated values of K in the thermodynamic limit have been extracted by using a linear function $f_1(1/L) = K_\infty + b/L$ and a quadratic function $f_2(1/L) = K_\infty + b/L + d/L^2$ in $1/L$ (see inset).

The first two terms in Eq. (6.31) represent the Gaussian part of the Hamiltonian, while the remaining nonlinear terms contribute to the potential

$$\mathscr{U}[\Phi] = \frac{m}{\pi\alpha} :\sin\sqrt{4\pi K}\Phi(x): - \frac{\lambda}{2(\pi\alpha)^2} :\cos\sqrt{16\pi K}\Phi(x):, \tag{6.33}$$

whose profile is determined by the relative strength and signs of the λ- and m-perturbations as explained in Sec. 2. In a strong coupling regime, the field Φ gets localized in one of the infinitely degenerate vacua of $\mathscr{U}[\Phi]$ thus determining the phase of the system. It is to be noted that when, in addition to V, the interaction also includes nearest-neighbor coupling along the chain,

$$H_\parallel = V_0 \sum_{j,\sigma} \hat{n}_{j,\sigma}\hat{n}_{j+1,\sigma}, \tag{6.34}$$

the DSG model (6.31) maintains its structure with a slightly modified velocity v_c and the parameter λ replaced by $\lambda = \tau^2(g - g_0)/2(1 + \tau^2)$, where $g_0 = V_0 a_0$.

6.2 Correlation effects

The relevance of the two operators entering the nonlinear potential $\mathscr{U}(\Phi)$ of the DSG model (6.31) is determined by their scaling dimensions: $d_m = K$ and $d_\lambda = 4K$. We will be mainly concerned with the case of a repulsive interchain interaction, $g > 0$, $K < 1$, and briefly comment on the attractive case $g < 0$, $K > 1$. At $K > 1/2$ the λ-term in (6.31), which describes interband pair-hopping processes, is irrelevant, and the properties of the model are determined by the single-particle mass perturbation. It is well known [102] that, in 1D models with short-range repulsive interactions, increasing local repulsion between the particles to push K to small enough values may not be enough; longer-range interaction should be also invoked. Therefore, we will phenomenologically assume that interaction in the model is generalized in such a way that the regime with $K < 1/2$, where the λ-perturbation becomes relevant, is feasible. In this case, the DSG model (6.31) describes the interplay of correlations and single-particle perturbations. Below we discuss the possible realization of different ground-state phases of the system.

6.2.1 $m = 0$ regime

This is the case of a symmetric TFL ($t_1 = t_2$, i.e., $m = 0$) in which bare fermions with momenta $k \sim \pi$ are massless. The effective Hamiltonian Eq. (6.31) reduces to a standard SG model (see appendix D):

$$\mathscr{H}(x) = \frac{v_c}{2}\left[\Pi^2(x) + (\partial_x \Phi(x))^2\right] - \frac{\lambda}{2(\pi\alpha)^2} :\cos\sqrt{16\pi K}\Phi(x):. \tag{6.35}$$

When interchain repulsion V is not strong enough and $K > 1/2$, the λ-perturbation is irrelevant, and in the infrared limit, the Hamiltonian Eq. (6.35) flows to a Gaussian model. The latter describes a TLL phase with a gapless spectrum of collective excitations and power-law correlations with K-dependent critical exponents. As follows from the definitions Eqs. (6.17)-(6.20), strong quantum fluctuations suppress any kind of ordering in the system, including charge imbalance between the legs of the ladder, dimerization along the zigzag links, and net current in the ground state. Within the range $1/2 < K < 1$, the τ-proportional part of the relative density Eq. (6.18) contributes to dominant correlations in the model: at distances $|x| > \alpha(K|\tau|)^{-\frac{1}{2(1-K)}}$ the corresponding correlation function follows the power law

$$\langle \rho_{\rm rel}(x)\rho_{\rm rel}(0)\rangle \simeq \frac{1}{2(\pi\alpha)^2}\frac{\tau^2}{1+\tau^2}\left(\frac{\alpha}{|x|}\right)^{2K}. \tag{6.36}$$

At $K < 1/2$, the λ-perturbation in Eq. (6.35) becomes relevant and the model flows towards strong coupling with a dynamical generation of a mass gap

$$m_\lambda \sim \frac{v_c}{\alpha}\left(\frac{|\lambda|}{v_c}\right)^{1/2(1-2K)}, \quad (K < 1/2). \tag{6.37}$$

Since $\lambda > 0$, the field Φ is locked in one of the infinitely degenerate vacuum values

$$(\Phi)_{\rm L} = \frac{1}{2}\sqrt{\frac{\pi}{K}}l, \quad l \in \mathbb{Z} \tag{6.38}$$

Therefore $\langle B_1\rangle = \langle B_2\rangle = 0$, but the average relative density turns out to be nonzero:

$$\langle \rho_{\mathrm{rel}}\rangle_\lambda = \pm\rho_0, \quad \rho_0 \sim |\tau|^{\frac{1-K}{1-2K}}. \tag{6.39}$$

According to Eqs. (6.18)-(6.19), the population imbalance between the chains is accompanied by a spontaneous generation of a net current

$$\langle j_0\rangle_\lambda = \langle j_z\rangle_\lambda = \frac{v_{\mathrm{F}}}{\pi\alpha}\frac{\tau}{1+\tau^2}\langle :\cos\sqrt{4\pi K}\Phi(x):\rangle_\lambda. \tag{6.40}$$

The spontaneous relative density, and hence the current, are non-analytic functions of the frustration parameter τ. Being zero at $K > 1/2$, they exponentially increase on decreasing K in the region $K < 1/2$ following the law Eq. (6.39). The quantum phase transition taking place at $K = 1/2$ belongs to the BKT universality class [99, 102].

Elementary excitations of the charge-transfer phase are topological quantum solitons of the SG model Eq. (6.35). They carry the mass given by Eq. (6.37) and a fractional fermionic number $Q_s = 1/2$. This number is identified with the topological charge of the soliton which interpolates between neighboring vacua of the cosine potential $\cos\sqrt{16\pi K}\Phi$:

$$Q_s = \sqrt{\frac{K}{\pi}}\int_{-\infty}^{\infty}\mathrm{d}x\ \partial_x\Phi(x) = \frac{1}{2}. \tag{6.41}$$

6.2.2 $m \neq 0$ regime with $K > 1/2$

At $K > 1/2$ and $m \neq 0$ the interband pair-hopping processes are irrelevant, and the effective theory is given by the SG model:

$$\mathscr{H}(x) = \frac{v_c}{2}\left[\Pi^2(x) + (\partial_x\Phi(x))^2\right] + \left(\frac{m}{\pi\alpha}\right) :\sin\sqrt{4\pi K}\Phi(x):. \tag{6.42}$$

It describes a bosonized version of the theory of marginally perturbed massive fermions – the so-called massive Thirring model [103]. The scalar field Φ is locked in one of the infinitely degenerate vacua

$$(\Phi)_l^{\mathrm{vac}} = \sqrt{\frac{\pi}{K}}\left(-\frac{1}{4}\mathrm{sgn}(m) + l\right), \quad l \in \mathbb{Z}. \tag{6.43}$$

Eq. (6.43) displays two subsets of the vacua corresponding to different signs of m, each subset describing a band insulator. The excitation spectrum has a mass gap m_s:

$$m_s = C(K)\left(\frac{v_c}{\alpha}\right)\left(\frac{|m|\alpha}{v_c}\right)^{1/(2-K)}\mathrm{sgn}(m), \tag{6.44}$$

where $C(K)$ is a dimensionless constant tending to 1 as $K \to 1$. The mass term in Eq. (6.42) explicitly breaks parity and, according to Eq. (6.13) and Eq. (6.20), leads to a finite dimerization $\langle B\rangle$ of the zigzag bonds of the ladder:

$$\langle B\rangle \sim |m_s|^K \mathrm{sgn}(m) \sim |m|^{K/(2-K)}\mathrm{sgn}(m). \tag{6.45}$$

The quantum soliton of the SG model Eq. (6.42) carries the mass m_s and topological charge $Q_{\mathrm{F}} = 1$ and thus is identified as the fundamental fermion of the related massive Thirring model [103].

In the ground state $\langle \partial_x \Phi \rangle = \langle \partial_x \Theta \rangle = 0$. Moreover, for the vacuum values of the field Φ given by Eq. (6.43) the average $\langle \cos\sqrt{4\pi K}\Phi \rangle$ vanishes. So at $\rho = 1$ and $m \neq 0$ the total and relative densities remain unaffected by the flux. Correlations of the relative density are short-ranged.

Thus, at $m \neq 0$ the SG model Eq. (6.42) describes band insulator phases. Their thermodynamic properties depend only on the magnitude of the spectral gap $|m_s|$, while their topological properties are determined by the sign of the bare mass m. With the sign of the "heavy" mass fixed ($M > 0$), the band insulator phase at $m > 0$ is topologically trivial, whereas the corresponding phase at $m < 0$ is topologically nontrivial as it has been shown in Sec. 5.5 by analysis of the non-interacting model.

A more complete characterization of the two band insulating phases described by the SG model in Eq. (6.42) is extracted from the mass dependence of non-local order parameters [104] – the parity ($\hat{O}_P$) and string-order ($\hat{O}_S$) operators:

$$\hat{O}_P(j) = \exp\left(i\pi \sum_{k\leq j} \delta\hat{n}_k\right), \quad \hat{O}_S(j) = \hat{O}_P(j)\delta\hat{n}_j. \tag{6.46}$$

Here j labels the diatomic unit cells of the ladder, and $\delta\hat{n}_j = \sum_\sigma : c^\dagger_{j\sigma} c_{j\sigma} :$ is the density fluctuation on the zigzag rung j. Non-local string and parity orders have been considered earlier for interacting bosons [105, 106, 107, 108] to specify the differences between the Mott and Haldane insulator gapped phases. It was shown that the two non-local order parameters are dual to each other [106]: $\langle \hat{O}_P \rangle \neq 0$, $\langle \hat{O}_S \rangle = 0$ for the Mott insulator, and $\langle \hat{O}_P \rangle = 0$, $\langle \hat{O}_S \rangle \neq 0$ for the Haldane insulator. Non-local parity and string order have been shown to characterize strongly correlated states of interacting fermions in strictly 1D systems [109, 110], as well as in fermionic ladder models [111, 112, 113]. A significant progress in the direct measurement of non-local parity and string correlations in low-dimensional ultra-cold Fermi and Bose systems has recently been reported [114, 115, 70, 116, 117].

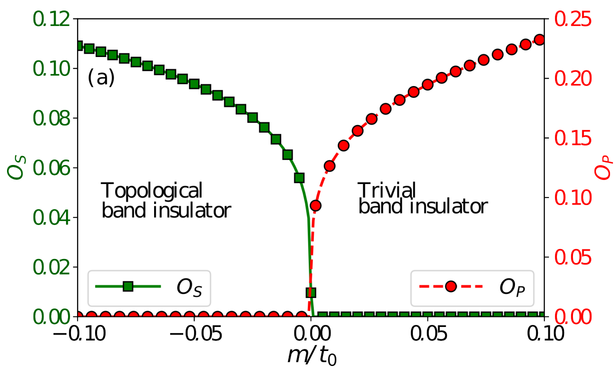

Figure 6.2: (Color online.) Numerical results for the string $\mathcal{O}_S$ and parity $\mathcal{O}_P$ correlations for varying m/t_0 and fixed $V/t_0 = 2$.

The string and parity order parameters, Eqs. (6.46), being non-local in terms of the densities $\hat{n}_k$, admit a local representation in terms of vertex operators of the effective SG model. In both Bose [106] and Fermi [113] cases, the perturbation to the Gaussian Hamiltonian for the field Φ was defined as $m\cos\sqrt{4\pi K}\Phi$, with the Luttinger-liquid constant K being close to 1. Using Abelian bosonization, with such a definition, one shows that in the continuum limit

$$\hat{O}_P(x) \sim \sin\sqrt{\pi K}\Phi(x), \quad \hat{O}_S(x) \sim \cos\sqrt{\pi K}\Phi(x). \tag{6.47}$$

However, in the SG model of Eq. (6.42) the perturbation is of the form $m\sin\sqrt{4\pi K}\Phi$. Therefore the bosonic representation of the operators $\hat{O}_P$ and $\hat{O}_S$ must be modified. The sine transforms to a cosine under the shift $\Phi \to \Phi - (1/4)\sqrt{\pi/K}$, implying the following the redefinition of the non-local order parameters

$$\begin{aligned}\hat{O}_P &\to \frac{1}{\sqrt{2}}\Big(\sin\sqrt{\pi K}\Phi - \cos\sqrt{\pi K}\Phi\Big),\\ \hat{O}_S &\to \frac{1}{\sqrt{2}}\Big(\cos\sqrt{\pi K}\Phi + \sin\sqrt{\pi K}\Phi\Big).\end{aligned} \tag{6.48}$$

Using the fact that in the ground state of the SG model (6.42) the vacuum values of the field Φ are given by Eq. (6.43), we conclude that the expectation values of $\hat{O}_P$ and $\hat{O}_S$ are given by

$$\begin{aligned}\big\langle \hat{O}_P(m;l)\big\rangle &= (-1)^{l-1}F(m)\theta(m),\\ \big\langle \hat{O}_S(m;l)\big\rangle &= (-1)^{l}F(m)\theta(-m),\end{aligned} \qquad l \in \mathbb{Z}, \tag{6.49}$$

where at $|m|\alpha/v \ll 1$ (i.e., in the vicinity of the Gaussian line $m = 0$) and

$$F(m) \sim \left(\frac{|m|\alpha}{v}\right)^{\frac{K}{4(2-K)}}.$$

Thus, the band insulator phase with $m > 0$ ($t_1 > t_2$) is topologically trivial ($\langle\hat{O}_S\rangle = 0$) and characterized by a non-zero non-local parity order ($\langle\hat{O}_P\rangle \neq 0$), whereas the phase with $m < 0$ ($t_1 < t_2$) represents a topological insulator with a non-zero string order ($\langle\hat{O}_S\rangle \neq 0$) but lacks parity order ($\langle\hat{O}_P\rangle = 0$).

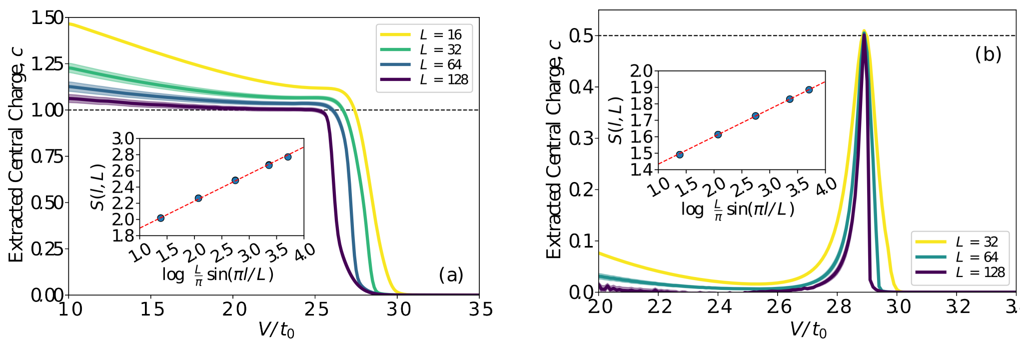

(a) (b)

Figure 6.3: (Color online.) Numerical values of the central charge for different system sizes for (a) $m = 0$ and (b) $m = 0.1t_0$. The critical line at $m = 0$ has central charge $c = 1$, i.e., a U(1) Gaussian criticality, while the bifurcated critical lines at $m \neq 0$ belong to the Ising universality class having the central charge $c = 1/2$. The shaded regions mark the errors in the fitting procedure. (Insets) The fitting of the entanglement entropy according to the equation $S(l,L) = \frac{c}{3}\ln\left[\frac{L}{\pi}\sin(\pi l/L)\right] + b'$, for (a) $m = 0$ and $V/t_0 = 2.3$ resulting in $c = 1.00(2)$, and (b) $m = 0.1t_0$ and $V/t_0 = 2.89$ resulting in $c = 0.50(1)$. For the insets, we have chosen the data for $L = 128$.

6.2.3 $m \neq 0$ regime with $K < 1/2$

The most interesting situation arises when both perturbations of the DSG model in Eq. (6.31) are relevant. This case can be realized when the interchain repulsion satisfies the condition $g \geq g_c$, where g_c is a non-universal value of the coupling constant such that $K(g_c) = 1/2$. At

$\lambda > 0$ the DSG potential of Eq. (6.31) is shown in Fig. 6.4. It represents a sequence of double-well potentials of the $\mathbb{Z}_2$-symmetric Ginzburg-Landau theory with the minima merging into ϕ^4 local wells at $2\pi\alpha m/\lambda = 4$. These semi-classical considerations (see Sec.2.1) lead to the conclusion that at $\lambda > 0$ the interplay of the two perturbations of the DSG model is resolved as the appearance of quantum criticalities belonging to the Ising universality class with central charge $c = 1/2$ [9].

As pointed out in Ref. [9], at a quantum level, the infrared behavior of the DSG model is determined by the ratio of the mass gaps separately generated by each of the two perturbations in the absence of the other. The parameter $\varrho \sim |m_s/m_\lambda|$ controls the two perturbative regimes of the DSG model ((6.31)): $\varrho \to 0$ and $\varrho \to \infty$. The Ising transitions occur in a non-perturbative region where the two masses are of the same order. The condition $\varrho \sim 1$ gives an order-of-magnitude estimate of the critical curves on the plane (λ, m):

$$m = \pm m^*(\lambda), \quad m^*(\lambda) \sim \frac{v_c}{\alpha}\left(\frac{\lambda}{v_c}\right)^{\frac{2-K}{2(1-2K)}}. \tag{6.50}$$

The two critical lines Eq. (6.50) separate the band-insulator phases, $|m| > m^*(\lambda)$, from the mixed phase occupying the region $-m^*(\lambda) < m < m^*(\lambda)$, in which charge imbalance coexists with dimerization of the zigzag bonds. As shown in Fig. 6.4, in the mixed phase the minima of the DSG potential decouple into two subsets

$$(\Phi)_k^{\mathrm{odd}} = \frac{1}{2}\sqrt{\frac{\pi}{K}}\left(2k+1+\frac{\eta}{\pi}\right), \quad (\Phi)_k^{\mathrm{even}} = \frac{1}{2}\sqrt{\frac{\pi}{K}}\left(2k-\frac{\eta}{\pi}\right), \tag{6.51}$$

where $k = 0, \pm1, \pm2, \ldots$ and $\eta = a/4 = 2\pi\alpha m/4\lambda$. Accordingly, there are two types of massive topological excitations carrying η-dependent fractional charge. These kinks are associated with the vacuum-vacuum interset transitions $(\Phi)_k^{\mathrm{odd}} \leftrightarrow (\Phi)_{k,k+1}^{\mathrm{even}}$. The long kinks carry the charge $Q_+ = 1/2 + |\eta|/\pi$ and interpolate between the solitons of the $m = 0$ phase with spontaneously broken $\mathscr{P}$-symmetry ($Q = 1/2$) and single-fermion excitations of the band-insulator phase ($Q = 1$). On the other hand, on approaching the Ising criticality, the short kinks with the topological quantum number $Q_- = 1/2 - |\eta|/\pi$ lose their charge and mass and transform to a neutral collective excitonic mode.

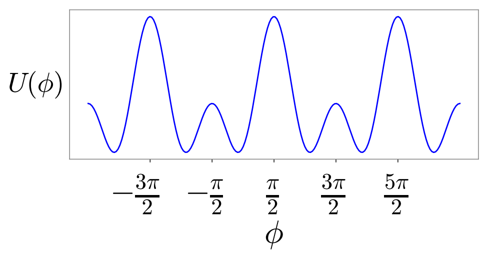

Figure 6.4: A pictorial representation of the potential $U(\phi) = a\sin\phi - \cos 2\phi$, $\phi = \sqrt{4\pi K}\Phi$, $a = (2\pi\alpha)m/\lambda$.

According to the analysis done in [10], in the vicinity of the critical lines Eq. (6.50) the gapped phases in the regions $|m| > m^*$ and $|m| < m^*$ are identified as Ising ordered and disordered phases, respectively. Near the transition the average relative density $:\rho_{\mathrm{rel}}(x):$ behaves as the disorder operator $\mu(x)$ of the underlying quantum Ising model [10]. Therefore, the phases realized at $|m| > m^*$ are the already discussed zigzag-dimerized insulating phases with equally populated chains: $\langle:\rho_{\mathrm{rel}}:\rangle = 0$. At $|m| < |m^*|$ the relative density acquires a finite expectation value which vanishes as

$$\langle:\rho_{\mathrm{rel}}:\rangle \sim (|m^*| - |m|)^{1/8} \tag{6.52}$$

on approaching the critical point from below: $|m| \to |m^*| - 0$.

The two Ising critical lines merge at the point $m = 0$, $K = 1/2$ and, as shown in Fig. 4.2 transform to a Gaussian critical line $m = 0$, $K > 1/2$ which describes a TLL phase. As it has been shown in chapter 2, *that the merging point of the Ising critical lines represents a bifurcation point of the AT model where the symmetry is enlarged to SU(2).*

6.3 Conclusions and outlook

In this thesis, we studied the phase diagram of a system of interacting spinless fermions on a two-leg triangular ladder at half-filling, with uniform t_0 intrachain and alternating $t_{1,2}$ interchain nearest-neighbor tunneling amplitudes, $f = 1/2$ magnetic flux per triangular plaquette (in units of π), and V nearest-neighbor density-density interchain interaction. It has been shown that the model exhibits interesting properties originating from the interplay of geometrical frustration of the lattice, the external magnetic flux, and dynamic correlations between fermions. The main results of our study apply to a broader class of frustrated ladders which can be unified into an asymmetric Creutz model depicted in Fig. 5.1, the TFL being the most frustrated member of this family. Contrary to the standard (rectangular) ladder, in a TFL the $k \to \pi - k$ particle-hole symmetry of the two-band spectrum is absent. At a weak interchain hopping qualitative differences between the two systems become evident when the flux per the diatomic plaquette is close to the flux quantum. In this regime, the removal of the double degeneracy of the spectral gap in the non-interacting limit leads to the appearance of two groups of low-energy Dirac-like excitations with different masses. Even for a nearly half-filled spectrum, this leads not to a single metal-insulator transition as in the standard ladder, but to a cascade of flux-induced Lifshitz transitions that separate phases with the number of Fermi points equal to 4, 2, 1, or 0, the latter case corresponding to the band insulator phase. The transitions take place when the flux is varied. At the critical points the orbital current and its derivative, the charge stiffness, display singular behavior: universal square-root singularities of the "commensurate-incommensurate" transition type when the chemical potential μ is constant, or cusps when a system is considered at a fixed particle density ρ. We have shown that the TFL displays a generic property that follows from the absence of $k \to \pi - k$ particle-hole symmetry – different patterns of Lifshitz transitions at a particle ($\rho > 1$) and hole ($\rho < 1$) doping.

Remarkably, for a translationally invariant TFL ($m = t_1 - t_2 = 0$) and the flux close to the value $f = 1/2$, the excitations close to the Brillouin zone boundary ($k = \pi$) become gapless and, in the low-energy limit, transform to a massless Dirac fermion. Such a system is very susceptible to inter-particle correlations.

At the microscopic level, the model exhibits a U(1) symmetry pertaining to the conservation of total fermion number and a $\mathbb{Z}_2$ symmetry – a combined parity transformation and the chain exchange operation.

To obtain the phase diagram, we use the bosonization approach in the weakly interacting regime ($|V| \ll t_0$), with $0 < t_{1,2} \ll t_0$ and $|t_1 - t_2| \ll t_1 + t_2$, and map the model onto the DSG model. We analytically predict various properties of the system, by utilizing the symmetries of the original lattice model, and RG analysis for the bosonized version. Specifically, for $t_1 \neq t_2$ and sufficiently weak repulsive interaction $V \ll V_c$, the system is a band insulator. If additionally $t_1 > t_2$ is the case, then the phase is a trivial band insulator with non-zero dimerization along t_1 links. If $t_1 < t_2$ holds, then the phase is instead a topological band insulator, with non-zero dimerization along t_2 links, and displays edge states for open boundary conditions. For $t_1 = t_2$, the system is described by a Gaussian model with central charge $c = 1$, separating two band insulator phases.

The Gaussian critical line for $t_1 = t_2$ terminates at $V = V_c$, where the symmetry of the system is enlarged from $\mathbb{Z}_2 \times \mathrm{U}(1)$ to SU(2), with the underlying field theory of the model corresponding to $\mathrm{SU}(2)_1$ WZNW model. This emergent non-Abelian SU(2) invariance, which is absent in the microscopic description of the system, is a remarkable effect coming from the interplay between the geometric frustration, magnetic flux, and many-body correlations.

At this $t_1 = t_2$ regime, when crossing $V = V_c$ critical point, the system undergoes a Berezinskii-Kosterlitz-Thouless transition to a gapped phase, with spontaneously broken $\mathbb{Z}_2$ symmetry. In this phase, we observe non-zero charge imbalance (i.e., a net relative density between the two chains) and total current along the chains. Additionally, the Gaussian critical line, terminated at emergent $\mathrm{SU}(2)_1$ symmetric point, bifurcates into two Ising critical lines, with central charge $c = 1/2$, similar to what is seen in the AT model. These Ising critical lines separate the strong-coupling symmetry-broken phase from the band insulators. Our work provides a unique example of non-Abelian SU(2) symmetry emerging in a fundamentally Abelian system.

Numerical simulations based on tensor network states, conducted by colleagues: Mikheil Tsitsishvili, Emanuele Tirrito, Marcello Dalmonte, and Titas Chanda, have fully confirmed our analytical predictions [2].

The model is based on experimental setups with cold atom gases in optical lattices, in the presence of off-resonant laser driving to Rydberg states. The regime of parameters under consideration is in principle accessible experimentally [65, 79, 88, 82, 118].

From the theoretical point of view, the solution of the two-leg TFL is expected to represent a building block for solving frustrated flux ladders with a larger number of chains. It is very interesting to formulate a field-theoretical approach to study non-perturbative effects in weakly coupled multi-chain ladders using methods of Abelian and non-Abelian bosonization [99]. A very different and complicated is the problem of frustrated ladders with a staggered flux. Here one faces a completely different physics already at the level of noninteracting fermions. One of the most challenging issues here is a chiral asymmetry of the spectrum and the breakdown of Lorentz invariance. Investigating the Hubbard model on a TFL constitutes one of the promising directions from our standpoint. An analytical study, using the bosonization method, predicts an interesting phase diagram consisting of trivial and topological band-insulating phases as well as a spontaneously broken symmetry phase with charge imbalance and nonzero total current.

Appendices

A Jordan-Wigner transformation

U(1) symmetric Heisenberg spin chain, usually referred to as an XXZ model, is described by the following Hamiltonian:

$$\begin{aligned}\mathscr{H}_{\mathrm{XXZ}} &= J\sum_{j=1}^{N}\left[S_j^x S_{j+1}^x + S_j^y S_{j+1}^y + \Delta S_j^z S_{j+1}^z\right] - h\sum_j S_j^z = \\ &= J\sum_{j=1}^{N}\left[\frac{1}{2}\left(S_j^+ S_{j+1}^- + S_j^- S_{j+1}^+\right) + \Delta S_j^z S_{j+1}^z\right] - h\sum_{j=1}^{N} S_j^z,,\end{aligned} \tag{A.1}$$

where $\mathbf{S}_j = (S_j^x, S_j^y, S_j^z)$ is spin-1/2 operator at cite j, $S_j^\pm \equiv S_j^x \pm \mathrm{i} S_j^y$ are spin rising/lowering operators, while $J > 0$ and h are exchange interactions between neighboring spins and an external magnetic field, respectively.

Usually, the first and last spins are identified, $\mathbf{S}_1 = \mathbf{S}_{N+1}$. In other words, periodic boundary conditions are imposed:

$$\mathbf{S}_{j+N} = \mathbf{S}_j. \tag{A.2}$$

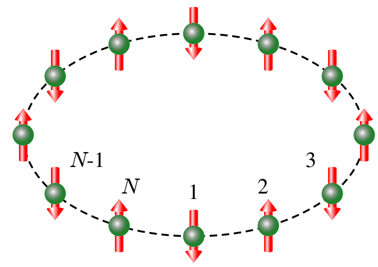

Figure 6.5: (Color online) Heisenberg spin chain with periodic boundary conditions.

Hence, the system has a ring geometry pictorially shown in Fig. 6.5. spin-1/2 has a remarkable property that its components alongside the usual SU(2) **commutation** algebra satisfy the **anticommutation** relations as well. In terms of ladder operators, the algebra has the following form:

$$[S_i^+, S_j^-] = 2\delta_{ij} S_j^z, \quad [S_i^z, S_j^\pm] = \pm\delta_{ij} S_j^\pm, \quad \{S_j^+, S_j^-\} = \mathbb{1}, \quad \{S_j^z, S_j^\pm\} = 0. \tag{A.3}$$

The U(1) symmetry is generated by the z-component of the total spin (the conserved charge) $S^z = \frac{1}{N}\sum_{j=1}^{N} S_j^z$, as a spin rotation around z-axes:

$$e^{\mathrm{i}\alpha S^z} S_j^\pm e^{-\mathrm{i}\alpha S^z} = e^{\pm\mathrm{i}\alpha} S_j^\pm, \quad e^{\mathrm{i}\alpha S^z} S_j^z e^{-\mathrm{i}\alpha S^z} = S_j^z. \tag{A.4}$$

with arbitrary angle $\alpha \in [0, 2\pi)$.

Full rotational symmetry is restored in the isotropic limit $\Delta = h = 0$:

$$\mathscr{H}_{\mathrm{XXX}} = J\sum_{j=1}^{N} \mathbf{S}_j \cdot \mathbf{S}_{j+1}. \tag{A.5}$$

Specifically, (A.5) is invariant under the full **non-Abelian** SU(2) group generated by all three components of the total spin operator:

$$S^a = \frac{1}{N}\sum_{j=1}^{N} S_j^a, \quad a = x, y, z. \tag{A.6}$$

Nontrivial commutation properties of spin operators (Eqs. (A.3)) allow mapping of the XX Hamiltonian onto the model of free spinless fermions, established by the so-called **Jordan-Wigner** (JW) transformation:

$$S_j^+ = c_j^\dagger \exp\left\{-\mathrm{i}\pi \sum_{n=1}^{j-1} c_n^\dagger c_n\right\}, \quad S_j^- = \left(S_j^+\right)^\dagger, \quad S_j^z = \frac{1}{2}[S_j^+, S_j^-] = c_j^\dagger c_j - \frac{1}{2}. \tag{A.7}$$

The exponential factor guarantees the correct transmutation of the spin algebra into fermion anti-commutation algebra (1.2) and vise versa.

Hence (A.1) becomes

$$\mathscr{H}_{\mathrm{XX}} = t\sum_{j=1}^{N}\left(c_j^\dagger c_{j+1} + c_{j+1}^\dagger c_j\right) + V\sum_{j=1}^{N}\left(n_j - \frac{1}{2}\right)\left(n_{j+1} - \frac{1}{2}\right) - \mu\sum_{j=1}^{N}\left(n_j - \frac{1}{2}\right), \tag{A.8}$$

where $t = J/2$, $V = J\Delta$ and $\mu = h$. The boundary conditions in terms of fermions depend on fermion parity

$$c_{j+N} = c_j, \quad \text{for } N_e \text{ odd}, \tag{A.9}$$

$$c_{j+N} = -c_j, \quad \text{for } N_e \text{ even}. \tag{A.10}$$

B Hubbard model

The simplest generalization of fermion models discussed so far to incorporate electron spin, is described by the following Hamiltonian known as the Hubbard model[119]:

$$\mathscr{H}_{\mathrm{H}} = -t\sum_{j=1}^{N}\sum_{\sigma=\uparrow,\downarrow}\left(c_{j,\sigma}^\dagger c_{j+1,\sigma} + \mathrm{h.c.}\right) + U\sum_{j=1}^{N} n_{j,\uparrow} n_{j,\downarrow} \tag{B.1}$$

where $c_{j,\sigma}^\dagger$ creates electron with spin projection $\sigma = \uparrow, \downarrow$, $n_{j,\sigma} = c_{j,\sigma}^\dagger c_{j,\sigma}$ is its density, while

$$n_j = n_{j,\uparrow} + n_{j,\downarrow} \tag{B.2}$$

is total electron density at site j. The electron spin operator on site j is defined by (1.98) or explicitly

$$S_j^+ \equiv S_j^x + \mathrm{i}S_j^y = c_{j,\uparrow}^\dagger c_{j,\downarrow}, \quad S_j^- \equiv \left(S_j^+\right)^\dagger, \quad S_j^z = \frac{1}{2}\left(n_{j,\uparrow} - n_{j,\downarrow}\right). \tag{B.3}$$

Obviously, electron spins satisfy usual spin algebra (A.3).

Hamiltonian (B.1) for arbitrary filling is U(1)⊗SU(2) invariant:

$$c_{j,\sigma} \longrightarrow e^{-\mathrm{i}\alpha} c_{j,\sigma}, \quad e^{\mathrm{i}\alpha} \in U(1); \tag{B.4}$$

$$c_{j,\sigma} \longrightarrow g_{\sigma\sigma'} c_{j,\sigma'}, \quad g \in SU(2). \tag{B.5}$$

generated by the total charge and spin operators,[2]

$$N_e = \sum_{j=1}^{N} n_j, \quad [\mathscr{H}_{\mathrm{H}}, N_e] = 0, \tag{B.6}$$

$$\mathbf{S} = \sum_{j=1}^{N} \mathbf{S}_j, \quad [\mathscr{H}_{\mathrm{H}}, \mathbf{S}] = 0, \tag{B.7}$$

respectively.

Particle-hole (ph) transformation,

$$c_{j,\sigma} \to (-1)^j c^\dagger_{j,\sigma}, \quad n_{j,\sigma} \to 1 - n_{j,\sigma}, \tag{B.8}$$

maps the Hubbard model as

$$\mathscr{H}_{\mathrm{H}}(t,U) \to \mathscr{H}_{\mathrm{H}}(t,U) + U(N - N_e). \tag{B.9}$$

At the half-filling $N = N_e$, the transformed Hamiltonian is identical to the original one and the system has ph symmetry.

The following important note should be made. In the case of a half-filled band, on-site repulsion tends to "freeze" one electron per site in the sense that pair creation costs energy penalty equal to U. This so-called, **Mott insulator** phase is characterized by 2^N-fold degenerate ground state. However, even small kinetic processes may result in electron delocalization, which is possible only when electrons confined in neighboring sites have opposite spins so the Pauli exclusion principle is respected. This way, the Mott insulator phase is antiferromagnetic. Perturbation expansion up to second-order in t/U gives the following Hamiltonian:

$$\mathscr{H}^{(2)} = J \sum_j \mathbf{S}_j \cdot \mathbf{S}_{j+1}, \tag{B.10}$$

which is identical to (A.5) with $J = \frac{4t^2}{U}$. This final observation is of fundamental importance in the non-Abelian bosonization of Heisenberg models.

In addition to (B.3), there is one more set of operators, the so-called pseudo-spin, given by:

$$\tilde{S}^+_j = (-1)^j c^\dagger_{j,\uparrow} c^\dagger_{j,\downarrow}, \quad \tilde{S}^-_j = (-1)^j c_{j,\downarrow} c_{j,\uparrow}, \quad \tilde{S}^z_j = \frac{1}{2}[\tilde{S}^+_j, \tilde{S}^-_j] = \frac{1}{2}(n_{j,\uparrow} + n_{j,\downarrow} - 1), \tag{B.11}$$

which constitute SU(2) algebra in the charge sector. In the half-filled Hubbard model, ph transformation in only one spin sector, say for $\sigma = \downarrow$,

$$c_{j,\downarrow} \to (-1)^j c^\dagger_{j,\downarrow}, \tag{B.12}$$

maps spin and the pseudo-spin operators onto each other,

$$\tilde{\mathbf{S}}_j \longleftrightarrow \mathbf{S}_j, \tag{B.13}$$

while at the same time, attractive and repulsive cases are interchanged:

$$\mathscr{H}_{\mathrm{H}}(t,U) \to \mathscr{H}_{\mathrm{H}}(t,-U) + UN_e. \tag{B.14}$$

Therefore, the half-filled Hubbard model has a larger $SU(2)_{\mathrm{charge}} \otimes SU(2)_{\mathrm{spin}}$ symmetry.

[2]The SU(2) invariance becomes manifest expressing the Hubbard interaction in terms of spin using the identity $\mathbf{S}^2_j = -\frac{3}{2} n_{j,\uparrow} n_{j,\downarrow} + \frac{3}{4} n_j$, where N_e is the total number of electrons.

To be more precise, $SU(2)_{\text{charge}}$ is not exact. Only the third component of total pseudo-spin

$$\tilde{\mathbf{S}} = \sum_{j=1}^{N} \tilde{\mathbf{S}}_j, \tag{B.15}$$

and the Casimir operator $\tilde{\mathbf{S}}^2 = \frac{1}{2}(\tilde{S}^+\tilde{S}^- + \tilde{S}^-\tilde{S}^+) + (\tilde{S}^z)^2$ commute with the Hubbard Hamiltonian:

$$\left[\tilde{S}^z, \mathscr{H}_{\text{H}}\right] = \left[\tilde{\mathbf{S}}^2, \mathscr{H}_{\text{H}}\right] = 0, \tag{B.16}$$

while

$$\left[\mathscr{H}_{\text{H}}, \tilde{S}^{\pm}\right] = \pm U \tilde{S}^{\pm}. \tag{B.17}$$

Therefore the "charge sector" enjoys just $U(1)\otimes U(1)$ symmetry generated by $\tilde{S}^z$ and $\tilde{\mathbf{S}}^2$.

It is known that the low-energy effective Hamiltonian of the Hubbard model can be described by the two mutually commuting contributions describing the charge and spin collective modes:

$$\begin{aligned}
\mathscr{H}_{\text{H}} &= \mathscr{H}_c + \mathscr{H}_s, \\
\mathscr{H}_c &= \int \mathrm{d}x \left[\frac{2\pi v_c}{3}(:\mathbf{I}_{\text{R}}^2: + :\mathbf{I}_{\text{L}}^2:) + 2g\mathbf{I}_{\text{R}}\cdot\mathbf{I}_{\text{L}}\right], \\
\mathscr{H}_s &= \int \mathrm{d}x \left[\frac{2\pi v_s}{3}(:\mathbf{J}_{\text{R}}^2: + :\mathbf{J}_{\text{L}}^2:) - 2g\mathbf{J}_{\text{R}}\cdot\mathbf{J}_{\text{L}}\right],
\end{aligned} \tag{B.18}$$

where

$$\mathbf{J}_{\text{R}}(x) \equiv \frac{1}{2}\sum_{\alpha,\beta=\uparrow\downarrow} R^{\dagger}_{\alpha}(x)\hat{\boldsymbol{\sigma}}_{\alpha\beta}R_{\beta}(x), \quad \mathbf{J}_{\text{L}}(x) \equiv \frac{1}{2}\sum_{\alpha,\beta=\uparrow\downarrow} L^{\dagger}_{\alpha}(x)\hat{\boldsymbol{\sigma}}_{\alpha\beta}L_{\beta}(x), \tag{B.19}$$

are SU(2)$_1$ spin currents, while $\mathbf{I}_{\text{R,L}}$ are SU(2)$_1$ pseudo spin currents which can be obtained from (B.19) by the particle-hole transformation (B.12) in $\sigma = \downarrow$ sector only (or in terms of slow fields $R_{\downarrow} \to R^{\dagger}_{\downarrow}, L_{\downarrow} \to L^{\dagger}_{\downarrow}$):

$$\begin{aligned}
J^+_{\text{R}} = J^x_{\text{R}} + \mathrm{i}J^y_{\text{R}} &\to I^+_{\text{R}} = I^x_{\text{R}} + \mathrm{i}I^y_{\text{R}} = R^{\dagger}_{\uparrow}R^{\dagger}_{\downarrow}, \\
J^-_{\text{R}} = J^x_{\text{R}} - \mathrm{i}J^y_{\text{R}} &\to I^-_{\text{R}} = I^x_{\text{R}} - \mathrm{i}I^y_{\text{R}} = R_{\downarrow}R_{\uparrow}, \\
J^z_{\text{R}} &\to I^z_{\text{R}} = \frac{1}{2}\left(R^{\dagger}_{\uparrow}R_{\uparrow} + R^{\dagger}_{\downarrow}R_{\downarrow}\right),
\end{aligned} \tag{B.20}$$

and similarly for Left currents.

The charge and spin Hamiltonians in (B.18) are structurally identical except for the sign of the current-current interaction term. For arbitrary (small) positive repulsion $g > 0$, the current-current interaction in the charge sector is marginally relevant in the RG sense, while it is marginally irrelevant in the spin sector (see Fig. 1.4). As a result, the charge Hamiltonian flows towards a strong coupling regime characterized by a spectral gap in charge excitations while the spin sector remains gapless. Assuming the energy scale of interest is much smaller than the scale set by the spectral gap in the charge sector, one can neglect $\mathscr{H}_c$ and consider $\mathscr{H}_s$ as a low-energy effective model for SU(2) invariant Heisenberg spin chain (A.5).

C Basic facts on conformal invariance

This appendix presents some basic facts from CFT. For a detailed treatment see [5].

Near the quantum critical point of second order phase transition, the correlation length (of the physical system under consideration) diverges rendering the system scale invariant. That is the system observed at different length scales looks self-similar. Scale invariance in $(1+1)$-dimensional theories leads to the invariance of the theory under local conformal transformations

$$z \to w = f(z), \quad \bar{z} \to \bar{w} = \bar{f}(\bar{z}) \quad z = x + \mathrm{i}v\tau, \quad \bar{z} = x - \mathrm{i}v\tau, \tag{C.1}$$

where x is a space coordinate and τ is imaginary time (in a sense of Wick's rotation $t \to -\mathrm{i}\tau$) and $f(z)$ ($\bar{f}(\bar{z})$) is an arbitrary holomorphic (anti-holomorphic) function of complex coordinate z ($\bar{z}$).

In CFTs the notion of primary fields is of central importance. A field $\phi(z,\bar{z})$ is called primary if under (C.1) it transforms as

$$\phi_j(w,\bar{w}) \;=\; \left(\frac{\partial w}{\partial z}\right)^{-h_j} \left(\frac{\partial \bar{w}}{\partial \bar{z}}\right)^{-\bar{h}_j} \phi_j(z,\bar{z}), \tag{C.2}$$

where $h_j, \bar{h}_j \in \mathbb{R}$ are called holomorphic and anti-holomorphic conformal dimensions, respectively. Every CFT is characterized by a set of primary fields $\{\phi_j(z,\bar{z})\}$ and corresponding conformal dimensions $(h_j, \bar{h}_j)$. Correlation functions of primary fields can be obtained in a closed form based on symmetry arguments only. With the suitable normalization, the following OPE algebra is satisfied

$$\phi_j(z,\bar{z})\phi_{j'}(w,\bar{w}) \;\sim\; \frac{\delta_{j,j'}}{(z-w)^{2h_j}(\bar{z}-\bar{w})^{2\bar{h}_j}}. \tag{C.3}$$

It is understood that the relations are valid only inside correlation functions.

If (C.2) is satisfied for only global conformal transformations, $f(z) = \frac{az+b}{cz+d}$, $a,b,c,d \in \mathbb{Z}$, then the field $\phi(z,\bar{z})$ is said to be quasi-primary. The most important quasi-primary field in CFT is an energy-momentum tensor (EMT) with holomorphic and anti-holomorphic components denoted by $T(z) = -\frac{\pi}{2} : T^{\bar{z}\bar{z}} :$ and $\overline{T}(\bar{z}) = -\frac{\pi}{2} : T^{zz} :$, respectively. The OPE of EMT with the primary field ϕ has particularly simple form:

$$\begin{aligned} T(z)\phi(w,\bar{w}) \;&\sim\; \frac{h}{(z-w)^2}\phi(w,\bar{w}) + \frac{1}{z-w}\partial_w \phi(w,\bar{w}) + \cdots, \\ \overline{T}(\bar{z})\phi(w,\bar{w}) \;&\sim\; \frac{\bar{h}}{(\bar{z}-\bar{w})^2}\phi(w,\bar{w}) + \frac{1}{\bar{z}-\bar{w}}\partial_{\bar{w}} \phi(w,\bar{w}) + \cdots, \end{aligned} \tag{C.4}$$

where "$\cdots$" denotes regular (non-singular) contribution, while the OPE with itself

$$T(z)T(w) \;\sim\; \frac{1}{2}\frac{c}{(z-w)^4} + \frac{2T(w)}{(z-w)^2} + \frac{\partial T(w)}{z-w} \tag{C.5}$$

and identical expression for anti-holomorphic counterpart. The real constant c is called the central charge of the CFT and represents a measure of degrees of freedom in the theory.

Below we present three relevant to this thesis examples of CFTs.

C.1 Free Gaussian field

In Euclidean formalism, massless Gaussian field action can be recast in the following manifestly conformally invariant form

$$\mathcal{S}_{\mathrm{E}} = \int \mathrm{d}^2\mathbf{x}\,\mathscr{L}_{\mathrm{E}}, \quad \mathscr{L}_{\mathrm{E}} = 2\partial\Phi\bar{\partial}\Phi \tag{C.6}$$

where $\partial \equiv \frac{\partial}{\partial z}$ and $\bar{\partial} \equiv \frac{\partial}{\partial \bar{z}}$. The EMT of the Gaussian field is given by

$$T^{\mu\nu} = \frac{\partial \mathscr{L}_{\mathrm{E}}}{\partial(\partial_\mu \Phi)}\partial^\nu\Phi - g^{\mu\nu}\mathscr{L}_{\mathrm{E}}, \quad \mu,\nu = z,\bar{z}, \tag{C.7}$$

only nonzero components of which are

$$T^{\bar{z}\bar{z}} = 2\frac{\partial \mathscr{L}_{\mathrm{E}}}{\partial(\bar{\partial}\Phi)}\partial\Phi = 4(\partial\varphi_{\mathrm{L}})^2(z), \quad T^{zz} = 2\frac{\partial \mathscr{L}_{\mathrm{E}}}{\partial(\partial\Phi)}\bar{\partial}\Phi = 4(\bar{\partial}\varphi_{\mathrm{R}})^2(\bar{z}),$$

where

$$\partial\varphi_{\mathrm{L}}(z) \equiv \partial\Phi(z,\bar{z}) \quad \text{and} \quad \bar{\partial}\varphi_{\mathrm{R}}(\bar{z}) \equiv \bar{\partial}\Phi(z,\bar{z}). \tag{C.8}$$

Hence, the renormalized EMT is

$$T(z) = -\frac{\pi}{2}T^{\bar{z}\bar{z}} = -2\pi :(\partial\varphi_{\mathrm{L}})^2(z):, \quad T(\bar{z}) = -\frac{\pi}{2}T^{zz} = -2\pi :(\bar{\partial}\varphi_{\mathrm{R}})^2(\bar{z}):. \tag{C.9}$$

Now we consider OPEs of the EMT with various fields. Using the correlation functions of Gaussian fields

$$\langle \partial\varphi_{\mathrm{L}}(z)\partial\varphi_{\mathrm{L}}(w)\rangle = -\frac{1}{4\pi}\frac{1}{(z-w)^2}, \quad \text{and} \quad \langle \bar{\partial}\varphi_{\mathrm{R}}(\bar{z})\bar{\partial}\varphi_{\mathrm{R}}(\bar{w})\rangle = -\frac{1}{4\pi}\frac{1}{(\bar{z}-\bar{w})^2} \tag{C.10}$$

and Wick's theorem we write the following OPEs,

$$\begin{aligned} T(z)\partial\varphi_{\mathrm{L}}(w) &\sim \frac{\partial\varphi_{\mathrm{L}}(w)}{(z-w)^2} + \frac{\partial^2\varphi_{\mathrm{L}}(w)}{(z-w)}, & \overline{T}(\bar{z})\bar{\partial}\varphi_{\mathrm{R}}(\bar{w}) &\sim \frac{\bar{\partial}\varphi_{\mathrm{R}}(w)}{(\bar{z}-\bar{w})^2} + \frac{\bar{\partial}^2\varphi_{\mathrm{R}}(w)}{(\bar{z}-\bar{w})}, \\ T(z)\bar{\partial}\varphi_{\mathrm{R}}(\bar{w}) &\sim 0, & \overline{T}(\bar{z})\partial\varphi_{\mathrm{L}}(w) &\sim 0 \end{aligned} \tag{C.11}$$

Hence, the fields $\partial\varphi_{\mathrm{L}}(z)$ and $\bar{\partial}\varphi_{\mathrm{R}}(\bar{z})$ are primary fields of conformal dimensions $(1,0)$ and $(0,1)$, respectively. Note that the Gaussian fields $\Phi(z,\bar{z})$ and $\Theta(z,\bar{z})$ are not a primary fields!

Now using the following OPEs of $\partial\varphi_{\mathrm{L}}(z)$ and $\bar{\partial}\varphi_{\mathrm{R}}(\bar{z})$ with (1.74) normal ordered bosonic exponents

$$\begin{aligned} \partial\varphi_{\mathrm{L}}(z)e^{\mathrm{i}\beta\varphi_{\mathrm{L}}} &\sim -\frac{\mathrm{i}\beta}{4\pi}\frac{e^{\mathrm{i}\beta\varphi_{\mathrm{L}}}}{z-w}, & \bar{\partial}\varphi_{\mathrm{R}}(\bar{z})e^{\mathrm{i}\beta\varphi_{\mathrm{R}}} &\sim -\frac{\mathrm{i}\bar{\beta}}{4\pi}\frac{e^{\mathrm{i}\beta\varphi_{\mathrm{R}}}}{\bar{z}-\bar{w}}, \\ \bar{\partial}\varphi_{\mathrm{R}}(\bar{z})e^{\mathrm{i}\beta\varphi_{\mathrm{L}}} &\sim 0 & \partial\varphi_{\mathrm{L}}(z)e^{\mathrm{i}\beta\varphi_{\mathrm{R}}} &\sim 0. \end{aligned}$$

one obtains:

$$T(z)e^{\mathrm{i}\beta\varphi_{\mathrm{L}}(w)} \sim \frac{\beta^2}{8\pi}\frac{e^{\mathrm{i}\beta\varphi_{\mathrm{L}}(w)}}{(z-w)^2} + \frac{\partial e^{\mathrm{i}\beta\varphi_{\mathrm{L}}(w)}}{z-w}, \tag{C.12}$$

$$\overline{T}(\bar{z})e^{\mathrm{i}\beta\varphi_{\mathrm{R}}(\bar{w})} \sim \frac{\bar{\beta}^2}{8\pi}\frac{e^{\mathrm{i}\beta\varphi_{\mathrm{R}}(\bar{w})}}{(\bar{z}-\bar{w})^2} + \frac{\bar{\partial}e^{\mathrm{i}\beta\varphi_{\mathrm{R}}(\bar{w})}}{\bar{z}-\bar{w}}. \tag{C.13}$$

Therefore, vertex operators $e^{\mathrm{i}\beta\varphi_{\mathrm{L}}(w)}$ and $e^{\mathrm{i}\beta\varphi_{\mathrm{R}}(\bar{w})}$ are primary fields with conformal dimensions $(h_{\mathrm{L}},\bar{h}_{\mathrm{L}}) = (\beta^2/8\pi\,,0)$ and $(h_{\mathrm{R}},\bar{h}_{\mathrm{R}}) = (0,\,\bar{\beta}^2/8\pi)$, respectively. Therefore, their correlation functions admit the form:

$$\langle e^{\mathrm{i}\beta\varphi_{\mathrm{L}}(z)}e^{-\mathrm{i}\beta\varphi_{\mathrm{L}}(w)}\rangle = \left(\frac{\alpha}{z-w}\right)^{\frac{\beta^2}{4\pi}},\quad \langle e^{\mathrm{i}\bar{\beta}\varphi_{\mathrm{R}}(z)}e^{-\mathrm{i}\bar{\beta}\varphi_{\mathrm{R}}(\bar{w})}\rangle = \left(\frac{\alpha}{\bar{z}-\bar{w}}\right)^{\frac{\bar{\beta}^2}{4\pi}} \tag{C.14}$$

Finally, the OPE of the EMT with itself

$$T(z)T(w) = \frac{1}{2}\frac{1}{(z-w)^4} + \frac{2T(w)}{(z-w)^2} + \frac{\partial T(w)}{(z-w)} \tag{C.15}$$

shows that the conformal charge of a single free Gaussian field is $c_{\mathrm{Gauss}} = 1$.

C.2 Conformal invariance of Dirac field

The action functional of the free Dirac field(1.31) in the Euclidean space admits the expression

$$\mathcal{S}_{\mathrm{E}} = 2\int \mathrm{d}^2\mathbf{x}\,[\psi_{\mathrm{L}}^{\dagger}\bar{\partial}\psi_{\mathrm{L}} + \psi_{\mathrm{R}}^{\dagger}\partial\psi_{\mathrm{R}}]. \tag{C.16}$$

If we suppose that the chiral components transform according to the:

$$\psi'_{\mathrm{L}}(w) = \left(\frac{\mathrm{d}w}{\mathrm{d}z}\right)^{-\frac{1}{2}}\psi_{\mathrm{L}}(z),\quad \psi'_{\mathrm{R}}(\bar{w}) = \left(\frac{\mathrm{d}\bar{w}}{\mathrm{d}\bar{z}}\right)^{-\frac{1}{2}}\psi_{\mathrm{R}}(\bar{z}). \tag{C.17}$$

then the action is invariant under (C.1) transformation. Hence, the fields ψ_{L} and ψ_{R} are primary fields of conformal dimensions (1/2, 0) and (0, 1/2), respectively, obeying the OPE algebra:

$$\psi_{\mathrm{L}}^{\dagger}(z)\psi_{\mathrm{L}}(w) \sim \frac{1}{2\pi}\frac{1}{z-w},\quad \psi_{\mathrm{R}}^{\dagger}(\bar{z})\psi_{\mathrm{R}}(\bar{w}) \sim \frac{1}{2\pi}\frac{1}{\bar{z}-\bar{w}}. \tag{C.18}$$

Complex components of Dirac EMT are

$$\begin{aligned} T(z) &= -\pi\big[:\psi_{\mathrm{L}}^{\dagger}(\partial\psi_{\mathrm{L}}): - :(\partial\psi_{\mathrm{L}}^{\dagger})\psi_{\mathrm{L}}:\big]_z, \\ \overline{T}(\bar{z}) &= -\pi\big[:\psi_{\mathrm{R}}^{\dagger}(\bar{\partial}\psi_{\mathrm{R}}): - :(\bar{\partial}\psi_{\mathrm{R}}^{\dagger})\psi_{\mathrm{R}}:\big]_{\bar{z}}. \end{aligned} \tag{C.19}$$

similar to the derivation of the Sugawara form of the Dirac Hamiltonian, one can express EMT in terms of chiral currents:

$$T(z) = 2\pi^2 : J_{\mathrm{L}}^2(z):,\quad \overline{T}(\bar{z}) = 2\pi^2 : J_{\mathrm{R}}^2(\bar{z}):. \tag{C.20}$$

The following OPEs follow using Wick's theorem,

$$\begin{aligned} J_{\mathrm{L}}(z)J_{\mathrm{L}}(w) &\sim \frac{1}{4\pi^2}\frac{1}{(z-w)^2}, & J_{\mathrm{R}}(\bar{z})J_{\mathrm{R}}(\bar{w}) &\sim \frac{1}{4\pi^2}\frac{1}{(\bar{z}-\bar{w})^2} \\ T(z)J_{\mathrm{L}}(w) &\sim \frac{J_{\mathrm{L}}(w)}{(z-w)^2} + \frac{\partial J_{\mathrm{L}}(w)}{z-w}, & \overline{T}(\bar{z})J_{\mathrm{R}}(\bar{w}) &\sim \frac{J_{\mathrm{R}}(\bar{w})}{(\bar{z}-\bar{w})^2} + \frac{\partial J_{\mathrm{R}}(\bar{w})}{\bar{z}-\bar{w}} \end{aligned} \tag{C.21}$$

using which the OPE of EMT with itself obtains the form:

$$T(z)T(w) \sim \frac{1}{2}\frac{1}{(z-w)^4} + \frac{2T(w)}{(z-w)^2} + \frac{\partial T(w)}{z-w} \tag{C.22}$$

and similar expression for anti-holomorphic counterpart. Therefore, the central charge of a single Dirac fermion is $c_{\mathrm{Dirac}} = 1$.

It is worth noting that it is the properties of correlation and the equality of central charges $c_{\mathrm{Dirac}} = c_{\mathrm{Gauss}}$ that leads to the bosonization formulas(1.72) and (1.75). Indeed, the behavior of bosonic and fermionic correlations coincide with each other provided that $\beta = \bar{\beta} = 4\pi$ in (C.14).

C.3 Quantum Ising model

The quantum Ising model in 1D is given by the lattice Hamiltonian:

$$\mathcal{H}_{\text{QI}} = -\sum_j \left(J\sigma_j^x\sigma_{j+1}^x + h\sigma_j^z\right), \tag{C.23}$$

where σ_j^a are Pauli matrices at site j. As in the case of the Heisenberg model, we implement (A.7) JW transformation:

$$\sigma_j^x = (-1)^j\left(c_j^\dagger + c_j\right)\exp\left(\mathrm{i}\pi\sum_{i<j} c_i^\dagger c_i\right), \quad \sigma_j^z = 2c_j^\dagger c_j - 1,$$

to obtain:

$$\mathcal{H}_{\text{QI}} = \sum_j \left[J\left(c_j^\dagger c_{j+1} + c_j^\dagger c_{j+1}^\dagger + \text{h.c.}\right) - h(2c_j^\dagger c_j - 1)\right]. \tag{C.24}$$

Before taking the continuum limit, we rewrite the Ising Hamiltonian in the following form:

$$\mathcal{H}_{\text{QI}} = \sum_j \left[J\left(c_j^\dagger - c_j\right)\left(c_{j+1}^\dagger + c_{j+1}\right) - h\left(c_j^\dagger - c_j\right)\left(c_j^\dagger + c_j\right)\right].$$

The immediate observation is that the only linear combinations $c_j^\dagger \pm c_j$ of JW fermions are present in the Hamiltonian. This permits us to introduce real or **Majorana** fermions on the lattice

$$\zeta_j = c_j^\dagger + c_j, \quad \eta_j = -\mathrm{i}\left(c_j^\dagger - c_j\right), \quad \{\zeta_i, \zeta_j\} = \{\eta_j, \eta_j\} = 2\delta_{i,j}, \quad \{\zeta_i, \eta_j\} = 0, \tag{C.25}$$

in terms of which,

$$\mathcal{H}_{\text{QI}} = \mathrm{i}\sum_j \left[J\eta_j\left(\zeta_{j+1} - \zeta_j\right) - (h-J)\eta_j\zeta_j\right]. \tag{C.26}$$

Now we turn to the continuum limit,

$$a_0 \to 0, \quad J, h \to \infty, \quad 2Ja_0 = v, \quad 2(h-J) = m, \tag{C.27}$$

and introduce continuum fields by

$$\zeta_j \to \sqrt{2a_0}\zeta(x), \quad \eta_j \to \sqrt{2a_0}\eta(x), \tag{C.28}$$

$$\left\{\zeta(x), \zeta(y)\right\} = \left\{\eta(x), \eta(y)\right\} = \delta(x-y), \quad \left\{\zeta(x), \eta(y)\right\} = 0. \tag{C.29}$$

Thus, the following effective Hamiltonian is obtained:

$$\mathcal{H}_{\text{QI}} = \int \mathrm{d}x \left[\mathrm{i}v\eta(x)\partial_x\zeta(x) - \mathrm{i}m\eta(x)\zeta(x)\right]. \tag{C.30}$$

Introducing more familiar chiral basis by $\pi/4$-rotation:

$$\xi_{\text{R}} = \frac{\eta - \zeta}{\sqrt{2}}, \quad \xi_{\text{L}} = \frac{\eta + \zeta}{\sqrt{2}}, \tag{C.31}$$

we write:

$$\mathcal{H}_{\text{QI}} = \int \mathrm{d}x \left[\mathrm{i}\frac{v}{2}(:\xi_{\text{L}}\partial_x\xi_{\text{L}}: - :\xi_{\text{R}}\partial_x\xi_{\text{R}}:) - \mathrm{i}m\xi_{\text{R}}\xi_{\text{L}}\right]. \tag{C.32}$$

In the massless limit, $m = 0$ or $J = h$ (critical regime) chiral sectors decouple from each other, rendering the system conformally invariant. Starting from the corresponding Euclidean action,

$$\mathcal{S}_{\mathrm{QI}} = \int \mathrm{d}^2\mathbf{x}\, \mathscr{L}_{\mathrm{QI}}(\xi_{\mathrm{L}}, \xi_{\mathrm{R}}), \quad \mathscr{L}_{\mathrm{QI}}(\xi_{\mathrm{L}}, \xi_{\mathrm{R}}) \equiv : \xi_{\mathrm{L}} \bar{\partial} \xi_{\mathrm{L}} : + : \xi_{\mathrm{R}} \partial \xi_{\mathrm{R}} :, \tag{C.33}$$

one easily proves that the fields ξ_{L} and ξ_{R} are primary fields of conformal dimensions $(1/2, 0)$ and $(0, 1/2)$, respectively, and obey the OPE algebra:

$$\xi_{\mathrm{L}}(z)\xi_{\mathrm{L}}(w) \sim \frac{1}{2\pi}\frac{1}{z-w}, \quad \xi_{\mathrm{R}}(\bar{z})\xi_{\mathrm{R}}(\bar{w}) \sim \frac{1}{2\pi}\frac{1}{\bar{z}-\bar{w}}. \tag{C.34}$$

The EMT has the form

$$T(z) = -\pi : \xi_{\mathrm{L}} \partial \xi_{\mathrm{L}} :, \quad \overline{T}(\bar{z}) = -\pi : \xi_{\mathrm{R}} \bar{\partial} \xi_{\mathrm{R}} : . \tag{C.35}$$

Hence, using Wick's theorem, one easily derives the OPE of the EMT with itself

$$T(z)T(w) \sim \frac{1}{2}\frac{1/2}{(z-w)^4} + \frac{2T(w)}{(z-w)^2} + \frac{\partial T(w)}{z-w}, \tag{C.36}$$

and identical expression for antiholomorphic counterpart. From this we extract the central charge of a single real fermion or the critical Ising model: $c_{\mathrm{Majorana}} = 1/2$.

The fact that the central charge of a single Dirac field can be expressed as a sum of the central charges of two Majorana fields – $c_{\mathrm{Dirac}} = c_{\mathrm{Majorana}} + c_{\mathrm{Majorana}}$ – permits us to represent the Dirac field as:

$$\begin{aligned} \psi_{\mathrm{L}} &= \frac{1}{\sqrt{2}}\big(\xi_{\mathrm{L}1} + \mathrm{i}\xi_{\mathrm{L}2}\big), \quad \psi_{\mathrm{L}}^{\dagger} = \frac{1}{\sqrt{2}}\big(\xi_{\mathrm{L}1} - \mathrm{i}\xi_{\mathrm{L}2}\big), \\ \psi_{\mathrm{R}} &= \frac{1}{\sqrt{2}}\big(\xi_{\mathrm{R}1} + \mathrm{i}\xi_{\mathrm{R}2}\big), \quad \psi_{\mathrm{R}}^{\dagger} = \frac{1}{\sqrt{2}}\big(\xi_{\mathrm{R}1} - \mathrm{i}\xi_{\mathrm{R}2}\big), \end{aligned} \tag{C.37}$$

in terms of two copies of the real Majorana field $\xi_{\mathrm{L}i}^{\dagger} = \xi_{\mathrm{L}i}$, $\xi_{\mathrm{R}i}^{\dagger} = \xi_{\mathrm{R}i}$, $i = 1, 2$, satisfying equal-time anticommutation relations

$$\begin{aligned} &\big\{\xi_{\mathrm{L}i}(\tau, x), \xi_{\mathrm{L}j}(\tau, x')\big\} = \big\{\xi_{\mathrm{R}i}(\tau, x), \xi_{\mathrm{R}j}(\tau, x')\big\} = \delta_{ij}\delta(x - x'), \\ &\big\{\xi_{\mathrm{L}i}(\tau, x), \xi_{\mathrm{R}j}(\tau, x')\big\} = 0. \end{aligned} \tag{C.38}$$

$$\mathscr{L}(\psi, \overline{\psi}) = \sum_{i=1,2} \mathscr{L}^{(i)}(\xi_{\mathrm{L}i}, \xi_{\mathrm{R}i}), \quad \mathscr{L}^{(i)}(\xi_{\mathrm{L}i}, \xi_{\mathrm{R}i}) \equiv : \xi_{\mathrm{R}i} \partial \xi_{\mathrm{R}i} : + : \xi_{\mathrm{L}i} \bar{\partial} \xi_{\mathrm{L}i} : . \tag{C.39}$$

Here gradient terms, $\partial\big(\xi_1\xi_2\big)$ and $\bar{\partial}\big(\xi_{\mathrm{R}1}\xi_{\mathrm{R}2}\big)$ have been neglected.

Being uncorrelated from each other, each species of Majorana fermions could be investigated separately. It must be noted, that $U(1) \otimes U(1)$ chiral symmetry of the Dirac model is represented by $O(2)$ rotation symmetry of the vector $\xi = (\xi_1,\ \xi_2)^{\mathrm{T}}$ and its antiholomorphic counterpart.

This remarkable result justifies a central charge as a measure of the number of degrees of freedom.

D Sine-Gordon model

In this appendix, we briefly summarize the properties of the SG model given by the Hamiltonian:

$$\mathcal{H}_{\rm SG} = \frac{v}{2}\int \mathrm{d}x \left[\frac{1}{v^2}(\partial_t\Theta)^2 + (\partial_x\Phi)^2\right] + \frac{gv}{\alpha^2}\int \mathrm{d}x \cos\beta\Phi \tag{D.1}$$

in the vicinity of marginal point $\beta = \sqrt{8\pi}$. Here g is the dimensionless coupling constant.

D.1 RG analysis

Following Ref. [99], we start with the Euclidean action

$$\mathcal{S}[\Phi] = \frac{1}{2}\int \mathrm{d}^2\mathbf{x}\left[(\partial_0\Theta)^2 + (\partial_1\Phi)^2\right] + g\int \frac{\mathrm{d}^2\mathbf{x}}{\alpha^2}\cos\beta\Phi, \tag{D.2}$$

where $\mathrm{d}^2\mathbf{x} = v\,\mathrm{d}\tau\,\mathrm{d}x$, $\partial_1 = \partial_x$, and $\partial_0 = v^{-1}\partial_\tau$. Then, we represent the Bose field as a sum of slow and fast contributions in the following way:

$$\Phi_\Lambda(\mathbf{x}) = \sum_{|\mathbf{k}|<\Lambda'} e^{\mathrm{i}\mathbf{k}\cdot\mathbf{x}}\Phi_{\mathbf{k},a} + \sum_{\Lambda'<|\mathbf{k}|<\Lambda} e^{\mathrm{i}\mathbf{k}\cdot\mathbf{x}}\Phi_{\mathbf{k},a} \equiv \Phi_{\Lambda'}(\mathbf{x}) + h(\mathbf{x}), \quad a = c,s. \tag{D.3}$$

Here Λ is a large momentum cutoff, and $\Lambda' \lesssim \Lambda$ is a renormalized cutoff. The idea is to express the Euclidean path integral in terms of slow and fast modes and integrate out all fast modes. If the resulting expression can be expressed as a path integral of slow modes with some effective action $\mathcal{S}_{\rm eff}[\Phi^{\Lambda'}_{c,s}(\mathbf{x})]$ which is identical to the original one with possibly renormalized couplings, one obtains the so-called RG flow in the space of couplings controlled by the RG parameter $l = \ln\frac{\Lambda'}{\Lambda}$. In particular,

$$\begin{aligned} Z_\Lambda &= \int \mathcal{D}\Phi_\Lambda e^{-\mathcal{S}[\Phi_\Lambda]} = \int \mathcal{D}\Phi_{\Lambda'}\mathcal{D}h e^{-\mathcal{S}_0[\Phi_{\Lambda'}]-\mathcal{S}_0[h]-\mathcal{S}'[\Phi_{\Lambda'}+h]} = \\ &= Z_h \int \mathcal{D}\Phi_{\Lambda'} e^{-\mathcal{S}_0[\Phi_{\Lambda'}]}\langle e^{-\mathcal{S}'[\Phi_{\Lambda'}+h]}\rangle_h = \\ &= \mathrm{const}\times\int \mathcal{D}\Phi_{\Lambda'} e^{-\mathcal{S}_{\rm eff}[\Phi_{\Lambda'}]}, \end{aligned}$$

where

$$Z_h = \int \mathcal{D}h e^{-\mathcal{S}_0[h]}, \quad \text{and} \quad \langle e^{-\mathcal{S}[\Phi_{\Lambda'}+h]}\rangle_h = \frac{1}{Z_h}\int \mathcal{D}h e^{-\mathcal{S}_0[h]} e^{-\mathcal{S}[\Phi_{\Lambda'}+h]}. \tag{D.4}$$

For small couplings, one can obtain the following perturbative expression for the effective action:

$$\begin{aligned} &\mathcal{S}_{\rm eff}[\Phi_{\Lambda'}] = \mathcal{S}_0[\Phi_{\Lambda'}] - \ln\langle e^{-\mathcal{S}[\Phi_{\lambda'}+h]}\rangle_h = \\ &= \mathcal{S}_0[\Phi_{\Lambda'}] + \langle \mathcal{S}'[\Phi_{\lambda'}+h]\rangle_h - \frac{1}{2}\left(\langle \mathcal{S}'^2[\Phi_{\lambda'}+h]\rangle_h - \langle \mathcal{S}'[\Phi_{\lambda'}+h]\rangle_h^2\right) + O(g^3). \end{aligned} \tag{D.5}$$

After some calculations, one derives the following effective action

$$\begin{aligned} \mathcal{S}_{\rm eff}[\Phi_{\Lambda'}] &= \frac{1}{2}\left[1 + \frac{\pi B g^2\beta^4}{4}\mathrm{d}l\right]\int \mathrm{d}^2\mathbf{x}\left[\left(\partial_0\Phi_{\Lambda'}\right)^2 + \left(\partial_0\Phi_{\Lambda'}\right)^2\right] + \\ &+ g\left[1 - \frac{\beta^2}{4\pi}\mathrm{d}l\right]\int \frac{\mathrm{d}^2\mathbf{x}}{\alpha^2}\cos\beta\Phi_{\Lambda'}(\mathbf{x}) \end{aligned}$$

Restoring the original cutoff by rescaling the momentum $\mathbf{k} \to \mathbf{k}' = (1+\mathrm{d}l)\mathbf{k}$ amounts to the coordinate rescaling by the inverse factor: $\mathbf{x} \to \mathbf{x}' = (1-\mathrm{d}l)\mathbf{x}$. Therefore, $\mathrm{d}^2\mathbf{x}$ is replaced by $(1+\mathrm{d}l)^2\,\mathrm{d}^2\mathbf{x}' \approx (1+2\,\mathrm{d}l)\,\mathrm{d}^2\mathbf{x}'$ and ∂_0 is replaced by $(1-\mathrm{d}l)\partial_0'$. Therefore (primes are omitted):

$$\begin{aligned}\mathcal{S}_{\mathrm{eff}}[\Phi_\Lambda] \;=\; & \frac{1}{2}\left[1+\frac{\pi A g^2\beta^4}{4}\,\mathrm{d}l\right]\int \mathrm{d}^2\mathbf{x}\left[\left(\partial_0\Phi_\Lambda\right)^2+\left(\partial_0\Phi_\Lambda\right)^2\right]+\\ & +g\left[1+\left(2-\frac{\beta^2}{4\pi}\right)\mathrm{d}l\right]\int\frac{\mathrm{d}^2\mathbf{x}}{\alpha^2}\cos\beta\Phi_\Lambda(\mathbf{x}),\end{aligned}$$

where $A>0$ is some non-universal constant. Finally, we rescale field and β

$$\widetilde{\Phi} = Z^{1/2}\Phi, \quad \beta' = Z^{-1/2}\beta, \tag{D.6}$$

where,

$$Z = 1+\frac{\pi A g^2\beta^4}{4}\,\mathrm{d}l\,, \tag{D.7}$$

to bring the Gaussian part of the effective action to its canonical form. Hence,

$$\mathcal{S}_{\mathrm{eff}}[\widetilde{\Phi}_\Lambda] \;=\; \frac{1}{2}\int \mathrm{d}^2\mathbf{x}\left[\left(\partial_0\widetilde{\Phi}_\Lambda\right)^2+\left(\partial_0\widetilde{\Phi}_\Lambda\right)^2\right]+g'\int\frac{\mathrm{d}^2\mathbf{x}}{\alpha^2}\cos\beta'\widetilde{\Phi}_\Lambda(\mathbf{x})$$

where

$$g' = g\left[1+\left(2-\frac{\beta^2}{4\pi}\right)\mathrm{d}l\right], \tag{D.8}$$

$$\beta'^2 = \beta^2\left[1-\frac{\pi A g^2\beta^4}{4}\,\mathrm{d}l\right]. \tag{D.9}$$

In terms of the scaling dimension of the cosine perturbation $\Delta = \beta^2/4\pi$, we write the following RG equations:

$$\frac{\mathrm{d}g(l)}{\mathrm{d}l} = (2-\Delta)g(l), \quad \frac{\mathrm{d}\Delta(l)}{\mathrm{d}l} = -4\pi^3 A g^2(l)\Delta^3(l). \tag{D.10}$$

Close to the critical point $\Delta = 2$, we introduce new variables

$$g_\parallel(l) = \Delta(l)-2, \quad g_\perp(l) = \frac{g(l)}{\sqrt{32\pi^3 A}}, \tag{D.11}$$

to recast the RG equations in a more familiar form (Berezinskii-Kosterlitz-Thouless equations):

$$\frac{\mathrm{d}g_\perp}{\mathrm{d}l} = -g_\parallel g_\perp, \quad \frac{\mathrm{d}g_\parallel}{\mathrm{d}l} = -g_\perp^2. \tag{D.12}$$

The corresponding RG phase diagram is shown in Fig. 1.4. The phase space consists of three distinct sectors:

- $g_\parallel \geq |g_\perp|$ – the weak coupling sector;
- $-|g_\perp| < g_\parallel < |g_\perp|$ - the crossover sector;
- $g_\parallel \leq |g_\perp|$ – the strong coupling sector.

D.2 Soliton mass and single point correlation functions

In the range $\beta > \sqrt{8\pi}$ the cosine perturbation is irrelevant and the SG model (D.2) reduces to the theory of critical Gaussian model with power low correlations and g-dependent critical exponents. In this appendix, we will concentrate on $0 \leq \beta \leq \sqrt{8\pi}$. The model (D.2) is an integrable model with explicitly known mass spectrum and scattering theory (see e.g. [120] and references therein). The mass spectrum contains topological soliton and anti-soliton doublets – fundamental fermions of the theory – representing kink and anti-kink type excitations interpolating between neighboring vacua (minimum of the cosine perturbation term) of Φ-field. The following topological charge characterizes soliton and anti-soliton excitations,

$$Q = \frac{\beta}{4\pi}\int_{-\infty}^{\infty} \mathrm{d}x\, \partial_x \Phi_x(x) = \pm\frac{1}{2}, \tag{D.13}$$

respectively.

The soliton mass m_s is related to the dimensionless coupling by the relation:

$$m_\mathrm{s} = C(\beta)\, |g|^{\frac{1}{2-\Delta_\beta}}, \tag{D.14}$$

where $\Delta_\beta = \beta^2/4\pi$ is the scaling dimension of the cosine perturbation term. The exact β dependence of $C(\beta)$ can be found in [120].

To obtain expectation values of various order parameters in Sec. 6.2 we will extensively make use of the exact expression of the expectation value of exponential operators $e^{\mathrm{i}\alpha\Phi}$:

$$\langle e^{\mathrm{i}\alpha\Phi}\rangle = C'(\alpha,\beta)\, |m_\mathrm{s}|^{\Delta_\alpha}, \quad \Delta_\alpha = \frac{\alpha^2}{4\pi}, \tag{D.15}$$

where m_s is the soliton mass (D.14) and numerical prefactor $C'(\alpha,\beta)$ in known explicitly [121].

Bibliography

[1] Bachana Beradze and Alexander Nersesyan. Spectrum, Lifshitz transitions and orbital current in frustrated fermionic ladders with a uniform flux. *The European Physical Journal B*, 96(1):2, January 2023. 11

[2] Bachana Beradze, Mikheil Tsitsishvili, Emanuele Tirrito, Marcello Dalmonte, Titas Chanda, and Alexander Nersesyan. Emergence of non-abelian su(2) invariance in abelian frustrated fermionic ladders. *Phys. Rev. B*, 108:075146, Aug 2023. 11, 83

[3] H. Bethe. Zur theorie der metalle. *Zeitschrift für Physik*, 71:205–226, 1931. 30

[4] Edward Witten. Nonabelian bosonization in two dimensions. *Communications in Mathematical Physics*, 92(4):455 – 472, 1984. 32

[5] Philippe Di Francesco, Pierre Mathieu, and David Sénéchal. *Conformal Field Theory*. Springer New York, 1997. 32, 89

[6] Ian Affleck. Exact critical exponents for quantum spin chains, non-linear σ-models at $\theta = \pi$ and the quantum hall effect. *Nuclear Physics B*, 265(3):409–447, 1986. 32

[7] F. D. M. Haldane. Spontaneous dimerization in the $s = \frac{1}{2}$ heisenberg antiferromagnetic chain with competing interactions. *Phys. Rev. B*, 25:4925–4928, Apr 1982. 33

[8] A. Luther and I. Peschel. Calculation of critical exponents in two dimensions from quantum field theory in one dimension. *Phys. Rev. B*, 12:3908–3917, Nov 1975. 33

[9] G. Delfino and G. Mussardo. Non-integrable aspects of the multi-frequency sine-gordon model. *Nuclear Physics B*, 516(3):675–703, 1998. 35, 36, 38, 76, 81

[10] M. Fabrizio, A.O. Gogolin, and A.A. Nersesyan. Critical properties of the double-frequency sine-gordon model with applications. *Nuclear Physics B*, 580(3):647–687, 2000. 35, 36, 38, 76, 81

[11] Ian Affleck. Soliton confinement and the excitation spectrum of spin-peierls antiferromagnets, 1997. 35

[12] Leo P Kadanoff and Alan C Brown. Correlation functions on the critical lines of the baxter and ashkin-teller models. *Annals of Physics*, 121(1):318–342, 1979. 36, 37

[13] Leo P. Kadanoff and Albert B. Zisook. Correlation functions on the critical line of the two-dimensional planar model: Logarithms and corrections to scaling. *Nuclear Physics B*, 180(1):61–76, 1981. 36, 37

[14] Gesualdo Delfino and Paolo Grinza. Universal ratios along a line of critical points. the ashkin–teller model. *Nuclear Physics B*, 682(3):521–550, mar 2004. 36

[15] Yacine Aoun, Moritz Dober, and Alexander Glazman. Phase diagram of the ashkin-teller model, 2023. 37

[16] Leo P. Kadanoff and Franz J. Wegner. Some critical properties of the eight-vertex model. *Phys. Rev. B*, 4:3989–3993, Dec 1971. 37

[17] F J Wegner. Duality relation between the ashkin-teller and the eight-vertex model. *Journal of Physics C: Solid State Physics*, 5(11):L131, jun 1972. 37

[18] R. J. Baxter. *Exactly solved models in statistical mechanics*. Dover Publications, 1982. 37

[19] John B. Kogut. An introduction to lattice gauge theory and spin systems. *Rev. Mod. Phys.*, 51:659–713, Oct 1979. 37

[20] Mahito Kohmoto, Marcel den Nijs, and Leo P. Kadanoff. Hamiltonian studies of the $d = 2$ ashkin-teller model. *Phys. Rev. B*, 24:5229–5241, Nov 1981. 37, 38

[21] Y.-J. Wang and A.A. Nersesyan. Ising model description of the su(2)1 quantum critical point in a dimerized two-leg spin-1/2 ladder. *Nuclear Physics B*, 583(3):671–690, 2000. 37

[22] L.D. Landau and E.M. Lifshitz. *Quantum Mechanics 3rd ed.* Pergamon, Oxford, 1977. 39

[23] R. E.Peierls. Zur theorie des diamagnetismus von leitungselektronen. *Z. Physik*, 80:763–791, 1933. 39

[24] L. Onsager. Interpretation of the de haas-van alphen effect. *Philos. Mag.*, 43:1006–1008, 1952. 39

[25] Gregory H. Wannier. Dynamics of band electrons in electric and magnetic fields. *Rev. Mod. Phys.*, 34:645–655, 1962. 39

[26] P. G. Harper. Single band motion of conduction electrons in a uniform magnetic field. *Proceedings of the Physical Society A*, 68(10):874–878, 1955. 39

[27] M. Ya Azbel'. Energy spectrum of a conduction electron in a magnetic field. *JETP*, 19(3):634, 1964. 39

[28] E. Brown. Bloch electrons in a uniform magnetic field. *Phys. Rev.*, 133:A1038–A1044, 1964. 39

[29] Douglas R. Hofstadter. Energy levels and wave functions of bloch electrons in rational and irrational magnetic fields. *Phys. Rev. B*, 14:2239–2249, 1976. 39

[30] Y. Hasegawa, P. Lederer, T. M. Rice, and P. B. Wiegmann. Theory of electronic diamagnetism in two-dimensional lattices. *Phys. Rev. Lett.*, 63:907–910, 1989. 39

[31] W. Barford and Ju H. Kim. Spinless fermions on frustrated lattices in a magnetic field. *Phys. Rev. B*, 43:559–568, 1991. 39

[32] Jean Dalibard, Fabrice Gerbier, Gediminas Juzeliūnas, and Patrik Öhberg. Colloquium: Artificial gauge potentials for neutral atoms. *Rev. Mod. Phys.*, 83:1523–1543, Nov 2011. 39, 41

[33] A. Celi, P. Massignan, J. Ruseckas, N. Goldman, I. B. Spielman, G. Juzeliūnas, and M. Lewenstein. Synthetic gauge fields in synthetic dimensions. *Phys. Rev. Lett.*, 112:043001, Jan 2014. 39, 41

[34] Victor Galitski, Gediminas Juzeliūnas, and Ian B. Spielman. Artificial gauge fields with ultracold atoms. *Physics Today*, 72(1):38–44, January 2019. 39, 41

[35] E. Orignac and T. Giamarchi. Meissner effect in a bosonic ladder. *Phys. Rev. B*, 64:144515, Sep 2001. 39

[36] Hirokazu Miyake, Georgios A. Siviloglou, Colin J. Kennedy, William Cody Burton, and Wolfgang Ketterle. Realizing the harper hamiltonian with laser-assisted tunneling in optical lattices. *Phys. Rev. Lett.*, 111:185302, Oct 2013. 39

[37] Marcos Atala, Monika Aidelsburger, Michael Lohse, Julio T. Barreiro, Belén Paredes, and Immanuel Bloch. Observation of chiral currents with ultracold atoms in bosonic ladders. *Nature Physics*, 10(8):588–593, July 2014. 39

[38] L. F. Livi, G. Cappellini, M. Diem, L. Franchi, C. Clivati, M. Frittelli, F. Levi, D. Calonico, J. Catani, M. Inguscio, and L. Fallani. Synthetic dimensions and spin-orbit coupling with an optical clock transition. *Phys. Rev. Lett.*, 117:220401, Nov 2016. 39

[39] B. N. Narozhny, S. T. Carr, and A. A. Nersesyan. Fractional charge excitations in fermionic ladders. *Phys. Rev. B*, 71:161101, Apr 2005. 39, 40, 51, 56

[40] Sam T. Carr, Boris N. Narozhny, and Alexander A. Nersesyan. Spinless fermionic ladders in a magnetic field: Phase diagram. *Phys. Rev. B*, 73:195114, May 2006. 39, 40, 51, 56

[41] J. C. Budich, A. Elben, M. Łącki, A. Sterdyniak, M. A. Baranov, and P. Zoller. Coupled atomic wires in a synthetic magnetic field. *Phys. Rev. A*, 95:043632, Apr 2017. 39, 40

[42] Simone Barbarino, Luca Taddia, Davide Rossini, Leonardo Mazza, and Rosario Fazio. Synthetic gauge fields in synthetic dimensions: interactions and chiral edge modes. *New Journal of Physics*, 18(3):035010, March 2016. 39

[43] Simone Barbarino, Marcello Dalmonte, Rosario Fazio, and Giuseppe E. Santoro. Topological phases in frustrated synthetic ladders with an odd number of legs. *Phys. Rev. A*, 97:013634, Jan 2018. 39

[44] Marcello Calvanese Strinati, Eyal Cornfeld, Davide Rossini, Simone Barbarino, Marcello Dalmonte, Rosario Fazio, Eran Sela, and Leonardo Mazza. Laughlin-like states in bosonic and fermionic atomic synthetic ladders. *Phys. Rev. X*, 7:021033, Jun 2017. 39

[45] Chen-How Huang, Masaki Tezuka, and Miguel A Cazalilla. Topological lifshitz transitions, orbital currents, and interactions in low-dimensional fermi gases in synthetic gauge fields. *New Journal of Physics*, 24(3):033043, March 2022. 39, 40, 54, 64

[46] J. Jünemann, A. Piga, S.-J. Ran, M. Lewenstein, M. Rizzi, and A. Bermudez. Exploring interacting topological insulators with ultracold atoms: The synthetic creutz-hubbard model. *Phys. Rev. X*, 7:031057, Sep 2017. 39, 52

[47] A. Bermudez, E. Tirrito, M. Rizzi, M. Lewenstein, and S. Hands. Gross–neveu–wilson model and correlated symmetry-protected topological phases. *Annals of Physics*, 399:149–180, 2018. 39

[48] E. Tirrito, M. Rizzi, G. Sierra, M. Lewenstein, and A. Bermudez. Renormalization group flows for wilson-hubbard matter and the topological hamiltonian. *Phys. Rev. B*, 99:125106, Mar 2019. 39

[49] E. Tirrito, M. Lewenstein, and A. Bermudez. Topological chiral currents in the gross-neveu model extension. *Phys. Rev. B*, 106:045147, Jul 2022. 39

[50] Zeno Bacciconi, Gian Marcello Andolina, Titas Chanda, Giuliano Chiriacò, Marco Schiró, and Marcello Dalmonte. First-order superradiant phase transition in magnetic cavities: A two-leg ladder model, 2023. 39

[51] Anton Mazurenko, Christie S. Chiu, Geoffrey Ji, Maxwell F. Parsons, Márton Kanász-Nagy, Richard Schmidt, Fabian Grusdt, Eugene Demler, Daniel Greif, and Markus Greiner. A cold-atom fermi–hubbard antiferromagnet. *Nature*, 545(7655):462–466, May 2017. 40

[52] Sebastian Krinner, Tilman Esslinger, and Jean-Philippe Brantut. Two-terminal transport measurements with cold atoms. *Journal of Physics: Condensed Matter*, 29(34):343003, July 2017. 40

[53] Luca Lepori, Anna Maraga, Alessio Celi, Luca Dell'Anna, and Andrea Trombettoni. Effective control of chemical potentials by rabi coupling with rf-fields in ultracold mixtures. *Condensed Matter*, 3(2), 2018. 40

[54] Peter Schauß, Marc Cheneau, Manuel Endres, Takeshi Fukuhara, Sebastian Hild, Ahmed Omran, Thomas Pohl, Christian Gross, Stefan Kuhr, and Immanuel Bloch. Observation of spatially ordered structures in a two-dimensional rydberg gas. *Nature*, 491(7422):87–91, October 2012. 40

[55] Y.-Y. Jau, A. M. Hankin, T. Keating, I. H. Deutsch, and G. W. Biedermann. Entangling atomic spins with a rydberg-dressed spin-flip blockade. *Nature Physics*, 12(1):71–74, October 2016. 40

[56] R. Faoro, C. Simonelli, M. Archimi, G. Masella, M. M. Valado, E. Arimondo, R. Mannella, D. Ciampini, and O. Morsch. van der waals explosion of cold rydberg clusters. *Phys. Rev. A*, 93:030701, Mar 2016. 40

[57] Johannes Zeiher, Rick van Bijnen, Peter Schauß, Sebastian Hild, Jae yoon Choi, Thomas Pohl, Immanuel Bloch, and Christian Gross. Many-body interferometry of a rydberg-dressed spin lattice. *Nature Physics*, 12(12):1095–1099, August 2016. 40

[58] Hannes Bernien, Sylvain Schwartz, Alexander Keesling, Harry Levine, Ahmed Omran, Hannes Pichler, Soonwon Choi, Alexander S. Zibrov, Manuel Endres, Markus Greiner, Vladan Vuletić, and Mikhail D. Lukin. Probing many-body dynamics on a 51-atom quantum simulator. *Nature*, 551(7682):579–584, November 2017. 40

[59] Daniel Barredo, Vincent Lienhard, Sylvain de Léséleuc, Thierry Lahaye, and Antoine Browaeys. Synthetic three-dimensional atomic structures assembled atom by atom. *Nature*, 561(7721):79–82, September 2018. 40

[60] Alexander Keesling, Ahmed Omran, Harry Levine, Hannes Bernien, Hannes Pichler, Soonwon Choi, Rhine Samajdar, Sylvain Schwartz, Pietro Silvi, Subir Sachdev, Peter Zoller, Manuel Endres, Markus Greiner, Vladan Vuletić, and Mikhail D. Lukin. Quantum kibble–zurek mechanism and critical dynamics on a programmable rydberg simulator. *Nature*, 568(7751):207–211, April 2019. 40

[61] Antoine Browaeys and Thierry Lahaye. Many-body physics with individually controlled rydberg atoms. *Nature Physics*, 16(2):132–142, January 2020. 40

[62] Christian Gross and Immanuel Bloch. Quantum simulations with ultracold atoms in optical lattices. *Science*, 357(6355):995–1001, September 2017. 40

[63] Sylvain de Léséleuc, Sebastian Weber, Vincent Lienhard, Daniel Barredo, Hans Peter Büchler, Thierry Lahaye, and Antoine Browaeys. Accurate mapping of multilevel rydberg atoms on interacting spin-1/2 particles for the quantum simulation of ising models. *Phys. Rev. Lett.*, 120:113602, Mar 2018. 40

[64] P. Scholl, H. J. Williams, G. Bornet, F. Wallner, D. Barredo, L. Henriet, A. Signoles, C. Hainaut, T. Franz, S. Geier, A. Tebben, A. Salzinger, G. Zürn, T. Lahaye, M. Weidemüller, and A. Browaeys. Microwave engineering of programmable xxz hamiltonians in arrays of rydberg atoms. *PRX Quantum*, 3:020303, Apr 2022. 40

[65] Alexander W. Glaetzle, Marcello Dalmonte, Rejish Nath, Christian Gross, Immanuel Bloch, and Peter Zoller. Designing frustrated quantum magnets with laser-dressed rydberg atoms. *Phys. Rev. Lett.*, 114:173002, Apr 2015. 40, 46, 83

[66] Pascal Scholl, Michael Schuler, Hannah J. Williams, Alexander A. Eberharter, Daniel Barredo, Kai-Niklas Schymik, Vincent Lienhard, Louis-Paul Henry, Thomas C. Lang, Thierry Lahaye, Andreas M. Läuchli, and Antoine Browaeys. Quantum simulation of 2d

antiferromagnets with hundreds of rydberg atoms. *Nature*, 595(7866):233–238, July 2021. 40

[67] Sepehr Ebadi, Tout T. Wang, Harry Levine, Alexander Keesling, Giulia Semeghini, Ahmed Omran, Dolev Bluvstein, Rhine Samajdar, Hannes Pichler, Wen Wei Ho, Soonwon Choi, Subir Sachdev, Markus Greiner, Vladan Vuletić, and Mikhail D. Lukin. Quantum phases of matter on a 256-atom programmable quantum simulator. *Nature*, 595(7866):227–232, July 2021. 40

[68] G. Semeghini, H. Levine, A. Keesling, S. Ebadi, T. T. Wang, D. Bluvstein, R. Verresen, H. Pichler, M. Kalinowski, R. Samajdar, A. Omran, S. Sachdev, A. Vishwanath, M. Greiner, V. Vuletić, and M. D. Lukin. Probing topological spin liquids on a programmable quantum simulator. *Science*, 374(6572):1242–1247, December 2021. 40

[69] T. Pohl, E. Demler, and M. D. Lukin. Dynamical crystallization in the dipole blockade of ultracold atoms. *Phys. Rev. Lett.*, 104:043002, Jan 2010. 40

[70] Sylvain de Léséleuc, Vincent Lienhard, Pascal Scholl, Daniel Barredo, Sebastian Weber, Nicolai Lang, Hans Peter Büchler, Thierry Lahaye, and Antoine Browaeys. Observation of a symmetry-protected topological phase of interacting bosons with rydberg atoms. *Science*, 365(6455):775–780, August 2019. 40, 79

[71] Ruben Verresen, Mikhail D. Lukin, and Ashvin Vishwanath. Prediction of toric code topological order from rydberg blockade. *Phys. Rev. X*, 11:031005, Jul 2021. 40

[72] P. S. Tarabunga, F. M. Surace, R. Andreoni, A. Angelone, and M. Dalmonte. Gauge-theoretic origin of rydberg quantum spin liquids. *Phys. Rev. Lett.*, 129:195301, Nov 2022. 40

[73] Zakaria Jouini, Natalia Chepiga, Loic Herviou, and Frédéric Mila. Emergent U(1) symmetry in non-particle-conserving 1D models, 2023. 40

[74] N. Henkel, R. Nath, and T. Pohl. Three-Dimensional Roton Excitations and Supersolid Formation in Rydberg-Excited Bose-Einstein Condensates. *Phys. Rev. Lett.*, 104:195302, May 2010. 40, 46

[75] Jens Honer, Hendrik Weimer, Tilman Pfau, and Hans Peter Büchler. Collective Many-Body Interaction in Rydberg Dressed Atoms. *Phys. Rev. Lett.*, 105:160404, Oct 2010. 40, 46

[76] G. Pupillo, A. Micheli, M. Boninsegni, I. Lesanovsky, and P. Zoller. Strongly Correlated Gases of Rydberg-Dressed Atoms: Quantum and Classical Dynamics. *Phys. Rev. Lett.*, 104:223002, Jun 2010. 40, 46

[77] T. Macrì and T. Pohl. Rydberg dressing of atoms in optical lattices. *Phys. Rev. A*, 89:011402, Jan 2014. 40, 46

[78] Marco Mattioli, Marcello Dalmonte, Wolfgang Lechner, and Guido Pupillo. Cluster luttinger liquids of rydberg-dressed atoms in optical lattices. *Phys. Rev. Lett.*, 111:165302, Oct 2013. 40

[79] M. Dalmonte, W. Lechner, Zi Cai, M. Mattioli, A. M. Läuchli, and G. Pupillo. Cluster Luttinger liquids and emergent supersymmetric conformal critical points in the one-dimensional soft-shoulder Hubbard model. *Phys. Rev. B*, 92:045106, Jul 2015. 40, 46, 83

[80] Adriano Angelone, Fabio Mezzacapo, and Guido Pupillo. Superglass phase of interaction-blockaded gases on a triangular lattice. *Phys. Rev. Lett.*, 116:135303, Apr 2016. 40

[81] Adriano Angelone, Tao Ying, Fabio Mezzacapo, Guido Masella, Marcello Dalmonte, and Guido Pupillo. Nonequilibrium scenarios in cluster-forming quantum lattice models. *Phys. Rev. A*, 101:063603, Jun 2020. 40

[82] Elmer Guardado-Sanchez, Benjamin M. Spar, Peter Schauss, Ron Belyansky, Jeremy T. Young, Przemyslaw Bienias, Alexey V. Gorshkov, Thomas Iadecola, and Waseem S. Bakr. Quench Dynamics of a Fermi Gas with Strong Nonlocal Interactions. *Phys. Rev. X*, 11:021036, May 2021. 41, 46, 83

[83] Mikheil Tsitsishvili, Titas Chanda, Matteo Votto, Pierre Fromholz, Marcello Dalmonte, and Alexander Nersesyan. Phase diagram of rydberg-dressed atoms on two-leg square ladders: Coupling supersymmetric conformal field theories on the lattice. *Phys. Rev. B*, 105:155159, Apr 2022. 41

[84] Pierre Fromholz, Mikheil Tsitsishvili, Matteo Votto, Marcello Dalmonte, Alexander Nersesyan, and Titas Chanda. Phase diagram of rydberg-dressed atoms on two-leg triangular ladders. *Phys. Rev. B*, 106:155411, Oct 2022. 41

[85] Thomas Botzung, Guido Pupillo, Pascal Simon, Roberta Citro, and Elisa Ercolessi. One-dimensional extended Hubbard model with soft-core potential, 2019. 41

[86] Madhumita Sarkar, Mainak Pal, Arnab Sen, and Krishnendu Sengupta. Quantum order-by-disorder induced phase transition in rydberg ladders with staggered detuning. *SciPost Physics*, 14(1):004, January 2023. 41

[87] Luisa Eck and Paul Fendley. Critical lines and ordered phases in a Rydberg-blockade ladder, 2023. 41

[88] D Jaksch and P Zoller. Creation of effective magnetic fields in optical lattices: the hofstadter butterfly for cold neutral atoms. *New Journal of Physics*, 5:56–56, May 2003. 41, 42, 43, 46, 83

[89] Simon Hollerith, Kritsana Srakaew, David Wei, Antonio Rubio-Abadal, Daniel Adler, Pascal Weckesser, Andreas Kruckenhauser, Valentin Walther, Rick van Bijnen, Jun Rui, Christian Gross, Immanuel Bloch, and Johannes Zeiher. Realizing distance-selective interactions in a rydberg-dressed atom array. *Phys. Rev. Lett.*, 128:113602, Mar 2022. 46

[90] Yotam Shapira, Tom Manovitz, Nitzan Akerman, Ady Stern, and Roee Ozeri. Quantum simulations of interacting systems with broken time-reversal symmetry. *Phys. Rev. X*, 13:021021, May 2023. 46

[91] G. E. Volovik. Topological lifshitz transitions. *Low Temp. Phys.*, 43(1):47–55, 2017. 53

[92] A Yu Kitaev. Unpaired majorana fermions in quantum wires. *Physics-Uspekhi*, 44(10S):131–136, October 2001. 54

[93] Jason Alicea. New directions in the pursuit of majorana fermions in solid state systems. *Reports on Progress in Physics*, 75(7):076501, June 2012. 54

[94] Andreas W W Ludwig. Topological phases: classification of topological insulators and superconductors of non-interacting fermions, and beyond. *Physica Scripta*, T168:014001, December 2015. 54

[95] G. I. Japaridze and A. A. Nersesyan. Magnetic-field phase transition in a one-dimensional system of electrons with attraction. *Pisma Zh. Eksp. Teor. Fiz.*, 27(6):356–359, 1878. 58, 59

[96] V. L. Pokrovsky and A. L. Talapov. Ground state, spectrum, and phase diagram of two-dimensional incommensurate crystals. *Phys. Rev. Lett.*, 42:65–67, Jan 1979. 58, 59

[97] B. Sriram Shastry and Bill Sutherland. Twisted boundary conditions and effective mass in heisenberg-ising and hubbard rings. *Phys. Rev. Lett.*, 65:243–246, Jul 1990. 59

[98] Thierry Giamarchi and B. Sriram Shastry. Persistent currents in a one-dimensional ring for a disordered hubbard model. *Phys. Rev. B*, 51:10915–10922, Apr 1995. 59

[99] Alexander O. Gogolin, Alexander A. Nersesyan, and Alexei M. Tsvelik. *Bosonization and Strongly Correlated Systems*. Cambridge University Press, Cambridge, 2004. 59, 73, 78, 83, 94

[100] T. Vekua. Susceptibility at the edge points of magnetization plateau of one-dimensional electron and spin systems. *Phys. Rev. B*, 80:104411, Sep 2009. 64

[101] Elliott H. Lieb and F. Y. Wu. Absence of mott transition in an exact solution of the short-range, one-band model in one dimension. *Phys. Rev. Lett.*, 20:1445–1448, Jun 1968. 67

[102] Thierry Giamarchi. *Quantum Physics in One Dimension*. Oxford University Press, Oxford, December 2003. 77, 78

[103] Sidney Coleman. Quantum sine-gordon equation as the massive thirring model. *Phys. Rev. D*, 11:2088–2097, Apr 1975. 78

[104] Kazuo Hida. Crossover between the haldane-gap phase and the dimer phase in the spin-1/2 alternating heisenberg chain. *Phys. Rev. B*, 45:2207–2212, Feb 1992. 79

[105] Emanuele G. Dalla Torre, Erez Berg, and Ehud Altman. Hidden order in 1d bose insulators. *Phys. Rev. Lett.*, 97:260401, Dec 2006. 79

[106] Erez Berg, Emanuele G. Dalla Torre, Thierry Giamarchi, and Ehud Altman. Rise and fall of hidden string order of lattice bosons. *Phys. Rev. B*, 77:245119, Jun 2008. 79

[107] G. G. Batrouni, R. T. Scalettar, V. G. Rousseau, and B. Grémaud. Competing supersolid and haldane insulator phases in the extended one-dimensional bosonic hubbard model. *Phys. Rev. Lett.*, 110:265303, Jun 2013. 79

[108] G. G. Batrouni, V. G. Rousseau, R. T. Scalettar, and B. Grémaud. Competing phases, phase separation, and coexistence in the extended one-dimensional bosonic hubbard model. *Phys. Rev. B*, 90:205123, Nov 2014. 79

[109] Arianna Montorsi and Marco Roncaglia. Nonlocal order parameters for the 1d hubbard model. *Phys. Rev. Lett.*, 109:236404, Dec 2012. 79

[110] Luca Barbiero, Arianna Montorsi, and Marco Roncaglia. How hidden orders generate gaps in one-dimensional fermionic systems. *Phys. Rev. B*, 88:035109, Jul 2013. 79

[111] Yasaman Bahri and Ashvin Vishwanath. Detecting majorana fermions in quasi-one-dimensional topological phases using nonlocal order parameters. *Phys. Rev. B*, 89:155135, Apr 2014. 79

[112] Gennady Y Chitov and Toplal Pandey. Constructing landau framework for topological order: quantum chains and ladders. *Journal of Statistical Mechanics: Theory and Experiment*, 2017(4):043101, April 2017. 79

[113] A. A. Nersesyan. Phase diagram of an interacting staggered su-schrieffer-heeger two-chain ladder close to a quantum critical point. *Phys. Rev. B*, 102:045108, Jul 2020. 79

[114] M. Endres, M. Cheneau, T. Fukuhara, C. Weitenberg, P. Schauß, C. Gross, L. Mazza, M. C. Bañuls, L. Pollet, I. Bloch, and S. Kuhr. Observation of correlated particle-hole pairs and string order in low-dimensional mott insulators. *Science*, 334(6053):200–203, October 2011. 79

[115] Timon A. Hilker, Guillaume Salomon, Fabian Grusdt, Ahmed Omran, Martin Boll, Eugene Demler, Immanuel Bloch, and Christian Gross. Revealing hidden antiferromagnetic correlations in doped hubbard chains via string correlators. *Science*, 357(6350):484–487, 2017. 79

[116] Pimonpan Sompet, Sarah Hirthe, Dominik Bourgund, Thomas Chalopin, Julian Bibo, Joannis Koepsell, Petar Bojović, Ruben Verresen, Frank Pollmann, Guillaume Salomon, Christian Gross, Timon A. Hilker, and Immanuel Bloch. Realizing the symmetry-protected haldane phase in fermi–hubbard ladders. *Nature*, 606(7914):484–488, June 2022. 79

[117] David Wei, Daniel Adler, Kritsana Srakaew, Suchita Agrawal, Pascal Weckesser, Immanuel Bloch, and Johannes Zeiher. Observation of brane parity order in programmable optical lattices. *Phys. Rev. X*, 13:021042, Jun 2023. 79

[118] Jin Hyoun Kang, Jeong Ho Han, and Y Shin. Creutz ladder in a resonantly shaken 1d optical lattice. *New Journal of Physics*, 22(1):013023, January 2020. 83

[119] Fabian H. L. Essler, Holger Frahm, Frank Göhmann, Andreas Klümper, and Vladimir E. Korepin. *The One-Dimensional Hubbard Model*. Cambridge University Press, 2005. 86

[120] AL. B. ZAMOLODCHIKOV. Mass scale in the sine–gordon model and its reductions. *International Journal of Modern Physics A*, 10(08):1125–1150, 1995. 96

[121] Sergei Lukyanov and Alexander Zamolodchikov. Exact expectation values of local fields in the quantum sine-gordon model. *Nuclear Physics B*, 493(3):571–587, 1997. 96